Aus dem

Institut für Schlaganfall- und Demenzforschung (ISD)

Klinikum der Ludwig-Maximilians-Universität München

Combining connectivity, related pathologies, and genetic factors to explain tau accumulation in Alzheimer's disease

Dissertation

zum Erwerb des Doctor of Philosophy (Ph.D.)

an der Medizinischen Fakultät der

Ludwig-Maximilians-Universität München

vorgelegt von

Lukai Zheng

aus

Zhejiang, China

Jahr

2024

Mit Genehmigung der Medizinischen Fakultät der
Ludwig-Maximilians-Universität München

Erstes Gutachten:	Prof. Dr. Michael Ewers
Zweites Gutachten:	Prof. Dr. Peter Graf zu Eulenburg
Drittes Gutachten:	Prof. Dr. Dr. h.c. Christian Haass
Viertes Gutachten:	Prof. Dr. Mikael Simons

Dekan: Prof. Dr. med. Thomas Gudermann

Tag der mündlichen Prüfung: 01.07.2024

Table of contents

List of abbreviations

Aβ = amyloid-beta

AD = Alzheimer's disease

AHBA = Allen Human Brain Atlas

APOE4 = apolipoprotein E ε4

APP = amyloid precursor protein

CNS = central nervous system

CSF = cerebrospinal fluid

MAPT = microtubule-associated protein tau

MBP = myelin basic protein

MRI = magnetic resonance imaging

MWF = myelin water fraction

MWI = myelin water imaging

NFT = neurofibrillary tangle

p-tau = hyperphosphorylated tau

PET = positron emission tomography

PHF = paired helical filament

R^2 = proportion variance explained

WM = white matter

List of publications included in this thesis

Manuscript I

Zheng, L., Rubinski, A., Denecke, J., Luan, Y., Smith, R., Strandberg, O., Stomrud, E., Ossenkoppele, R., Svaldi, D. O., Higgins, I. A., Shcherbinin, S., Pontecorvo, M. J., Hansson, O., Franzmeier, N., Ewers, M., for the Alzheimer's Disease Neuroimaging Initiative. (2024). Combined Connectomics, *MAPT* Gene Expression, and Amyloid Deposition to Explain Regional Tau Deposition in Alzheimer Disease. *Annals of Neurology*, 95(2), 274–287. https://doi.org/10.1002/ana.26818

Manuscript II

Rubinski, A., Dewenter, A., **Zheng, L.**, Franzmeier, N., Stephenson, H., Deming, Y., Duering, M., Gesierich, B., Denecke, J., Pham, A.-V., Bendlin, B., Ewers, M., for the Alzheimer's Disease Neuroimaging Initiative. (2024). Florbetapir PET-assessed demyelination is associated with faster tau accumulation in an *APOE ε4*-dependent manner. *European Journal of Nuclear Medicine and Molecular Imaging*, 51(4), 1035–1049. https://doi.org/10.1007/s00259-023-06530-8

Contribution to the publications

Contribution to Manuscript I

The author of this thesis (LZ) is the first author on this manuscript. LZ contributed to the processing and analysis of data, drafting of the manuscript and preparation of the figures.

Contribution of other coauthors: ME and NF contributed to the conception and design of the study, drafting of the manuscript and preparation of the figures. AR, YL, and JD contributed to the processing of the data. RS, OS, ES, RO, DOS, IAH, SS, MJP, and OH contributed to initial data acquisition.

Contribution to Manuscript II

LZ processed the data and revised the manuscript. Specifically, he performed quality control of the results of automated white matter hyperintensity segmentation, removed any artifacts from the results, and critically revised the manuscript.

Contribution of other coauthors: AR designed the study, processed the data, conducted the analysis, interpreted the results, and wrote the manuscript. ME designed the study, interpreted the results, and wrote the manuscript. AD, NF, MD, BG, JD, and A-VP processed the data, and revised the manuscript. HS, YD, and BB assisted with data and imaging analysis, and revised the manuscript.

Introductory summary

Alzheimer’s disease

Alzheimer’s disease (AD) is a neurodegenerative disease that accounts for 60-80% of all cases of dementia in the elderly (Alzheimer's Association, 2024). Clinically, it is characterized by progressive cognitive decline over years to decades, with memory loss typically being the earliest and most prominent symptom (Cummings & Benson, 1992). The pathological hallmarks of AD include extracellular amyloid-beta (Aβ) plaques and neuronal tau tangles, which may occur long before symptom onset (Birdsill et al., 2022; Scheltens et al., 2021). Although the complete molecular processes linking these pathologic protein alterations to dementia symptoms are still unknown, the higher brain levels of Aβ and, in particular, pathologic tau have been found across a large number of studies to be associated with neuron loss and cognitive decline (Hanseeuw et al., 2019; Sato et al., 2018), therefore holding great promise as targets for diagnosis and treatment of AD (Golde, 2022; Guo et al., 2022).

Tau pathology in Alzheimer’s disease

Tau is a highly soluble protein that plays a critical role in the stability of neuronal microtubules (Drubin & Kirschner, 1986; Weingarten et al., 1975). Under normal conditions, tau protein undergoes a balance of phosphorylation and dephosphorylation, which ensures its physiological functionality (Xia et al., 2021). However, in AD, tau becomes hyperphosphorylated, likely due to overactivation of tau kinases and resistance to proteolysis (Alonso et al., 2018; Noble et al., 2013). While hyperphosphorylated tau (p-tau) exhibits reduced microtubule binding, the protein misfolds and self-assembles into relatively insoluble paired helical filaments (PHFs) (Grundke-Iqbal et al., 1986; Lee et al., 1991; Mandelkow et al., 2007). As PHFs accumulate

and mature, they form dense and insoluble neurofibrillary tangles (NFTs) (Kidd, 1963; Mena et al., 1991). The formation of NFTs within neurons is closely correlated with neuronal dysfunction and degeneration, contributing to cognitive decline in AD (Wang & Mandelkow, 2016).

Several biomarkers are available for tau pathology in AD (Barthelemy et al., 2020; Janelidze et al., 2020; Leuzy et al., 2020; Ossenkoppele et al., 2018; Palmqvist et al., 2020), including cerebrospinal fluid (CSF) and blood tests for soluble p-tau, and positron emission tomography (PET) imaging for insoluble tau aggregates (i.e., PHFs and NFTs). These biomarkers have shown strong correlations with cognitive and functional outcomes in patients with AD (Bucci et al., 2021; Ossenkoppele et al., 2022), making them important tools for monitoring disease progression and evaluating potential treatments.

Spatial tau progression in Alzheimer's disease: tau propagation hypothesis and connectivity-based models

Our comprehension of the spatial pattern of tau progression in AD has been traditionally guided by the classical Braak staging, which is derived from post-mortem assessments of NFT deposits in the brain (Braak & Braak, 1991). This staging system categorizes the severity of tau pathology in AD based on the spatially increasing extent of NFT deposits in specific brain regions, including the entorhinal cortex (Stage I), hippocampus and limbic areas (Stages II-III), and neocortex (Stages IV-VI). In contrast, the distribution of Aβ plaques, another hallmark of AD, tends to be more diffuse throughout the brain, as characterized by the Thal staging system (Thal et al., 2002). While Aβ plaques exhibit a less structured spatial pattern, the Braak staging implies a distinct and hierarchical pattern of tau progression. However, post-mortem studies have revealed "atypical" AD cases that do not conform to the spatial

tau trajectory (Murray et al., 2011), and the advent of tau-PET imaging has shed new light on this perspective. Tau-PET ligands, such as ^{18}F-flortaucipir, bind to tau aggregates in the central nervous system (CNS), allowing for the visualization of tau pathology in the living brain (Marquié et al., 2015; Xia et al., 2013). Using tau-PET imaging, recent studies have shown that spatial patterns of tau pathology vary among individuals and may not strictly adhere to the Braak staging (Mohanty et al., 2023; Vogel et al., 2021). Understanding the biological underpinning of the susceptibility of brain regions to tau deposition is critical in AD, as tau-PET-defined subtypes of AD have been associated with different clinical manifestations, structural brain changes, and cognitive prognosis (Mohanty et al., 2023; Vogel et al., 2021).

One of the leading hypotheses concerning the spatial tau progression is the tau propagation hypothesis, postulating that pathological tau spreads trans-neuronally (Liu et al., 2019). Similar to the transmission of prions, it is hypothesized that the misfolded and aggregated state of tau can be transmitted between connected neurons, likely through the release, uptake, and trafficking of tau aggregates (Frost et al., 2009). In vitro and in vivo studies suggest that synaptic contacts between neurons contribute to the transmission, and neuronal activity promotes tau propagation (Calafate et al., 2015; de Calignon et al., 2012). Therefore, the axonal connections between neurons and brain regions may serve as anatomical pathways for the spreading of pathologic tau in the brain (Ahmed et al., 2014). On a cautionary note, it remains to be demonstrated that the transsynaptic transmission of tau aggregates causes the spatial expansion of tau pathology in the brain, and no direct evidence on “prion-like” spreading of tau aggregates has been observed in humans yet. Nevertheless, consistent with the notion of tau spreading between connected brain regions, human neuroimaging studies have indicated that higher functional or structural connectivity between brain regions could facilitate the spreading of tau aggregates in the brain (Franzmeier et al., 2019; Ossenkoppele et al., 2019; Vogel et al., 2020).

Driven by these findings, an approach, known as connectivity-based models, has emerged to predict the spatial tau patterns in AD, as well as other “prion-like” spreading pathologies in the brain (Vogel et al., 2023). In a widely used approach, *tau epicenters* are identified as brain areas with the earliest tau accumulation, and the functional or structural connectivity of tau epicenters is leveraged to predict the regional tau deposition level in each connected region (Franzmeier et al., 2020). Those regions that are strongly connected to tau epicenters are hypothesized to be more susceptible to developing tau pathology in the course of AD. By integrating information about tau epicenters and the strength of epicenter-connectivity, these models consistently demonstrated that higher epicenter-connectivity was predictive of higher tau deposition in the corresponding brain region among individuals exhibiting biomarker evidence of AD (Franzmeier et al., 2020; Vogel et al., 2020). Nevertheless, they still explain limited variance: in one study (Franzmeier et al., 2020), the R^2 values of connectivity-based models ranged from 18% to 49% in predicting 9 independent component analysis-derived AD tau-PET patterns. Yet when predicting some patient-specific tau deposition maps, the model fit dropped even below 10%. Despite exceeding chance and spatial proximity (Franzmeier et al., 2020; Vogel et al., 2020), the limited variance explained by connectivity-based models indicates that, in addition to interregional connectivity, other factors, in particular region-intrinsic properties, may also play a role in the spatial progression of tau deposition in AD.

Factors of local susceptibility to tau in the brain

Amyloid deposition

Extracellular deposition of Aβ peptides as plaques is the other disease-defining pathology of AD. The Aβ peptides are proteolytic products of amyloid precursor protein (APP), with the 42-amino acid form (Aβ42) being the most prone to aggregation

(Jarrett & Lansbury, 1993). In AD, there is an imbalance in APP production and clearing, leading to increased level of Aβ40 and Aβ42 (Haass et al., 2012), which aggregate to form oligomers, protofibrils, and further insoluble Aβ plaques over time (Pfundstein et al., 2022). The presence of Aβ plaques often precedes tau pathology and is thought to promote the spread of tau pathology (Hardy, 2006). Experimental findings suggest that Aβ interacts with p-tau in a variety of ways, promoting the aggregation and propagation of tau pathology (Busche & Hyman, 2020). For example, a recent study using postmortem brain specimens has showed that Aβ can enhance the seeding potential of synaptically released p-tau, which supports a heterotypic seeding of p-tau by Aβ within synaptic terminals (Miyoshi et al., 2021). Furthermore, Aβ aggregates can lead to synaptic dysfunction, which may trigger downstream signaling events impacting tau phosphorylation, aggregation, and spread (Hampel et al., 2021). Other possible mechanisms include Aβ-induced neuroinflammation (Ising et al., 2019), activation of tau phosphatases (Fan et al., 2022), and impaired tau clearance mechanisms (Chesser et al., 2013). In human brains, Aβ plaques accumulate in a diffuse pattern that demonstrates limited overlap with the distribution of tau pathology (Thal et al., 2002). Nevertheless, while medial temporal lobe deposition of PHF-tau frequently occurs as part of aging (Sanchez et al., 2021), the progression of tau pathology to the cortex is greatly facilitated by the presence of cortical amyloid pathology (Therriault et al., 2022), and regions with higher Aβ burden show greater tau deposition than predicted by connectivity patterns (Lee et al., 2022; Vogel et al., 2020). Together, these findings suggest that regional deposition of amyloid enhances the development of tau pathologies in AD.

Gene expression

As mentioned above, the progression of tau pathology in the brain occurs in predilection areas such as the entorhinal cortex, and amyloid deposition may facilitate the

spreading of tau aggregates in these brain areas. Yet the question remains: what factors render a brain region a predilection area for tau pathology?

Regional expression of specific genes may play a crucial role in this differential susceptibility of brain regions. It has been observed that most genes expressed in the brain exhibit region-specific preponderance, possibly reflecting developmental and pathological differences of brain regions (Kang et al., 2011; Seidlitz et al., 2020). One of these genes, microtubule-associated protein tau (*MAPT*), is notably significant. *MAPT* is the gene that encodes tau protein (Goedert et al., 1991), which could serve as a substrate for tau hyperphosphorylation and aggregation. Population genetics have demonstrated associations between the *MAPT* H2 haplotype with both decreased brain *MAPT* expression and reduced AD risk (Allen et al., 2014; Gerrish et al., 2012). Additionally, several other variants in *MAPT* were found to be associated with enhanced *MAPT* expression and increased tau pathology (Kauwe et al., 2008). These findings indicate that genetic mutations in *MAPT* are associated with tau aggregation and play a critical role in tauopathies.

The Allen Human Brain Atlas (AHBA) has made available whole-brain maps of gene expressions based on transcriptomics in six post-mortem healthy adult brains (Shen et al., 2012). Leveraging the brain transcriptomic maps from AHBA, recent studies showed a strong similarity between the expression pattern of *MAPT* and the spatial patterns of tau-PET deposition (Sepulcre et al., 2018) as well as gray matter atrophy (Grothe et al., 2018). Taken together, these findings suggest that the region-specific expression of *MAPT* may contribute to the vulnerability of certain brain regions to tau pathology.

Combining functional connectivity, amyloid deposition, and MAPT expression to explain spatial tau deposition

In the first study (Manuscript I), we sought to improve upon epicenter-connectivity based explanation of the distribution of tau aggregates (Franzmeier et al., 2020) in individuals within AD spectrum (i.e., amyloid-positive). We achieved this by combining interregional connectivity and factors of local susceptibility to tau, including the normative expression pattern of *MAPT* obtained from AHBA and participants' amyloid-PET scans. Our results showed that stronger connectivity to tau epicenters, higher regional *MAPT* expression, and higher regional amyloid-PET deposition were associated with elevated tau-PET deposition in the corresponding region. When explaining group-averaged spatial tau patterns separately derived from three cohorts of amyloid-positive participants, tau epicenter-connectivity alone accounted for 22%-39% of the variance in regional tau-PET values. Upon further addition of *MAPT* expression and amyloid-PET as predictors, the proportion of explained variance substantially increased, eventually reaching 45%-50%. Importantly, this observation was consistent not only at the group level but also at the patient level across our analysis of three independent samples, underscoring a robust benefit of the integrated model compared to single modalities.

Myelin damage in Alzheimer's disease

While tau deposition seems to adhere to pathways guided by connectivity and influenced by local factors in the connected region, damage to axonal pathways may introduce an additional mechanism for the propagation of tau aggregates in AD. In particular, findings from post-mortem studies suggest that myelin alterations may be associated with higher susceptibility to the development of tau pathology. A significant observation is that brain regions maintaining a higher degree of myelination display relatively higher resistance to NFTs in AD, such as the superior temporal gyrus compared to other temporal areas (Braak & Del Tredici, 2015).

Demyelination has been commonly observed in aging and is even greater in AD (Bouhrara et al., 2018; de Faria et al., 2021). During the process, the sheath-like structure of myelin around axons is compromised or lost, which disrupts neuronal communication and has been linked to pathological consequences including axonal degeneration, neuronal degeneration, and cognitive decline in neurodegenerative diseases including AD (Carmeli et al., 2013; Chen et al., 2021; You et al., 2019). Produced by oligodendrocytes in the CNS, myelin is primarily composed of lipids, such as cholesterol and phospholipids, and specific proteins like myelin basic protein (MBP) (Stadelmann et al., 2019). These components collectively support myelin's role in facilitating neuronal communication processes, including transsynaptic transmission (Hughes & Appel, 2016). While connectivity involves the connections and interactions between brain regions, myelin provides structural support and enhances the speed and efficiency of transmission along axonal pathways. Therefore, myelin integrity is crucial to healthy brain functioning and may play a different role in network propagation of tau aggregates compared to connectivity.

Although it remains unclear whether demyelination is a primary event in AD pathogenesis, growing evidence suggests complex interactions between tau pathology and demyelination in AD. Murine studies have demonstrated that myelin damage can occur prior to amyloid and tau pathologies (Desai et al., 2009; Stokin et al., 2005), indicating that myelin abnormalities might contribute to the early stages of the disease. Furthermore, the spatial pattern of myelogenesis shows intriguing associations with the Braak staging scheme, indicating a reverse relationship between myelination development and tau pathology progression (Braak & Braak, 1996). A recent study also suggests that brain regions connected by lower myelinated fiber tracts exhibit greater susceptibility to tau accumulation (Rubinski et al., 2022). Taken together, these findings suggest that the degree of regional (de)myelination may influence the

spread and progression of tau pathology. Further investigation is necessary to uncover the underlying mechanisms and identify potential therapeutic targets associated with demyelination and its impact on tau pathology.

Understanding the relationship between *APOE4*, demyelination, and subsequent tau accumulation

Apolipoprotein E (*APOE*) gene is widely recognized as the strongest genetic risk factor for AD (Saunders et al., 1993; St Clair et al., 1995). The ε4 allele of *APOE* (*APOE4*) is associated with an increased susceptibility to developing AD and has been linked to key pathologies of AD (Benson et al., 2022; Joie et al., 2021; Lumsden et al., 2020).

Role of APOE4 in demyelination

A growing body of literature suggests a potential link between *APOE4* and demyelination with or without the presence of AD pathologies. *APOE4* carriers, compared to individuals with other *APOE* isoforms, have been found to exhibit reduced myelin integrity and density, as well as a decreased number of oligodendrocytes in both aging and AD brains (Bartzokis et al., 2006; Blanchard et al., 2022; Cheng et al., 2022). Recent studies have shed light on the underlying mechanisms, suggesting that *APOE4* is associated with altered cholesterol metabolism and impaired repairing mechanisms in oligodendrocytes, contributing to demyelination (Blanchard et al., 2022; Mok et al., 2023). Furthermore, *APOE4* might also impair myelination via lipid dysregulation in microglia, which are cells responsible for eliminating cellular debris and dysfunctional synapses in the CNS (Wang et al., 2022). These findings collectively support the notion that *APOE4* is associated with impaired lipid metabolism in the brain and thereby could contribute to demyelination processes. However, it is important to note that this is an active area of research and findings can vary. Further

research is needed to confirm the association between *APOE4* and demyelination in different populations.

Role of APOE4 in tau pathology

In addition to its involvement in demyelination, *APOE4* is also implicated in the development and progression of tau pathology. It is well established that *APOE4* promotes the seeding of Aβ (Liu et al., 2017; Namba et al., 1991), which can further induce tau aggregation in AD (Zhao et al., 2018). However, more recent studies have demonstrated that *APOE4* is associated with increased levels of tau pathology in human brains even independent of Aβ (Salvadó et al., 2021; Therriault et al., 2020). Furthermore, *APOE4* has been linked to enhanced neurodegeneration in non-demented older adults, with the strongest associations observed in the hippocampus and entorhinal cortex (Régy et al., 2022), i.e., the same regions where tau first accumulates in AD. A mouse model of tauopathy consistently showed that *APOE4* exacerbates tau-mediated neurodegeneration (Shi et al., 2017). The precise mechanisms underlying the role of *APOE4* in tau pathology are still being investigated, but evidence from experimental studies suggests that *APOE4* may exert its influence on tau through multiple mechanisms, including altered tau phosphorylation (Brecht et al., 2004; Harris et al., 2004), impaired tau clearance (Montagne et al., 2020; Parcon et al., 2018), and enhanced tau cleavage (Kang et al., 2021).

Lower myelination associated with faster tau accumulation in an APOE4-dependent manner

Despite the evidence suggesting, on the one hand, that *APOE4* genotype is associated with higher tau pathology in AD, and on the other hand, that *APOE4* may enhance age-related demyelination, there is a dearth of studies investigating whether the association between *APOE4* and tau pathology can be explained by its effect on myelin in the brain. For this aim, various myelin-sensitive imaging methods can be

employed to quantify the regional myelin content in the brain. One such method is myelin water imaging (MWI), which acquires magnetic resonance imaging (MRI) signals from water compartments confined between myelin lipid bilayers (MacKay et al., 1994; Whittall et al., 1997). MWI and its specific parameter, the myelin water fraction (MWF), have been shown to be highly specific for myelin content (Lee et al., 2021). However, the utilization of WMI and other MRI techniques for myelin imaging has been constrained by the availability of these techniques, as well as the potential interference from iron, inflammation, and other confounding factors (van der Weijden et al., 2023). In contrast, recent investigations have explored the use of the PET radiotracer ^{18}F-florbetapir for measuring myelin (Auvity et al., 2020; Carotenuto et al., 2020; Meng et al., 2022; Moscoso et al., 2021; Zhang et al., 2021). Originally developed for cortical amyloid imaging (European Medicines Agency, 2013), this radiotracer also binds to myelin in the white matter (WM), most likely the β-sheet structure of MBP (Catafau & Bullich, 2015), thereby offering the potential for sensitive and accessible measurements of WM myelin.

In Manuscript II of this thesis, we aimed to investigate the association between *APOE4*, myelin alterations, and tau accumulation within the AD spectrum. We employed ^{18}F-florbetapir PET binding in the WM as a measure of myelin in patients with biomarker evidence of AD. We found that lower myelination in the WM, as assessed by ^{18}F-florbetapir PET, was predictive of faster tau accumulation and associated cognitive decline in participants within the AD spectrum. Notably, individuals with the *APOE4* genotype exhibited lower ^{18}F-florbetapir uptake in the WM, and a higher rate of tau-PET accumulation. A mediation analysis indicated that the effect of *APOE4* on the rate of tau accumulation in cortical limbic areas (Braak stages III-IV) is partially mediated by global ^{18}F-florbetapir uptake in WM. Additionally, *APOE4* carriers showed stronger association between global ^{18}F-florbetapir uptake in the WM and tau-PET accumulation in Braak III-IV regions. These findings suggest that myelin

alterations are associated with faster tau progression, particularly in an *APOE4*-dependent manner.

Conclusions and summary

The major findings of the current thesis were 1) the integration of region-specific factors, such as *MAPT* expression and amyloid deposition, into connectivity-based models enhanced the explanation of spatial tau deposition within the AD spectrum, and 2) lower myelination was associated with faster tau accumulation in AD spectrum individuals in an *APOE4*-dependent manner.

In our first study, we expanded on a previously developed connectivity-based model of spatial tau deposition (Franzmeier et al., 2020) by incorporating two region-specific factors. Specifically, we showed that higher regional levels of amyloid-PET deposition and *MAPT* expression were associated with higher regional tau-PET deposition, and the integration of both factors enhanced the explanatory power of the model. While brain connectivity has been speculated to facilitate tau propagation (Lamontagne-Kam et al., 2023), our findings, supported by other studies (Lee et al., 2022; Vogel et al., 2020), suggest that connectivity-based models are not exhaustive in explaining spatial tau deposition. *MAPT* expression and amyloid deposition, on the other hand, may additionally contribute to regional susceptibility to tau pathology. Therefore, our first study highlights the value of considering both epicenter-connectivity and local factors in the connected region, when explaining spatial tau deposition in AD.

In addition to connectivity and region-specific factors, our second study shed light on another potential mechanism influencing tau pathology in AD: damage to the myelin sheath surrounding axons. This study provides in vivo neuroimaging evidence supporting an association between lower WM myelination and subsequent faster tau

accumulation. Consistent with previous post-mortem studies (Braak & Del Tredici, 2019), our findings suggest that the propagation of tau aggregates may be facilitated by demyelination. Furthermore, the study highlights an *APOE4*-dependent mechanism underlying this association, including an indirect effect of *APOE4* on tau accumulation through its association with demyelination, and a synergistic effect between *APOE4* and demyelination in promoting tau pathology in AD. Given that *APOE4* has also been found to associate with lower MWF in infants in another study (Mc Donald & Krainc, 2014), these effects of *APOE4* might be prenatal and persisting. It remains to be investigated whether remyelination-promoting drugs (Caprariello & Adams, 2022) could mitigate disease progression and cognitive decline in AD, with or without *APOE4*.

Collectively, the two studies expand our understanding of pathological tau accumulation in AD, considering not only activity-dependent spreading proposed by the tau propagation hypothesis, but also the intricate interplay of connectivity, myelin integrity, and local factors. While brain connectomes may reflect neuronal activity at the system level and shape spatial tau patterns, local factors in the connected region may influence the local vulnerability to tau pathology. Furthermore, in contrast to the role of neuronal connectivity, myelin sheath around the axonal pathways appears to be a protective factor against tau accumulation, influenced by genetic factors such as *APOE4*. Thus, the integration of diverse imaging modalities and genetic information provides a more comprehensive perspective. Further investigation employing additional modalities and advanced myelin imaging is warranted to explore the interrelationships, with the potential to contribute to improved diagnostics, monitoring, and targeted interventions for individuals affected by AD.

References

Ahmed, Z., Cooper, J., Murray, T. K., Garn, K., McNaughton, E., Clarke, H., Parhizkar, S., Ward, M. A., Cavallini, A., Jackson, S., Bose, S., Clavaguera, F., Tolnay, M., Lavenir, I., Goedert, M., Hutton, M. L., & O'Neill, M. J. (2014). A novel in vivo model of tau propagation with rapid and progressive neurofibrillary tangle pathology: the pattern of spread is determined by connectivity, not proximity. *Acta Neuropathologica*, *127*(5), 667-683. https://doi.org/10.1007/s00401-014-1254-6

Allen, M., Kachadoorian, M., Quicksall, Z., Zou, F., Chai, H. S., Younkin, C., Crook, J. E., Pankratz, V. S., Carrasquillo, M. M., Krishnan, S., Nguyen, T., Ma, L., Malphrus, K., Lincoln, S., Bisceglio, G., Kolbert, C. P., Jen, J., Mukherjee, S., Kauwe, J. K., . . . Alzheimer's Disease Genetics Consortium. (2014). Association of MAPT haplotypes with Alzheimer's disease risk and MAPT brain gene expression levels. *Alzheimer's Research & Therapy*, *6*(4), 39. https://doi.org/10.1186/alzrt268

Alonso, A. D., Cohen, L. S., Corbo, C., Morozova, V., ElIdrissi, A., Phillips, G., & Kleiman, F. E. (2018). Hyperphosphorylation of Tau Associates With Changes in Its Function Beyond Microtubule Stability. *Front Cell Neurosci*, *12*, 338. https://doi.org/10.3389/fncel.2018.00338

Alzheimer's Association. (2024). 2024 Alzheimer's disease facts and figures. *Alzheimer's & Dementia*, *20*(5), 3708-3821. https://doi.org/10.1002/alz.13809

Auvity, S., Tonietto, M., Caillé, F., Bodini, B., Bottlaender, M., Tournier, N., Kuhnast, B., & Stankoff, B. (2020). Repurposing radiotracers for myelin imaging: a study comparing 18F-florbetaben, 18F-florbetapir, 18F-flutemetamol, 11C-MeDAS, and 11C-PiB. *European journal of nuclear medicine and molecular imaging*, *47*, 490–501.

Barthelemy, N. R., Li, Y., Joseph-Mathurin, N., Gordon, B. A., Hassenstab, J., Benzinger, T. L. S., Buckles, V., Fagan, A. M., Perrin, R. J., Goate, A. M., Morris, J. C., Karch, C. M., Xiong, C., Allegri, R., Mendez, P. C., Berman, S. B., Ikeuchi, T., Mori, H., Shimada, H., . . . Dominantly Inherited Alzheimer Network. (2020). A soluble phosphorylated tau signature links tau, amyloid and the evolution of stages of dominantly inherited Alzheimer's disease. *Nature Medicine*, *26*(3), 398-407. https://doi.org/10.1038/s41591-020-0781-z

Bartzokis, G., Lu, P. H., Geschwind, D. H., Edwards, N., Mintz, J., & Cummings, J. L. (2006). Apolipoprotein E Genotype and Age-Related Myelin Breakdown in Healthy Individuals: Implications for Cognitive Decline and Dementia. *Archives of General Psychiatry*, *63*(1), 63-72. https://doi.org/10.1001/archpsyc.63.1.63

Benson, G. S., Bauer, C., Hausner, L., Couturier, S., Lewczuk, P., Peters, O., Hüll, M., Jahn, H., Jessen, F., Pantel, J., Teipel, S. J., Wagner, M., Schuchhardt, J., Wiltfang, J., Kornhuber, J., & Frölich, L. (2022). Don't forget about tau: the effects of ApoE4 genotype on Alzheimer's disease cerebrospinal fluid biomarkers in subjects with mild cognitive impairment—data from the Dementia Competence Network. *Journal of Neural Transmission*, *129*(5), 477-486. https://doi.org/10.1007/s00702-022-02461-0

Birdsill, A. C., Koscik, R. L., Cody, K. A., Jonaitis, E. M., Cadman, R. V., Erickson, C. M., Chin, N. A., Przybelski, R. J., Carlsson, C. M., Asthana, S., Christian, B. T., Eisenmenger, L. B., Betthauser, T. J., & Johnson, S. C. (2022). Trajectory of clinical symptoms in relation to amyloid chronicity. *Alzheimer's & Dementia: Diagnosis, Assessment & Disease Monitoring*, *14*(1), e12360. https://doi.org/10.1002/dad2.12360

Blanchard, J. W., Akay, L. A., Davila-Velderrain, J., von Maydell, D., Mathys, H., Davidson, S. M., Effenberger, A., Chen, C.-Y., Maner-Smith, K., Hajjar, I., Ortlund, E. A., Bula, M., Agbas, E., Ng, A., Jiang, X., Kahn, M., Blanco-Duque, C., Lavoie, N., Liu, L., . . . Tsai, L.-H. (2022). APOE4 impairs myelination via cholesterol dysregulation in oligodendrocytes. *Nature*, *611*(7937), 769-779. https://doi.org/10.1038/s41586-022-05439-w

Bouhrara, M., Reiter, D. A., Bergeron, C. M., Zukley, L. M., Ferrucci, L., Resnick, S. M., & Spencer, R. G. (2018). Evidence of demyelination in mild cognitive impairment and dementia using a direct and specific magnetic resonance imaging measure of myelin

content. *Alzheimer's & Dementia*, *14*(8), 998-1004. https://doi.org/10.1016/j.jalz.2018.03.007

Braak, H., & Braak, E. (1991). Neuropathological stageing of Alzheimer-related changes. *Acta Neuropathologica*, *82*(4), 239-259. https://doi.org/10.1007/BF00308809

Braak, H., & Braak, E. (1996). Development of Alzheimer-related neurofibrillary changes in the neocortex inversely recapitulates cortical myelogenesis. *Acta Neuropathologica*, *92*(2), 197-201. https://doi.org/10.1007/s004010050508

Braak, H., & Del Tredici, K. (2015). Neuroanatomy and pathology of sporadic Alzheimer's disease. *Adv Anat Embryol Cell Biol*, *215*, 1-162. https://www.ncbi.nlm.nih.gov/pubmed/25920101

Braak, H., & Del Tredici, K. (2019). Top-Down Projections Direct the Gradual Progression of Alzheimer-Related Tau Pathology Throughout the Neocortex. *Adv Exp Med Biol*, *1184*, 291-303. https://doi.org/10.1007/978-981-32-9358-8_22

Brecht, W. J., Harris, F. M., Chang, S., Tesseur, I., Yu, G.-Q., Xu, Q., Dee Fish, J., Wyss-Coray, T., Buttini, M., Mucke, L., Mahley, R. W., & Huang, Y. (2004). Neuron-specific apolipoprotein e4 proteolysis is associated with increased tau phosphorylation in brains of transgenic mice. *The Journal of Neuroscience*, *24*(10), 2527-2534. https://doi.org/10.1523/JNEUROSCI.4315-03.2004

Bucci, M., Chiotis, K., & Nordberg, A. (2021). Alzheimer's disease profiled by fluid and imaging markers: tau PET best predicts cognitive decline. *Molecular Psychiatry*, *26*(10), 5888-5898. https://doi.org/10.1038/s41380-021-01263-2

Busche, M. A., & Hyman, B. T. (2020). Synergy between amyloid-β and tau in Alzheimer's disease. *Nature Neuroscience*, *23*(10), 1183-1193. https://doi.org/10.1038/s41593-020-0687-6

Calafate, S., Buist, A., Miskiewicz, K., Vijayan, V., Daneels, G., De Strooper, B., de Wit, J., Verstreken, P., & Moechars, D. (2015). Synaptic contacts enhance cell-to-cell tau pathology propagation. *Cell Reports*, *11*(8), 1176-1183. https://doi.org/10.1016/j.celrep.2015.04.043

Caprariello, A. V., & Adams, D. J. (2022). The Landscape of Targets and Lead Molecules for Remyelination. *Nature chemical biology*, *18*(9), 925-933. https://doi.org/10.1038/s41589-022-01115-2

Carmeli, C., Donati, A., Antille, V., Viceic, D., Ghika, J., von Gunten, A., Clarke, S., Meuli, R., Frackowiak, R. S., & Knyazeva, M. G. (2013). Demyelination in mild cognitive impairment suggests progression path to Alzheimer's disease. *PLoS One*, *8*(8), e72759. https://doi.org/10.1371/journal.pone.0072759

Carotenuto, A., Giordano, B., Dervenoulas, G., Wilson, H., Veronese, M., Chappell, Z., Polychronis, S., Pagano, G., Mackewn, J., & Turkheimer, F. E. (2020). [18 F] Florbetapir PET/MR imaging to assess demyelination in multiple sclerosis. *European journal of nuclear medicine and molecular imaging*, *47*, 366–378. https://doi.org/10.1007/s00259-019-04533-y

Catafau, A. M., & Bullich, S. (2015). Amyloid PET imaging: applications beyond Alzheimer's disease. *Clin Transl Imaging*, *3*(1), 39-55. https://doi.org/10.1007/s40336-014-0098-3

Chen, J.-F., Liu, K., Hu, B., Li, R.-R., Xin, W., Chen, H., Wang, F., Chen, L., Li, R.-X., Ren, S.-Y., Xiao, L., Chan, J. R., & Mei, F. (2021). Enhancing myelin renewal reverses cognitive dysfunction in a murine model of Alzheimer's disease. *Neuron*, *109*(14), 2292-2307.e2295. https://doi.org/10.1016/j.neuron.2021.05.012

Cheng, G. W.-Y., Mok, K. K.-S., Yeung, S. H.-S., Kofler, J., Herrup, K., & Tse, K.-H. (2022). Apolipoprotein E ε4 Mediates Myelin Breakdown by Targeting Oligodendrocytes in Sporadic Alzheimer Disease. *Journal of Neuropathology & Experimental Neurology*, *81*(9), 717-730. https://doi.org/10.1093/jnen/nlac054

Chesser, A. S., Pritchard, S. M., & Johnson, G. V. W. (2013). Tau Clearance Mechanisms and Their Possible Role in the Pathogenesis of Alzheimer Disease. *Frontiers in Neurology*, *4*, 122. https://doi.org/10.3389/fneur.2013.00122

Cummings, J. L., & Benson, D. F. (1992). *Dementia: A clinical approach*.

de Calignon, A., Polydoro, M., Suárez-Calvet, M., William, C., Adamowicz, D. H., Kopeikina, K. J., Pitstick, R., Sahara, N., Ashe, K. H., Carlson, G. A., Spires-Jones, T. L., & Hyman, B. T. (2012). Propagation of Tau Pathology in a Model of Early Alzheimer's Disease. *Neuron*, *73*(4), 685-697. https://doi.org/10.1016/j.neuron.2011.11.033

de Faria, O., Pivonkova, H., Varga, B., Timmler, S., Evans, K. A., & Káradóttir, R. T. (2021). Periods of synchronized myelin changes shape brain function and plasticity. *Nature Neuroscience*, *24*(11), 1508-1521. https://doi.org/10.1038/s41593-021-00917-2

Desai, M. K., Sudol, K. L., Janelsins, M. C., Mastrangelo, M. A., Frazer, M. E., & Bowers, W. J. (2009). Triple-transgenic Alzheimer's disease mice exhibit region-specific abnormalities in brain myelination patterns prior to appearance of amyloid and tau pathology. *Glia*, *57*(1), 54-65. https://doi.org/10.1002/glia.20734

Drubin, D. G., & Kirschner, M. W. (1986). Tau protein function in living cells. *J Cell Biol*, *103*(6 Pt 2), 2739-2746. https://doi.org/10.1083/jcb.103.6.2739

European Medicines Agency. (2013). *Amyvid: EPAR-Product Information*. https://ec.europa.eu/health/documents/community-register/2013/20130114124958/anx_124958_en.pdf

Fan, X., Xia, L., Zhou, Z., Qiu, Y., Zhao, C., Yin, X., & Qian, W. (2022). Tau Acts in Concert With Kinase/Phosphatase Underlying Synaptic Dysfunction. *Frontiers in Aging Neuroscience*, *14*. https://www.frontiersin.org/articles/10.3389/fnagi.2022.908881

Franzmeier, N., Dewenter, A., Frontzkowski, L., Dichgans, M., Rubinski, A., Neitzel, J., Smith, R., Strandberg, O., Ossenkoppele, R., Buerger, K., Duering, M., Hansson, O., & Ewers, M. (2020). Patient-centered connectivity-based prediction of tau pathology spread in Alzheimer's disease. *Science Advances*, *6*(48), eabd1327. https://doi.org/10.1126/sciadv.abd1327

Franzmeier, N., Rubinski, A., Neitzel, J., Kim, Y., Damm, A., Na, D. L., Kim, H. J., Lyoo, C. H., Cho, H., Finsterwalder, S., Duering, M., Seo, S. W., Ewers, M., & Alzheimer's Disease Neuroimaging Initiative. (2019). Functional connectivity associated with tau levels in ageing, Alzheimer's, and small vessel disease. *Brain*, *142*(4), 1093-1107. https://doi.org/10.1093/brain/awz026

Frost, B., Jacks, R. L., & Diamond, M. I. (2009). Propagation of Tau Misfolding from the Outside to the Inside of a Cell *. *Journal of Biological Chemistry*, *284*(19), 12845-12852. https://doi.org/10.1074/jbc.M808759200

Gerrish, A., Russo, G., Richards, A., Moskvina, V., Ivanov, D., Harold, D., Sims, R., Abraham, R., Hollingworth, P., Chapman, J., Hamshere, M., Pahwa, J. S., Dowzell, K., Williams, A., Jones, N., Thomas, C., Stretton, A., Morgan, A. R., Lovestone, S., . . . Williams, J. (2012). The role of variation at AβPP, PSEN1, PSEN2, and MAPT in late onset Alzheimer's disease. *Journal of Alzheimer's disease: JAD*, *28*(2), 377-387. https://doi.org/10.3233/JAD-2011-110824

Goedert, M., Crowther, R. A., & Garner, C. C. (1991). Molecular characterization of microtubule-associated proteins tau and MAP2. *Trends in Neurosciences*, *14*(5), 193-199. https://doi.org/10.1016/0166-2236(91)90105-4

Golde, T. E. (2022). Disease-Modifying Therapies for Alzheimer's Disease: More Questions than Answers. *Neurotherapeutics*, *19*(1), 209-227. https://doi.org/10.1007/s13311-022-01201-2

Grothe, M. J., Sepulcre, J., Gonzalez-Escamilla, G., Jelistratova, I., Schöll, M., Hansson, O., Teipel, S. J., & Alzheimer's Disease Neuroimaging Initiative. (2018). Molecular properties underlying regional vulnerability to Alzheimer's disease pathology. *Brain*, *141*(9), 2755-2771. https://doi.org/10.1093/brain/awy189

Grundke-Iqbal, I., Iqbal, K., Tung, Y. C., Quinlan, M., Wisniewski, H. M., & Binder, L. I. (1986). Abnormal phosphorylation of the microtubule-associated protein tau (tau) in Alzheimer cytoskeletal pathology. *Proceedings of the National Academy of Sciences of the United States of America*, *83*(13), 4913-4917. https://doi.org/10.1073/pnas.83.13.4913

Guo, Y., Li, S., Zeng, L.-H., & Tan, J. (2022). Tau-targeting therapy in Alzheimer's disease: critical advances and future opportunities. *Ageing and Neurodegenerative Diseases*, *2*(3), 11. https://doi.org/10.20517/and.2022.16

Haass, C., Kaether, C., Thinakaran, G., & Sisodia, S. (2012). Trafficking and proteolytic processing of APP. *Cold Spring Harb Perspect Med*, *2*(5), a006270. https://doi.org/10.1101/cshperspect.a006270

Hampel, H., Hardy, J., Blennow, K., Chen, C., Perry, G., Kim, S. H., Villemagne, V. L., Aisen, P., Vendruscolo, M., Iwatsubo, T., Masters, C. L., Cho, M., Lannfelt, L., Cummings, J. L., & Vergallo, A. (2021). The Amyloid-β Pathway in Alzheimer's Disease. *Molecular Psychiatry*, *26*(10), 5481-5503. https://doi.org/10.1038/s41380-021-01249-0

Hanseeuw, B. J., Betensky, R. A., Jacobs, H. I. L., Schultz, A. P., Sepulcre, J., Becker, J. A., Cosio, D. M. O., Farrell, M., Quiroz, Y. T., Mormino, E. C., Buckley, R. F., Papp, K. V., Amariglio, R. A., Dewachter, I., Ivanoiu, A., Huijbers, W., Hedden, T., Marshall, G. A., Chhatwal, J. P., . . . Johnson, K. (2019). Association of Amyloid and Tau With Cognition in Preclinical Alzheimer Disease: A Longitudinal Study. *JAMA Neurology*, *76*(8), 915-924. https://doi.org/10.1001/jamaneurol.2019.1424

Hardy, J. (2006). Alzheimer's disease: the amyloid cascade hypothesis: an update and reappraisal. *J Alzheimers Dis*, *9*(3 Suppl), 151-153. https://doi.org/10.3233/jad-2006-9s317

Harris, F. M., Brecht, W. J., Xu, Q., Mahley, R. W., & Huang, Y. (2004). Increased tau Phosphorylation in Apolipoprotein E4 Transgenic Mice Is Associated with Activation of Extracellular Signal-regulated Kinase: MODULATION BY ZINC *. *Journal of Biological Chemistry*, *279*(43), 44795-44801. https://doi.org/10.1074/jbc.M408127200

Hughes, E. G., & Appel, B. (2016). The cell biology of CNS myelination. *Curr Opin Neurobiol*, *39*, 93-100. https://doi.org/10.1016/j.conb.2016.04.013

Ising, C., Venegas, C., Zhang, S., Scheiblich, H., Schmidt, S. V., Vieira-Saecker, A., Schwartz, S., Albasset, S., McManus, R. M., Tejera, D., Griep, A., Santarelli, F., Brosseron, F., Opitz, S., Stunden, J., Merten, M., Kayed, R., Golenbock, D. T., Blum, D., . . . Heneka, M. T. (2019). NLRP3 inflammasome activation drives tau pathology. *Nature*, *575*(7784), 669-673. https://doi.org/10.1038/s41586-019-1769-z

Janelidze, S., Mattsson, N., Palmqvist, S., Smith, R., Beach, T. G., Serrano, G. E., Chai, X., Proctor, N. K., Eichenlaub, U., Zetterberg, H., Blennow, K., Reiman, E. M., Stomrud, E., Dage, J. L., & Hansson, O. (2020). Plasma P-tau181 in Alzheimer's disease: relationship to other biomarkers, differential diagnosis, neuropathology and longitudinal progression to Alzheimer's dementia. *Nature Medicine*, *26*(3), 379-386. https://doi.org/10.1038/s41591-020-0755-1

Jarrett, J. T., & Lansbury, P. T., Jr. (1993). Seeding "one-dimensional crystallization" of amyloid: a pathogenic mechanism in Alzheimer's disease and scrapie? *Cell*, *73*(6), 1055-1058. https://doi.org/10.1016/0092-8674(93)90635-4

Joie, R. L., Visani, A. V., Lesman-Segev, O. H., Baker, S. L., Edwards, L., Iaccarino, L., Soleimani-Meigooni, D. N., Mellinger, T., Janabi, M., Miller, Z. A., Perry, D. C., Pham, J., Strom, A., Gorno-Tempini, M. L., Rosen, H. J., Miller, B. L., Jagust, W. J., & Rabinovici, G. D. (2021). Association of APOE4 and Clinical Variability in Alzheimer Disease With the Pattern of Tau- and Amyloid-PET. *Neurology*, *96*(5), e650-e661. https://doi.org/10.1212/WNL.0000000000011270

Kang, H. J., Kawasawa, Y. I., Cheng, F., Zhu, Y., Xu, X., Li, M., Sousa, A. M. M., Pletikos, M., Meyer, K. A., Sedmak, G., Guennel, T., Shin, Y., Johnson, M. B., Krsnik, Ž., Mayer, S., Fertuzinhos, S., Umlauf, S., Lisgo, S. N., Vortmeyer, A., . . . Šestan, N. (2011). Spatio-temporal transcriptome of the human brain. *Nature*, *478*(7370), 483-489. https://doi.org/10.1038/nature10523

Kang, S. S., Ahn, E. H., Liu, X., Bryson, M., Miller, G. W., Weinshenker, D., & Ye, K. (2021). ApoE4 inhibition of VMAT2 in the locus coeruleus exacerbates Tau pathology in Alzheimer's disease. *Acta Neuropathologica*, *142*(1), 139-158. https://doi.org/10.1007/s00401-021-02315-1

Kauwe, J. S. K., Cruchaga, C., Mayo, K., Fenoglio, C., Bertelsen, S., Nowotny, P., Galimberti, D., Scarpini, E., Morris, J. C., Fagan, A. M., Holtzman, D. M., & Goate, A. M. (2008). Variation in MAPT is associated with cerebrospinal fluid tau levels in the presence of amyloid-beta deposition. *Proceedings of the National Academy of Sciences of the United States of America*, *105*(23), 8050-8054. https://doi.org/10.1073/pnas.0801227105

Kidd, M. (1963). Paired helical filaments in electron microscopy of Alzheimer's disease. *Nature*, *197*, 192-193. https://doi.org/10.1038/197192b0

Lamontagne-Kam, D., Ulfat, A. K., Herve, V., Vu, T. M., & Brouillette, J. (2023). Implication of tau propagation on neurodegeneration in Alzheimer's disease. *Frontiers in Neuroscience*, *17*, 1219299. https://doi.org/10.3389/fnins.2023.1219299

Lee, J., Hyun, J. W., Lee, J., Choi, E. J., Shin, H. G., Min, K., Nam, Y., Kim, H. J., & Oh, S. H. (2021). So You Want to Image Myelin Using MRI: An Overview and Practical Guide for Myelin Water Imaging. *J Magn Reson Imaging*, *53*(2), 360-373. https://doi.org/10.1002/jmri.27059

Lee, V. M., Balin, B. J., Otvos, L., Jr., & Trojanowski, J. Q. (1991). A68: a major subunit of paired helical filaments and derivatized forms of normal Tau. *Science*, *251*(4994), 675-678. https://doi.org/10.1126/science.1899488

Lee, W. J., Brown, J. A., Kim, H. R., La Joie, R., Cho, H., Lyoo, C. H., Rabinovici, G. D., Seong, J.-K., Seeley, W. W., & Alzheimer's Disease Neuroimaging Initiative. (2022). Regional Aβ-tau interactions promote onset and acceleration of Alzheimer's disease tau spreading. *Neuron*, *110*(12), 1932-1943.e1935. https://doi.org/10.1016/j.neuron.2022.03.034

Leuzy, A., Smith, R., Ossenkoppele, R., Santillo, A., Borroni, E., Klein, G., Ohlsson, T., Jogi, J., Palmqvist, S., Mattsson-Carlgren, N., Strandberg, O., Stomrud, E., & Hansson, O. (2020). Diagnostic Performance of RO948 F 18 Tau Positron Emission Tomography in the Differentiation of Alzheimer Disease From Other Neurodegenerative Disorders. *JAMA Neurology*, *77*(8), 955-965. https://doi.org/10.1001/jamaneurol.2020.0989

Liu, C. C., Zhao, N., Fu, Y., Wang, N., Linares, C., Tsai, C. W., & Bu, G. (2017). ApoE4 Accelerates Early Seeding of Amyloid Pathology. *Neuron*, *96*(5), 1024-1032 e1023. https://doi.org/10.1016/j.neuron.2017.11.013

Liu, P.-P., Xie, Y., Meng, X.-Y., & Kang, J.-S. (2019). History and progress of hypotheses and clinical trials for Alzheimer's disease. *Signal Transduction and Targeted Therapy*, *4*(1), 1-22. https://doi.org/10.1038/s41392-019-0063-8

Lumsden, A. L., Mulugeta, A., Zhou, A., & Hyppönen, E. (2020). Apolipoprotein E (APOE) genotype-associated disease risks: a phenome-wide, registry-based, case-control study utilising the UK Biobank. *eBioMedicine*, *59*. https://doi.org/10.1016/j.ebiom.2020.102954

MacKay, A., Whittall, K., Adler, J., Li, D., Paty, D., & Graeb, D. (1994). In vivo visualization of myelin water in brain by magnetic resonance. *Magn Reson Med*, *31*(6), 673-677. https://doi.org/10.1002/mrm.1910310614

Mandelkow, E., von Bergen, M., Biernat, J., & Mandelkow, E. M. (2007). Structural principles of tau and the paired helical filaments of Alzheimer's disease. *Brain Pathol*, *17*(1), 83-90. https://doi.org/10.1111/j.1750-3639.2007.00053.x

Marquié, M., Normandin, M. D., Vanderburg, C. R., Costantino, I. M., Bien, E. A., Rycyna, L. G., Klunk, W. E., Mathis, C. A., Ikonomovic, M. D., Debnath, M. L., Vasdev, N., Dickerson, B. C., Gomperts, S. N., Growdon, J. H., Johnson, K. A., Frosch, M. P., Hyman, B. T., & Gómez-Isla, T. (2015). Validating novel tau positron emission tomography tracer [F-18]-AV-1451 (T807) on postmortem brain tissue. *Annals of Neurology*, *78*(5), 787-800. https://doi.org/10.1002/ana.24517

Mc Donald, J., & Krainc, D. (2014). Alzheimer gene APOE epsilon4 linked to brain development in infants. *JAMA*, *311*(3), 298-299. https://doi.org/10.1001/jama.2013.285400

Mena, R., Wischik, C. M., Novak, M., Milstein, C., & Cuello, A. C. (1991). A progressive deposition of paired helical filaments (PHF) in the brain characterizes the evolution of dementia in Alzheimer's disease. An immunocytochemical study with a monoclonal antibody against the PHF core. *J Neuropathol Exp Neurol*, *50*(4), 474-490. https://doi.org/10.1097/00005072-199107000-00008

Meng, H., Zheng, S., Yuan, S., Zhou, Q., Gao, Y., Ni, Y., He, L., Yin, D., Zhang, M., & Chen, S. (2022). Hybrid 18F-florbetapir PET/MRI for assessing myelin recovery in GFAP-A patients. *Translational Neuroscience*, *13*(1), 120–124.

Miyoshi, E., Bilousova, T., Melnik, M., Fakhrutdinov, D., Poon, W. W., Vinters, H. V., Miller, C. A., Corrada, M., Kawas, C., Bohannan, R., Caraway, C., Elias, C., Maina, K. N., Campagna, J. J., John, V., & Gylys, K. H. (2021). Exosomal tau with seeding activity is released from Alzheimer's disease synapses, and seeding potential is associated with amyloid beta. *Laboratory Investigation*, *101*(12), 1605-1617. https://doi.org/10.1038/s41374-021-00644-z

Mohanty, R., Ferreira, D., Nordberg, A., Westman, E., & Alzheimer's Disease Neuroimaging Initiative. (2023). Associations between different tau-PET patterns and longitudinal atrophy in the Alzheimer's disease continuum: biological and methodological perspectives from disease heterogeneity. *Alzheimer's Research & Therapy*, *15*(1), 37. https://doi.org/10.1186/s13195-023-01173-1

Mok, K. K.-S., Yeung, S. H.-S., Cheng, G. W.-Y., Ma, I. W.-T., Lee, R. H.-S., Herrup, K., & Tse, K.-H. (2023). Apolipoprotein E ε4 disrupts oligodendrocyte differentiation by interfering with astrocyte-derived lipid transport. *Journal of Neurochemistry*, *165*(1), 55-75. https://doi.org/10.1111/jnc.15748

Montagne, A., Nation, D. A., Sagare, A. P., Barisano, G., Sweeney, M. D., Chakhoyan, A., Pachicano, M., Joe, E., Nelson, A. R., D'Orazio, L. M., Buennagel, D. P., Harrington, M. G., Benzinger, T. L. S., Fagan, A. M., Ringman, J. M., Schneider, L. S., Morris, J. C., Reiman, E. M., Caselli, R. J., . . . Zlokovic, B. V. (2020). APOE4 leads to blood–brain barrier dysfunction predicting cognitive decline. *Nature*, *581*(7806), 71-76. https://doi.org/10.1038/s41586-020-2247-3

Moscoso, A., Silva-Rodríguez, J., Aldrey, J. M., Cortés, J., Pías-Peleteiro, J. M., Ruibal, A., Aguiar, P., & Alzheimer's Disease Neuroimaging Initiative. (2021). 18 F-florbetapir PET as a marker of myelin integrity across the Alzheimer's disease spectrum. *European journal of nuclear medicine and molecular imaging*, 1–12. https://doi.org/10.1007/s00259-021-05493-y

Murray, M. E., Graff-Radford, N. R., Ross, O. A., Petersen, R. C., Duara, R., & Dickson, D. W. (2011). Neuropathologically defined subtypes of Alzheimer's disease with distinct clinical characteristics: a retrospective study. *The Lancet Neurology*, *10*(9), 785-796. https://doi.org/10.1016/S1474-4422(11)70156-9

Namba, Y., Tomonaga, M., Kawasaki, H., Otomo, E., & Ikeda, K. (1991). Apolipoprotein E immunoreactivity in cerebral amyloid deposits and neurofibrillary tangles in Alzheimer's disease and kuru plaque amyloid in Creutzfeldt-Jakob disease. *Brain Res*, *541*(1), 163-166. https://doi.org/10.1016/0006-8993(91)91092-f

Noble, W., Hanger, D. P., Miller, C. C., & Lovestone, S. (2013). The importance of tau phosphorylation for neurodegenerative diseases. *Frontiers in Neurology*, *4*, 83. https://doi.org/10.3389/fneur.2013.00083

Ossenkoppele, R., Iaccarino, L., Schonhaut, D. R., Brown, J. A., La Joie, R., O'Neil, J. P., Janabi, M., Baker, S. L., Kramer, J. H., Gorno-Tempini, M.-L., Miller, B. L., Rosen, H. J., Seeley, W. W., Jagust, W. J., & Rabinovici, G. D. (2019). Tau covariance patterns in Alzheimer's disease patients match intrinsic connectivity networks in the healthy brain. *NeuroImage. Clinical*, *23*, 101848. https://doi.org/10.1016/j.nicl.2019.101848

Ossenkoppele, R., Rabinovici, G. D., Smith, R., Cho, H., Scholl, M., Strandberg, O., Palmqvist, S., Mattsson, N., Janelidze, S., Santillo, A., Ohlsson, T., Jogi, J., Tsai, R., La Joie, R., Kramer, J., Boxer, A. L., Gorno-Tempini, M. L., Miller, B. L., Choi, J. Y., . . . Hansson, O. (2018). Discriminative Accuracy of [18F]flortaucipir Positron Emission Tomography for Alzheimer Disease vs Other Neurodegenerative Disorders. *JAMA*, *320*(11), 1151-1162. https://doi.org/10.1001/jama.2018.12917

Ossenkoppele, R., van der Kant, R., & Hansson, O. (2022). Tau biomarkers in Alzheimer's disease: towards implementation in clinical practice and trials. *The Lancet Neurology*, *21*(8), 726-734. https://doi.org/10.1016/S1474-4422(22)00168-5

Palmqvist, S., Janelidze, S., Quiroz, Y. T., Zetterberg, H., Lopera, F., Stomrud, E., Su, Y., Chen, Y., Serrano, G. E., Leuzy, A., Mattsson-Carlgren, N., Strandberg, O., Smith, R., Villegas, A., Sepulveda-Falla, D., Chai, X., Proctor, N. K., Beach, T. G., Blennow, K., . . . Hansson, O. (2020). Discriminative Accuracy of Plasma Phospho-tau217 for Alzheimer Disease vs Other Neurodegenerative Disorders. *JAMA*, *324*(8), 772-781. https://doi.org/10.1001/jama.2020.12134

Parcon, P. A., Balasubramaniam, M., Ayyadevara, S., Jones, R. A., Liu, L., Shmookler Reis, R. J., Barger, S. W., Mrak, R. E., & Griffin, W. S. T. (2018). Apolipoprotein E4 inhibits autophagy gene products through direct, specific binding to CLEAR motifs. *Alzheimer's & Dementia*, *14*(2), 230-242. https://doi.org/10.1016/j.jalz.2017.07.754

Pfundstein, G., Nikonenko, A. G., & Sytnyk, V. (2022). Amyloid precursor protein (APP) and amyloid beta (Abeta) interact with cell adhesion molecules: Implications in Alzheimer's disease and normal physiology. *Front Cell Dev Biol*, *10*, 969547. https://doi.org/10.3389/fcell.2022.969547

Régy, M., Dugravot, A., Sabia, S., Fayosse, A., Mangin, J.-F., Chupin, M., Fischer, C., Bouteloup, V., Dufouil, C., Chêne, G., Paquet, C., Hanseeuw, B., Singh-Manoux, A., & Dumurgier, J. (2022). Association of APOE ε4 with cerebral gray matter volumes in non-demented older adults: The MEMENTO cohort study. *NeuroImage*, *250*, 118966. https://doi.org/10.1016/j.neuroimage.2022.118966

Rubinski, A., Franzmeier, N., Dewenter, A., Luan, Y., Smith, R., Strandberg, O., Ossenkoppele, R., Dichgans, M., Hansson, O., Ewers, M., & Alzheimer's Disease Neuroimaging Initiative. (2022). Higher levels of myelin are associated with higher resistance against tau pathology in Alzheimer's disease. *Alzheimer's Research & Therapy*, *14*(1), 139. https://doi.org/10.1186/s13195-022-01074-9

Salvadó, G., Grothe, M. J., Groot, C., Moscoso, A., Schöll, M., Gispert, J. D., Ossenkoppele, R., & Alzheimer's Disease Neuroimaging Initiative. (2021). Differential associations of APOE-ε2 and APOE-ε4 alleles with PET-measured amyloid-β and tau deposition in older individuals without dementia. *European journal of nuclear medicine and molecular imaging*, *48*(7), 2212-2224. https://doi.org/10.1007/s00259-021-05192-8

Sanchez, J. S., Becker, J. A., Jacobs, H. I. L., Hanseeuw, B. J., Jiang, S., Schultz, A. P., Properzi, M. J., Katz, S. R., Beiser, A., Satizabal, C. L., O'Donnell, A., DeCarli, C., Killiany, R., El Fakhri, G., Normandin, M. D., Gomez-Isla, T., Quiroz, Y. T., Rentz, D. M., Sperling, R. A., . . . Johnson, K. A. (2021). The cortical origin and initial spread of medial temporal tauopathy in Alzheimer's disease assessed with positron emission tomography. *Science Translational Medicine*, *13*(577). https://doi.org/10.1126/scitranslmed.abc0655

Sato, C., Barthelemy, N. R., Mawuenyega, K. G., Patterson, B. W., Gordon, B. A., Jockel-Balsarotti, J., Sullivan, M., Crisp, M. J., Kasten, T., Kirmess, K. M., Kanaan, N. M., Yarasheski, K. E., Baker-Nigh, A., Benzinger, T. L. S., Miller, T. M., Karch, C. M., & Bateman, R. J. (2018). Tau Kinetics in Neurons and the Human Central Nervous System. *Neuron*, *98*(4), 861-864. https://doi.org/10.1016/j.neuron.2018.04.035

Saunders, A. M., Strittmatter, W. J., Schmechel, D., George-Hyslop, P. H., Pericak-Vance, M. A., Joo, S. H., Rosi, B. L., Gusella, J. F., Crapper-MacLachlan, D. R., Alberts, M. J., & et al. (1993). Association of apolipoprotein E allele epsilon 4 with late-onset familial and sporadic Alzheimer's disease. *Neurology*, *43*(8), 1467-1472. https://doi.org/10.1212/wnl.43.8.1467

Scheltens, P., De Strooper, B., Kivipelto, M., Holstege, H., Chételat, G., Teunissen, C. E., Cummings, J., & van der Flier, W. M. (2021). Alzheimer's disease. *The Lancet*, *397*(10284), 1577-1590. https://doi.org/10.1016/S0140-6736(20)32205-4

Seidlitz, J., Nadig, A., Liu, S., Bethlehem, R. A. I., Vertes, P. E., Morgan, S. E., Vasa, F., Romero-Garcia, R., Lalonde, F. M., Clasen, L. S., Blumenthal, J. D., Paquola, C., Bernhardt, B., Wagstyl, K., Polioudakis, D., de la Torre-Ubieta, L., Geschwind, D. H., Han, J. C., Lee, N. R., . . . Raznahan, A. (2020). Transcriptomic and cellular decoding of regional brain vulnerability to neurogenetic disorders. *Nature Communications*, *11*(1), 3358. https://doi.org/10.1038/s41467-020-17051-5

Sepulcre, J., Grothe, M. J., Uquillas, F. d. O., Ortiz-Terán, L., Díez, I., Yang, H.-S., Jacobs, H. I. L., Hanseeuw, B., Li, Q., El-Fakhri, G., Sperling, R. A., & Johnson, K. A. (2018).

Neurogenetic contributions to amyloid beta and tau spreading in the human cortex. *Nature Medicine*, *24*(12), 1910. https://doi.org/10.1038/s41591-018-0206-4

Shen, E. H., Overly, C. C., & Jones, A. R. (2012). The Allen Human Brain Atlas: Comprehensive gene expression mapping of the human brain. *Trends in Neurosciences*, *35*(12), 711-714. https://doi.org/10.1016/j.tins.2012.09.005

Shi, Y., Yamada, K., Liddelow, S. A., Smith, S. T., Zhao, L., Luo, W., Tsai, R. M., Spina, S., Grinberg, L. T., Rojas, J. C., Gallardo, G., Wang, K., Roh, J., Robinson, G., Finn, M. B., Jiang, H., Sullivan, P. M., Baufeld, C., Wood, M. W., . . . Holtzman, D. M. (2017). ApoE4 markedly exacerbates tau-mediated neurodegeneration in a mouse model of tauopathy. *Nature*, *549*(7673), 523-527. https://doi.org/10.1038/nature24016

St Clair, D., Rennie, M., Slorach, E., Norrman, J., Yates, C., & Carothers, A. (1995). Apolipoprotein E epsilon 4 allele is a risk factor for familial and sporadic presenile Alzheimer's disease in both homozygote and heterozygote carriers. *J Med Genet*, *32*(8), 642-644. https://doi.org/10.1136/jmg.32.8.642

Stadelmann, C., Timmler, S., Barrantes-Freer, A., & Simons, M. (2019). Myelin in the Central Nervous System: Structure, Function, and Pathology. *Physiological Reviews*, *99*(3), 1381-1431. https://doi.org/10.1152/physrev.00031.2018

Stokin, G. B., Lillo, C., Falzone, T. L., Brusch, R. G., Rockenstein, E., Mount, S. L., Raman, R., Davies, P., Masliah, E., Williams, D. S., & Goldstein, L. S. B. (2005). Axonopathy and transport deficits early in the pathogenesis of Alzheimer's disease. *Science (New York, N.Y.)*, *307*(5713), 1282-1288. https://doi.org/10.1126/science.1105681

Thal, D. R., Rub, U., Orantes, M., & Braak, H. (2002). Phases of A beta-deposition in the human brain and its relevance for the development of AD. *Neurology*, *58*(12), 1791-1800. https://doi.org/10.1212/wnl.58.12.1791

Therriault, J., Benedet, A. L., Pascoal, T. A., Mathotaarachchi, S., Chamoun, M., Savard, M., Thomas, E., Kang, M. S., Lussier, F., Tissot, C., Parsons, M., Qureshi, M. N. I., Vitali, P., Massarweh, G., Soucy, J.-P., Rej, S., Saha-Chaudhuri, P., Gauthier, S., & Rosa-Neto, P. (2020). Association of Apolipoprotein E ε4 With Medial Temporal Tau Independent of Amyloid-β. *JAMA Neurology*, *77*(4), 470-479. https://doi.org/10.1001/jamaneurol.2019.4421

Therriault, J., Pascoal, T. A., Lussier, F. Z., Tissot, C., Chamoun, M., Bezgin, G., Servaes, S., Benedet, A. L., Ashton, N. J., Karikari, T. K., Lantero-Rodriguez, J., Kunach, P., Wang, Y.-T., Fernandez-Arias, J., Massarweh, G., Vitali, P., Soucy, J.-P., Saha-Chaudhuri, P., Blennow, K., . . . Rosa-Neto, P. (2022). Biomarker modeling of Alzheimer's disease using PET-based Braak staging. *Nature Aging*, *2*(6), 526-535. https://doi.org/10.1038/s43587-022-00204-0

van der Weijden, C. W. J., Biondetti, E., Gutmann, I. W., Dijkstra, H., McKerchar, R., de Paula Faria, D., de Vries, E. F. J., Meilof, J. F., Dierckx, R. A. J. O., Prevost, V. H., & Rauscher, A. (2023). Quantitative myelin imaging with MRI and PET: an overview of techniques and their validation status. *Brain*, *146*(4), 1243-1266. https://doi.org/10.1093/brain/awac436

Vogel, J. W., Corriveau-Lecavalier, N., Franzmeier, N., Pereira, J. B., Brown, J. A., Maass, A., Botha, H., Seeley, W. W., Bassett, D. S., Jones, D. T., & Ewers, M. (2023). Connectome-based modelling of neurodegenerative diseases: towards precision medicine and mechanistic insight. *Nature Reviews. Neuroscience*, *24*(10), 620-639. https://doi.org/10.1038/s41583-023-00731-8

Vogel, J. W., Iturria-Medina, Y., Strandberg, O. T., Smith, R., Levitis, E., Evans, A. C., & Hansson, O. (2020). Spread of pathological tau proteins through communicating neurons in human Alzheimer's disease. *Nature Communications*, *11*(1), 2612. https://doi.org/10.1038/s41467-020-15701-2

Vogel, J. W., Young, A. L., Oxtoby, N. P., Smith, R., Ossenkoppele, R., Strandberg, O. T., La Joie, R., Aksman, L. M., Grothe, M. J., Iturria-Medina, Y., Alzheimer's Disease Neuroimaging Initiative, Pontecorvo, M. J., Devous, M. D., Rabinovici, G. D., Alexander, D. C., Lyoo, C. H., Evans, A. C., & Hansson, O. (2021). Four distinct trajectories of tau deposition identified in Alzheimer's disease. *Nature Medicine*, *27*(5), 871-881. https://doi.org/10.1038/s41591-021-01309-6

Wang, N., Wang, M., Jeevaratnam, S., Rosenberg, C., Ikezu, T. C., Shue, F., Doss, S. V., Alnobani, A., Martens, Y. A., Wren, M., Asmann, Y. W., Zhang, B., Bu, G., & Liu, C.-C. (2022). Opposing effects of apoE2 and apoE4 on microglial activation and lipid metabolism in response to demyelination. *Molecular Neurodegeneration*, *17*(1), 75. https://doi.org/10.1186/s13024-022-00577-1

Wang, Y., & Mandelkow, E. (2016). Tau in physiology and pathology. *Nature Reviews Neuroscience*, *17*(1), 22-35. https://doi.org/10.1038/nrn.2015.1

Weingarten, M. D., Lockwood, A. H., Hwo, S. Y., & Kirschner, M. W. (1975). A protein factor essential for microtubule assembly. *Proceedings of the National Academy of Sciences of the United States of America*, *72*(5), 1858-1862. https://doi.org/10.1073/pnas.72.5.1858

Whittall, K. P., MacKay, A. L., Graeb, D. A., Nugent, R. A., Li, D. K., & Paty, D. W. (1997). In vivo measurement of T2 distributions and water contents in normal human brain. *Magn Reson Med*, *37*(1), 34-43. https://doi.org/10.1002/mrm.1910370107

Xia, C. F., Arteaga, J., Chen, G., Gangadharmath, U., Gomez, L. F., Kasi, D., Lam, C., Liang, Q., Liu, C., Mocharla, V. P., Mu, F., Sinha, A., Su, H., Szardenings, A. K., Walsh, J. C., Wang, E., Yu, C., Zhang, W., Zhao, T., & Kolb, H. C. (2013). [(18)F]T807, a novel tau positron emission tomography imaging agent for Alzheimer's disease. *Alzheimer's & Dementia*, *9*(6), 666-676. https://doi.org/10.1016/j.jalz.2012.11.008

Xia, Y., Prokop, S., & Giasson, B. I. (2021). "Don't Phos Over Tau": recent developments in clinical biomarkers and therapies targeting tau phosphorylation in Alzheimer's disease and other tauopathies. *Molecular Neurodegeneration*, *16*(1), 37. https://doi.org/10.1186/s13024-021-00460-5

You, Y., Joseph, C., Wang, C., Gupta, V., Liu, S., Yiannikas, C., Chua, B. E., Chitranshi, N., Shen, T., Dheer, Y., Invernizzi, A., Borotkanics, R., Barnett, M., Graham, S. L., & Klistorner, A. (2019). Demyelination precedes axonal loss in the transneuronal spread of human neurodegenerative disease. *Brain*, *142*(2), 426-442. https://doi.org/10.1093/brain/awy338

Zhang, M., Ni, Y., Zhou, Q., He, L., Meng, H., Gao, Y., Huang, X., Meng, H., Li, P., & Chen, M. (2021). 18F-florbetapir PET/MRI for quantitatively monitoring myelin loss and recovery in patients with multiple sclerosis: A longitudinal study. *EClinicalMedicine*, *37*, 100982. https://doi.org/10.1016/j.eclinm.2021.100982

Zhao, N., Liu, C. C., Qiao, W., & Bu, G. (2018). Apolipoprotein E, Receptors, and Modulation of Alzheimer's Disease. *Biol Psychiatry*, *83*(4), 347-357. https://doi.org/10.1016/j.biopsych.2017.03.003

Manuscript I

Combined connectomics, *MAPT* gene expression, and amyloid deposition to explain regional tau deposition in Alzheimer disease

RESEARCH ARTICLE

Combined Connectomics, *MAPT* Gene Expression, and Amyloid Deposition to Explain Regional Tau Deposition in Alzheimer Disease

Lukai Zheng, MD, MMed,[1] Anna Rubinski, PhD,[1] Jannis Denecke, MSc,[1] Ying Luan, MD, PhD,[1,2] Ruben Smith, MD, PhD,[3] Olof Strandberg, PhD,[3] Erik Stomrud, MD, PhD,[3,4] Rik Ossenkoppele, PhD,[3,5,6] Diana Otero Svaldi, PhD,[7] Ixavier Alonzo Higgins, PhD,[7] Sergey Shcherbinin, PhD,[7] Michael J. Pontecorvo, PhD,[7,8] Oskar Hansson, MD, PhD,[3,4] Nicolai Franzmeier, PhD,[1,9,10] and Michael Ewers, PhD,[1,11] for the Alzheimer's Disease Neuroimaging Initiative

Objective: We aimed to test whether region-specific factors, including spatial expression patterns of the tau-encoding gene *MAPT* and regional levels of amyloid positron emission tomography (PET), enhance connectivity-based modeling of the spatial variability in tau-PET deposition in the Alzheimer disease (AD) spectrum.
Methods: We included 685 participants (395 amyloid-positive participants within AD spectrum and 290 amyloid-negative controls) with tau-PET and amyloid-PET from 3 studies (Alzheimer's Disease Neuroimaging Initiative, ^{18}F-AV-1451-A05, and BioFINDER-1). Resting-state functional magnetic resonance imaging was obtained in healthy controls (n = 1,000) from the Human Connectome Project, and *MAPT* gene expression from the Allen Human Brain Atlas. Based on a brain-parcellation atlas superimposed onto all modalities, we obtained region of interest (ROI)-to-ROI functional connectivity, ROI-level PET values, and *MAPT* gene expression. In stepwise regression analyses, we tested connectivity, *MAPT* gene expression, and amyloid-PET as predictors of group-averaged and individual tau-PET ROI values in amyloid-positive participants.
Results: Connectivity alone explained 21.8 to 39.2% (range across 3 studies) of the variance in tau-PET ROI values averaged across amyloid-positive participants. Stepwise addition of *MAPT* gene expression and amyloid-PET increased the proportion of explained variance to 30.2 to 46.0% and 45.0 to 49.9%, respectively. Similarly, for the prediction of patient-level tau-PET ROI values, combining all 3 predictors significantly improved the variability explained

View this article online at wileyonlinelibrary.com. DOI: 10.1002/ana.26818

Received May 19, 2023, and in revised form Sep 7, 2023. Accepted for publication Oct 3, 2023.

Address correspondence to Dr Ewers, Institute for Stroke and Dementia Research, University Hospital, LMU Munich, Feodor-Lynen Str 17, 81377 Munich, Germany. E-mail: michael.ewers@med.uni-muenchen.de

Data used in preparation of this article were obtained in part from the Alzheimer's Disease Neuroimaging Initiative (ADNI) database (adni.loni.usc.edu). As such, the investigators within ADNI contributed to the design and implementation of ADNI and/or provided data but did not participate in the analysis or writing of this report. A complete listing of ADNI investigators can be found at: http://adni.loni.usc.edu/wp-content/uploads/how_to_apply/ADNI_Acknowledgement_List.pdf.

From the [1]Institute for Stroke and Dementia Research, University Hospital, LMU, Munich, Germany; [2]Department of Radiology, Zhongda Hospital, School of Medicine, Southeast University, Nanjing, China; [3]Clinical Memory Research Unit, Department of Clinical Sciences Malmö, Lund University, Lund, Sweden; [4]Memory Clinic, Skåne University Hospital, Malmö, Sweden; [5]Alzheimer Center Amsterdam, Neurology, Vrije Universiteit Amsterdam, Amsterdam UMC Location VUmc, Amsterdam, the Netherlands; [6]Amsterdam Neuroscience, Neurodegeneration, Amsterdam, the Netherlands; [7]Eli Lilly and Company, Indianapolis, IN, USA; [8]Avid Radiopharmaceuticals, Philadelphia, PA, USA; [9]Munich Cluster for Systems Neurology, Munich, Germany; [10]Department of Psychiatry and Neurochemistry, Institute of Neuroscience and Physiology, Sahlgrenska Academy, University of Gothenburg, Gothenburg, Sweden; and [11]German Center for Neurodegenerative Diseases, Munich, Germany

Additional supporting information can be found in the online version of this article.

(mean adjusted R^2 range across studies = 0.118–0.148, 0.156–0.196, and 0.251–0.333 for connectivity alone, connectivity plus *MAPT* expression, and all 3 modalities combined, respectively).
Interpretation: Across 3 study samples, combining the functional connectome and molecular properties substantially enhanced the explanatory power compared to single modalities, providing a valuable tool to explain regional susceptibility to tau deposition in AD.

ANN NEUROL 2024;95:274–287

Neurofibrillary tau tangles (NFTs) constitute a core pathology of Alzheimer disease (AD) and are closely correlated with neurodegeneration and cognitive decline.[1] During the course of the disease, NFTs typically emerge in circumscribed brain areas, including the entorhinal cortex, and subsequently progress to other cortical brain areas.[2] However, the regional patterns of tau deposition differ substantially between subjects at a given level of disease severity,[3,4] which contributes to the heterogeneity in cognitive and clinical symptoms in AD.[5,6] Therefore, it is of great clinical value to understand which factors influence the spatial differences in tau accumulation in AD.

One major potential source that influences the spatial distribution of tau deposition in the brain is the connectivity between brain regions.[3] Multiple lines of evidence have suggested that pathologic tau trans-synaptically propagates between neurons in vitro,[7] and spreads along axonal connections in the brain of transgenic mouse models of tauopathy,[8] consistent with the hypothesis of a prionlike spreading of fibrillar tau between interconnected regions.[9] In humans, the assessment of transaxonal transfer cannot be measured directly at the system level. However, functional and structural connectomes of large-scale networks can be employed to assess connectivity between brain regions in humans as a predictor of the spatial progression of tau between brain regions. Based on the combination of the normative human functional connectome and positron emission tomography (PET) scans of fibrillar tau in patients of AD, we and others have previously shown that higher connectivity of tau epicenters (assumed to reflect the earliest tau-affected regions) is predictive of higher tau accumulation in the connected region,[3,10] consistent with the view that fibrillar tau progresses from initial seed regions preferentially to closely connected brain regions. Despite these encouraging results, a substantial portion of variability in the spatial patterns of tau deposition remained unexplained,[3,10] prompting urgent research needs to advance patient-level explanation of regional patterns of tau deposition.

Here, we propose combining functional connectivity and markers of local vulnerability to enhance the explanation of region-specific susceptibility to fibrillar tau. Our approach was motivated by previous findings suggesting that region-specific cellular properties such as differences in gene expression[11,12] and the presence of other major pathologies including cortical amyloid deposition[13] may influence regional tau accumulation in AD. For gene expression, recent results from human transcriptomics suggest that the normative brain expression patterns of specific genes spatially resemble predilection areas of tau pathology.[14] Specifically, the expression pattern of the gene called microtubule-associated protein tau (*MAPT*) strongly resembled the spatial patterns of tau-PET spreading and gray matter atrophy.[11,14] Because *MAPT* encodes the tau protein, which serves as the substrate for NFTs, brain regions with high *MAPT* expression may be particularly prone to develop NFTs in AD. In terms of the influence of regional amyloid-beta (Aβ) deposition on tau accumulation, the Aβ protein was previously reported to facilitate the formation of fibrillar tau in transgenic mouse models of Aβ and tau pathology.[15,16] In humans, cortical fibrillar tau is almost exclusively found in the presence of abnormally elevated levels of Aβ in cortical brain areas as measured by PET imaging,[17,18] suggesting that regional cortical Aβ facilitates the spread of tau from medial temporal to connected neocortical brain areas.[13] Therefore, regional variability in the severity of amyloid-PET accumulation may contribute to the regional heterogeneity in the spreading of tau pathology in AD. Whereas higher connectivity to epicenter may contribute to explaining the tau spreading between different regions, the accumulation of tau in the connected region may be facilitated by local Aβ levels.[13] Yet, despite the evidence supporting the contribution of such local factors to regional tau susceptibility in the brain, robust multimodal modeling that integrates regional molecular properties and interregional connectivity for explaining tau-PET accumulation patterns is still lacking.

Here, we addressed that research gap by combining the functional connectome, normative transcriptomic brain maps of *MAPT* expression, and individual measurements of regional Aβ deposition to explain regional susceptibility to tau-PET deposition. We tested the models in 3 different samples of patients with biomarker evidence of AD to assess the robustness of our findings. Overall, we provide a framework to leverage both regional factors and connectivity and thereby present a powerful approach toward precision medicine-guided explanation of tau-PET deposition patterns at the patient level in AD.

Subjects and Methods

Participants

Alzheimer's Disease Neuroimaging Initiative. We included 410 participants encompassing 279 cognitively normal (CN) subjects, 80 subjects with mild cognitive impairment (MCI), and 51 subjects with AD dementia from the Alzheimer's Disease Neuroimaging Initiative (ADNI) study (NCT01231971 and NCT02854033).[19] A detailed description of the ADNI study can be found in the ADNI General Procedures Manual.[20] In addition to the inclusion criteria of ADNI,[21] selection criteria for our study included the availability of ^{18}F-flortaucipir PET (to assess fibrillar tau) and ^{18}F-florbetapir PET (to assess Aβ deposition) spaced no longer than 6 months apart. The clinical classification of CN, MCI, or dementia was assessed by ADNI investigators as previously described.[21] Briefly, the criteria for CN were the absence of major depression, Mini-Mental State Examination (MMSE) score ≥ 24, and Clinical Dementia Rating (CDR) = 0; for MCI, objective memory loss on education-adjusted Wechsler Memory Scale II, preserved activities of daily living, MMSE ≥ 24, and CDR = 0.5; and for AD dementia, fulfillment of the National Institute of Neurological and Communicative Disorders and Stroke–Alzheimer's Disease and Related Disorders Association (NINCDS-ADRDA) probable AD criteria,[22] MMSE ≤ 26, and CDR > 0.5. Beyond the above criteria, we excluded participants with non-AD-related (ie, amyloid-negative [Aβ$^-$]) cognitive impairment.

Ethical approval was obtained by the ADNI investigators. All participants provided written informed consent.

^{18}F-AV-1451-A05. A total of 220 participants comprising 67 CN subjects, 85 MCI patients, and 68 participants with dementia were included from the ^{18}F-AV-1451-A05 study (henceforth referred to as "A05"; NCT02016560), which is a completed observational trial to assess the association between ^{18}F-flortaucipir uptake and subsequent cognitive decline.[23] In addition to the inclusion criteria of A05,[23] other criteria included the availability of ^{18}F-florbetapir PET obtained at baseline (within 2 months from the ^{18}F-flortaucipir PET scan). The classification criteria for CN subjects were MMSE ≥ 29 and no history of cognitive impairment; for MCI subjects, 24 ≤ MMSE ≤ 29 and fulfillment of the 2011 National Institute on Aging/Alzheimer's Association (NIA-AA) MCI criteria[24]; and for dementia patients, 10 < MMSE < 24, and fulfillment of the 2011 NIA-AA possible or probable AD criteria.[25] Similar to ADNI, we further excluded participants with non-AD-related cognitive impairment (determined as Aβ$^-$ MCI and Aβ$^-$ dementia).

The A05 study was approved by the relevant institutional review boards, and all participants signed informed consent.[26]

Swedish BioFINDER-1. We included 55 participants, encompassing 30 CN, 7 MCI, and 18 dementia cases from the Swedish BioFINDER-1 cohort (NCT01208675).[27] In addition to the inclusion criteria of BioFINDER-1,[27] further requirements were the availability of ^{18}F-flutemetamol PET (to assess Aβ deposition) and ^{18}F-flortaucipir PET. The classification criteria for CN were MMSE ≥ 28 and no measurable cognitive deficits on a neuropsychological battery examining verbal, visuospatial, episodic memory, and executive functions[28]; for MCI, MMSE ≥ 24 and objective memory loss on the above neuropsychological battery; and for dementia, fulfillment of the Diagnostic and Statistical Manual of Mental Disorders (third edition, revised) dementia criteria,[29] as well as the NINCDS-ADRDA probable AD criteria. Furthermore, we excluded participants classified as Aβ$^-$ MCI and Aβ$^-$ dementia.

The BioFINDER-1 study was approved by the regional ethical review board in Lund, Sweden. Participants gave their written informed consent to participate.

Image Acquisition and Processing

Alzheimer's Disease Neuroimaging Initiative. Structural magnetic resonance imaging (MRI) data were acquired on 3T scanners using 3-dimensional T1-weighted magnetization-prepared rapid acquisition gradient echo (MPRAGE) sequences with 1mm isotropic resolution and a repetition time (TR)/echo time (TE) of 3,000/30 milliseconds. ^{18}F-flortaucipir PET was acquired using 6 × 5-minute frames from 75 to 105 minutes after injection of 370MBq of the tracer. Amyloid-PET was acquired in 4 × 5-minute frames, 50 to 70 minutes after injection of ^{18}F-florbetapir (370MBq). The standardized imaging acquisition protocol for ADNI can be found online.[30]

For each participant, the T1 magnetic resonance (MR) images were segmented and the high-dimensional spatial normalization parameters for registration to the Montreal Neurological Institute (MNI) 152 space[31] were estimated using the Advanced Normalization Tools (ANTs) cortical-thickness pipeline (see Tustison et al[32] for a detailed description). The parameters were subsequently applied to each participant's corresponding ^{18}F-flortaucipir and ^{18}F-florbetapir PET scans for registration to MNI space. The thus registered ^{18}F-flortaucipir PET scans were intensity-normalized, using the inferior cerebellar cortex as the reference region,[33] and the regional standardized uptake value ratios (SUVRs) were extracted for 200 cortical regions of interest (ROIs) based on the Schaefer atlas.[34] Finally, the ROI values of ^{18}F-flortaucipir SUVRs were

converted into z scores (henceforth called ^{18}F-flortaucipir z scores) based on the data from the Aβ$^-$ CN reference group for each specific ROI.[35] This involved transforming each participant's ROI value by subtracting the average ROI value of the reference group and then dividing it by the standard deviation of the reference group's ROI values. For ^{18}F-florbetapir PET scans, the registered images were intensity-normalized to the mean signal in the whole cerebellum, and the global ^{18}F-florbetapir SUVRs were calculated as the average SUVR of frontal, anterior/posterior cingulate, lateral parietal, and lateral temporal regions according to a previously described protocol.[36,37] The Aβ status was determined based on established cut-points of global ^{18}F-florbetapir SUVR > 1.11.[30] We also extracted regional mean ^{18}F-florbetapir SUVRs for 200 Schaefer ROIs and calculated ^{18}F-florbetapir z scores using the ^{18}F-florbetapir PET scans from the Aβ$^-$ CN group as reference data.

^{18}F-AV-1451-A05. Structural MRI data were acquired across multiple scanners (1.5 or 3T) using volumetric T1-weighted sequences. ^{18}F-flortaucipir PET was acquired using 4 × 5-minute frames from 80 to 100 minutes after injection of 370MBq of the tracer. Amyloid-PET was acquired in 2 × 5-minute frames, 50 to 60 minutes after injection of ^{18}F-florbetapir (370MBq). A detailed description of imaging acquisition in A05 was given elsewhere.[23]

All MR and PET images were processed as previously described.[23] Briefly, structural T1 MR images were segmented into tissue compartments using Statistical Parametric Mapping (SPM) and spatially normalized to the MNI space using FMRIB's nonlinear image registration tool (FNIRT).[38] The derived spatial normalization parameters were applied to the coregistered ^{18}F-flortaucipir PET scans, which were subsequently intensity-normalized to the inferior cerebellar gray as the reference region. For the ^{18}F-florbetapir PET data, summed motion-corrected scans were spatially normalized to a ^{18}F-florbetapir PET template in MNI space using nonlinear registration methods in SPM and subsequently intensity-normalized using the whole cerebellum as the reference region. All ^{18}F-florbetapir PET images were visually interpreted by experienced Avid investigators and classified by consensus as Aβ$^-$ or Aβ$^+$.[23] Readers had access to regional and global average quantitative PET scan information, which was used as an adjunct to the visual read.[23] Regional mean SUVRs were extracted for 200 Schaefer ROIs for both the ^{18}F-flortaucipir and ^{18}F-florbetapir PET scans, followed by the conversion of these values into z scores referenced to the Aβ$^-$ CN group.

BioFINDER-1. For all BioFINDER-1 participants, structural MRI data were acquired on 3T scanners using T1-weighted MPRAGE (1mm isotropic resolution, TR/TE = 1,900/2.64 milliseconds) sequences. Tau-PET was acquired 80 to 100 minutes after injection of ^{18}F-flortaucipir, whereas amyloid-PET was acquired 90 to 110 minutes after injection of ^{18}F-flutemetamol. A detailed description of MRI and PET data acquisition in BioFINDER-1 can be found elsewhere.[39]

All MR and PET images were processed centrally by the BioFINDER imaging core in Lund.[40] In brief, T1 MR images were segmented via FreeSurfer,[41] and high-dimensional spatial normalization parameters were estimated using ANTs.[40] Attenuation- and motion-corrected ^{18}F-flortaucipir and ^{18}F-flutemetamol PET images were intensity-normalized to the inferior cerebellar gray matter as the reference region for ^{18}F-flortaucipir PET images and to the pons for the ^{18}F-flutemetamol PET images, and subsequently normalized to MNI space by applying the T1-derived transformation parameters. Global ^{18}F-flutemetamol SUVR was defined as an average SUVR across prefrontal, parietal, temporal lateral, anterior cingulate, posterior cingulate, and precuneus cortices.[42] A previously defined cutoff (global ^{18}F-flutemetamol SUVR > 0.575) was applied to determine Aβ status.[43] Regional SUVRs of each PET image were also extracted for 200 Schaefer ROIs and then converted into z scores referenced to the Aβ$^-$ CN group.

Identification of Tau Epicenters

Following a previously developed approach,[3] we determined tau epicenters for each Aβ$^+$ participant, defined as those ROIs that show the highest ^{18}F-flortaucipir z scores among the 200 ROIs within a given participant. The number of epicenters was kept constant across all Aβ$^+$ participants. The optimal number of epicenters was defined based on the maximal R^2 value of epicenter–connectivity distance to explain the ^{18}F-flortaucipir deposition at a given number of epicenter ROIs in the ADNI sample. To this end, we first averaged all ^{18}F-flortaucipir z score maps across the Aβ$^+$ participants and ranked the ROIs in descending order of the group-averaged ROI values of ^{18}F-flortaucipir z scores in the ADNI sample. Next, we systematically varied the number of ROIs as candidate epicenters (ranging from top 1 to top 30 ROIs of highest ^{18}F-flortaucipir z score, increasing by steps of 1). For each number of ROIs, the R^2 value of the connectivity-based prediction of the ROI levels of ^{18}F-flortaucipir z scores was determined. The number 5 ROIs yielded the highest R^2, which also gained high model performance in the other two datasets. Finally, we determined for each participant the tau epicenters as the 5 highest ranking ROIs within the participant's ^{18}F-flortaucipir z score map.

Functional Connectivity Template and Connectivity Distance

We computed pairwise functional connectivity for all ROI pairs in the 200-ROI Schaefer atlas using the resting state functional MRI (fMRI) scans from 1,000 healthy participants recruited within the Human Connectome Project (HCP), as described previously.[3] Briefly, minimally preprocessed 3T resting-state fMRI images (spatially normalized to MNI space; for details see Smith et al[44]) were downloaded from the HCP database, and further processed by detrending, bandpass filtering (0.01–0.08Hz), despiking, and motion correction. As an additional measure to control for motion artifacts, frames with displacement > 0.5mm were scrubbed along with 1 preceding and 2 subsequent frames. Based on the processed fMRI images, we extracted regional-average time course within each of the 200 ROIs and assessed Pearson moment correlations of the time courses for each pair of ROIs, resulting in participant-level functional connectivity matrices. The correlation coefficients were Fisher *z*-transformed and averaged across participants to create a group-level connectivity matrix.

For the computation of connectivity distance (ie, the length of the shortest path connecting two ROIs in the functional network),[45] we retained 70% of the strongest positive connections within the group-level connectivity matrix to eliminate weak and potentially noisy connections.[3] Connectivity distance was computed for each pair of ROIs using Floyd's algorithm,[46] resulting in a distance matrix. Floyd's distance is defined as the shortest distance between two nodes in a graph, where the edges are weighted by the connectivity. Epicenter–connectivity distance of an ROI was defined as the average connectivity distance of a target ROI to all 5 epicenter ROIs for a given participant.

Spatial Maps of MAPT Gene Expression

For our hypothesis-driven analysis focusing on *MAPT* gene expression, the spatial gene expression data of *MAPT* were derived from mRNA profiling of 6 healthy human brains in the Allen Human Brain Atlas (AHBA).[47] Specifically, we used a whole-brain gene expression map, where the *MAPT* mRNA levels were interpolated at all locations throughout the brain in MNI standard space as described previously.[48] In brief, mRNA microarray data obtained from AHBA were symmetrized across hemispheres, filtered, and averaged across probes, mean-centering normalized across donors, and finally fitted into a variogram model to predict mRNA level for each voxel in MNI space. Several probe filtering methods were applied, including intensity-based filtering of background signal (>1%), correlation-based filtering of probes (Pearson $r > 0.3$), and a stepwise selection based on spatial variability of the variogram modeling.[48]

Based on the whole-brain map, we computed the average *MAPT* gene expression level in each of the 200 ROIs from the Schaefer atlas. To this end, we created a gray matter mask (thresholded at the probability of >0.3) from the segmented T1 scans in the ADNI sample and superimposed the mask onto the *MAPT* gene expression map to obtain the ROI expression values.

Statistical Analysis

All statistical analyzes were performed with R version 4.2.0 (www.R-project.org). First, we tested whether the spatial similarity between the *MAPT* gene expression and group-average ^{18}F-flortaucipir *z* scores in corresponding ROIs was exceptionally high among the 18,686 gene expression maps of protein-encoding genes mapped in the AHBA.[48] To this end, we computed for each gene the spatial correlation (Pearson correlation coefficient) at the ROI level between gene expression ROI levels and the average ^{18}F-flortaucipir *z* score ROI levels among $A\beta^+$ participants, rendering a sampling distribution of the spatial correlation coefficients across genes. We determined the percentile rank of the spatial correlation coefficient for the *MAPT* gene within the sampling distribution. Additionally, we extended this analysis by narrowing down the gene pool to include only those genes labeled as brain-elevated genes (n = 2,098) in the Human Protein Atlas.[49] These brain-elevated genes show at least 4-fold higher expression in the brain compared to other organs and tissues, thus providing a more stringent reference for assessing the spatial similarity to ^{18}F-flortaucipir deposition. To control for spatial autocorrelation, the significance (p_{spin}) of the correlation between ^{18}F-florbetapir *z* scores and *MAPT* expression was established against 10,000 spatial permutations using Vasa's method, which is an implementation of the nonparametric spin test for parcellated brain map.[50]

Next, to replicate our previous findings that shorter epicenter–connectivity distance was associated with higher ^{18}F-flortaucipir *z* scores in the connected ROIs,[3] we performed linear regression with group-average ROI values of ^{18}F-flortaucipir *z* scores as the dependent variable and epicenter–connectivity distance as the independent variable within the $A\beta^+$ group. To test our hypothesis that regional *MAPT* expression and amyloid-PET *z* scores enhance connectivity-based prediction of ^{18}F-flortaucipir *z* scores, we added in a stepwise manner the terms *MAPT* expression and amyloid-PET *z* scores (all at the ROI level) to the initial connectivity-only model. The explanatory power of the above models was assessed by adjusted R^2 values (R^2_{adj}) and compared between the models by likelihood ratio tests. To account for spatial autocorrelation, we also performed 10,000 spatial permutations per modality (epicenter–connectivity distance/*MAPT* expression/amyloid-PET) and assessed the significance (p_{spin}) of R^2_{adj} against a null distribution of R^2_{adj} derived from the permuted maps.

For participant-level analyses, the above-described regression analyzes were repeated for each $A\beta^+$ participant separately. To this end, the tau epicenters (5 ROIs with the highest ^{18}F-flortaucipir *z* score) were determined for each participant separately, and the epicenter–connectivity distance was calculated accordingly on the HCP-derived connectivity matrix. R^2_{adj} values of the models were compared with paired *t* tests across participants within each sample.

Results

Sample Characteristics

Basic demographic and clinical characteristics are summarized by diagnostic group and study in Table 1. The

TABLE 1. Demographic and Basic Participant Characteristics

ADNI, N = 410	Aβ⁻ CN, n = 211	Aβ⁺ CN, n = 68	Aβ⁺ MCI, n = 80	AD dementia, n = 51	*p*
Age, yr	73.3 ± 7.5	77.0 ± 7.1	76.3 ± 7.5	78.6 ± 8.9	<0.001
Male, n (%)	95 (45.0)	25 (36.8)	47 (58.8)	28 (54.9)	0.031
Education, yr	17 ± 3	17 ± 2	16 ± 3	15 ± 2	0.001
MMSE	29.0 ± 1.2	28.83 ± 1.4	26.93 ± 2.3	21.9 ± 4.6	<0.001
ADAS-13	8.18 ± 4.16	9.04 ± 5.32	17.80 ± 6.89	31.00 ± 9.83	<0.001
APOE-ε4, n (%)[a]	59 (29.4)	34 (51.5)	47 (61.8)	30 (60.0)	<0.001
A05, N = 220	**Aβ⁻ CN, n = 63**	**Aβ⁺ CN, n = 4**	**Aβ⁺ MCI, n = 85**	**AD dementia, n = 68**	***p***
Age, yr	58.5 ± 19.7	78.1 ± 8.0	74.5 ± 9.2	75.0 ± 9.66	<0.001
Male, n (%)	36 (57.1)	3 (75.0)	49 (57.6)	32 (47.1)	0.451
Education, n (%)					0.554
≥13 years	54 (85.7)	4 (100.0)	66 (77.6)	55 (80.9)	-
Otherwise	9 (14.3)	0 (0)	19 (22.4)	13 (19.1)	-
MMSE	29.4 ± 0.8	28.8 ± 1.9	25.6 ± 3.2	22.0 ± 10.5	<0.001
ADAS-11	5.29 ± 3.26	5.75 ± 3.95	13.7 ± 5.84	22.0 ± 10.5	<0.001
APOE-ε4, n (%)	13 (21.0)	1 (25.0)	44 (52.4)	42 (64.6)	<0.001
BioFINDER-1, N = 55	**Aβ⁻ CN, n = 16**	**Aβ⁺ CN, n = 14**	**Aβ⁺ MCI, n = 7**	**AD dementia, n = 18**	***p***
Age, yr	73.9 ± 5.3	76.2 ± 5.0	72.7 ± 6.6	69.8 ± 10.5	0.126
Male, n (%)	10 (62.5)	6 (42.9)	2 (28.6)	11 (61.1)	0.357
Education, yr	13 ± 4	11 ± 3	11 ± 3	13 ± 3	0.118
MMSE	29.0 ± 1.1	29.2 ± 1.1	25.6 ± 2.9	22.1 ± 5.2	<0.001
ADAS-delayed recall	1.81 ± 1.47	2.29 ± 1.59	6.17 ± 2.40	7.62 ± 2.45	<0.001
APOE-ε4, n (%)	0 (0)	8 (57.1)	4 (57.1)	11 (61.1)	<0.001

Note: Values are n (%) for categorical variables and mean ± standard deviation for continuous variables; *p* values are derived from χ^2 tests for categorical variables, and analyses of variance for continuous variables.

[a]Proportion of *APOE-ε4* carriers was based on individuals who had information on *APOE* genotype, which was available for 393 of 410 participants in the ADNI sample, 215 of 220 participants in the A05 sample, and all the participants in the BioFINDER-1 sample.

Abbreviations: A05 = ^{18}F-AV-1451-A05; AD = Alzheimer disease; ADAS = Alzheimer's Disease Assessment Scale; ADNI = Alzheimer's Disease Neuroimaging Initiative; Aβ = amyloid-beta; CN = cognitively normal; MCI = mild cognitive impairment; MMSE = Mini-Mental State Examination.

group-average maps of cortical ^{18}F-flortaucipir SUVRs in the Aβ$^+$ groups are shown for all 3 samples in Figure 1A. Higher ^{18}F-flortaucipir *z* scores (>3) were observed on average primarily in the temporal lobe and medial posterior parietal cortex for each of the 3 studies (see Supplementary Fig S1 for average ^{18}F-flortaucipir *z* score maps split by clinical group within each study). The *MAPT* expression was primarily observed in the posterior parietal, lateral temporal, entorhinal, precuneus, and cingulate cortex (see Fig 1B).

Spatial Similarity between Flortaucipir z Scores and MAPT Expression

Higher regional *MAPT* expression was associated with higher ^{18}F-flortaucipir *z* scores across spatially corresponding ROIs within the Aβ$^+$ group (ADNI: $r = 0.375$, $p_{spin} = 0.004$;

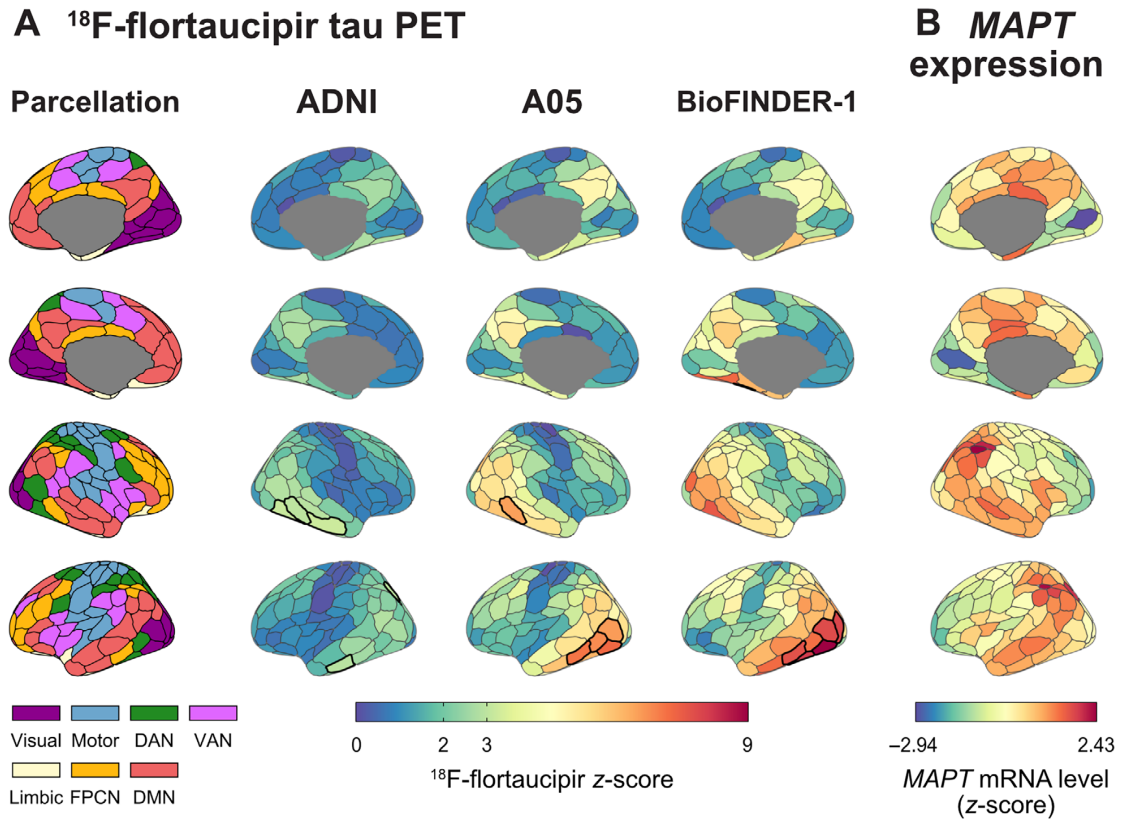

FIGURE 1: Spatial distribution of ^{18}F-flortaucipir deposition and *MAPT* expression. (A) Surface rendering of the ^{18}F-flortaucipir *z* scores within regions of interest (ROIs) defined by a 200-ROI brain parcellation atlas (first column; resting-state functional networks are color-coded) applied to ^{18}F-flortaucipir PET scans from Aβ^+ participants in each study. (B) Average *MAPT* gene expression in spatially corresponding ROIs. Tau epicenter ROIs are displayed in bold colors. A05 = ^{18}F-AV-1451-A05; ADNI = Alzheimer's Disease Neuroimaging Initiative; DAN = dorsal attention network; DMN = default mode network; FPCN = frontoparietal control network; PET = positron emission tomography; VAN = ventral attention network.

A05: $r = 0.371$, $p_{spin} = 0.019$; BioFINDER-1: $r = 0.386$, $p_{spin} = 0.024$). To test whether the spatial correlation between ^{18}F-flortaucipir *z* scores and *MAPT* stands out against that between tau and the expression of other genes in the brain, we computed the distribution of spatial correlations between group-averaged ^{18}F-flortaucipir maps of Aβ^+ participants and the spatial expression of each of the 18,686 genes in the AHBA atlas. The correlation scores for ^{18}F-flortaucipir versus *MAPT* ranked between the top 2rd and 3th percentile when compared to those between the ^{18}F-flortaucipir *z* scores and the expression of any other of the 18,686 genes in the AHBA atlas (ADNI: top 2th percentile; A05: top 2th percentile; BioFINDER1: top 3rd percentile; Fig 2), confirming a higher spatial match between ^{18}F-flortaucipir *z* scores and *MAPT* expression when compared to most other genes in the AHBA across study samples. Furthermore, we replicated this analysis in a subset of genes that are highly expressed in the brain (n = 2,098). The percentile rank of the correlation between *MAPT* gene expression and ^{18}F-flortaucipir *z* scores remained high compared to that of most other genes (ADNI: top 5th percentile; A05: top 5th percentile; BioFINDER-1: top 5th percentile; Supplementary Fig S2).

MAPT *Expression and Amyloid-PET for Explaining Interregional Tau Variation at the Group Level within the Aβ^+ Group*

First, we replicated our previous findings of the association between epicenter–connectivity distance and ^{18}F-flortaucipir *z* scores in the connected brain regions in each of the 3 samples of Aβ^+ participants (Table 2, Fig 3A).[3,51] Overall, shorter epicenter–connectivity distance was associated with higher average ^{18}F-flortaucipir *z* scores in the connected ROIs, with $R^2_{adj} = 0.392$ (in ADNI study), 0.218 (A05), and 0.221 (BioFINDER-1) within the Aβ^+ participants (ADNI: $p_{spin} < 0.001$; A05: $p_{spin} < 0.001$; BioFINDER-1:

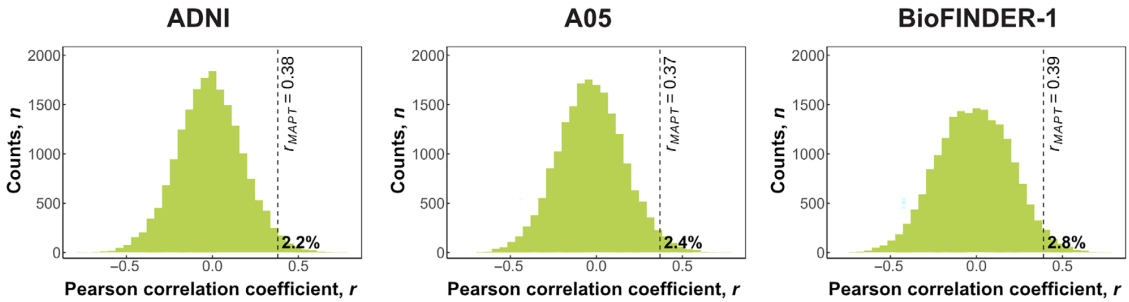

FIGURE 2: Association between ^{18}F-flortaucipir and gene expression across 18,686 genes. The vertical dotted lines indicate the percentiles of the correlation coefficients for the associations between *MAPT* gene expression versus ^{18}F-flortaucipir *z* scores for each of the 3 studies. A05 = ^{18}F-AV-1451-A05; ADNI = Alzheimer's Disease Neuroimaging Initiative.

$p_{spin} = 0.013$), confirming our previous findings that epicenter–connectivity distance partially explains the interregional variability in tau-PET deposition in AD.[3,51] When adding *MAPT* expression to the epicenter–connectivity distance for the prediction of regional ^{18}F-flortaucipir *z* score, the combined model led to a significant improvement by 7 to 12% in explanatory power (connectivity-only model vs 2-predictor combined model, ADNI: $R^2_{adj} = 0.392$ vs 0.460, $p < 0.001$; A05: $R^2_{adj} = 0.218$ vs 0.302, $p < 0.001$; BioFINDER-1: $R^2_{adj} = 0.221$ vs 0.343, $p < 0.001$). In contrast, *MAPT* expression alone explained only 11.5%/13.6%/15.7% of the variance in ADNI/A05/BioFINDER-1 samples (ADNI: $p_{spin} = 0.010$; A05: $p_{spin} = 0.010$; BioFINDER-1: $p_{spin} = 0.008$).

In a final step, we tested whether adding amyloid-PET *z* scores as a third independent variable further enhanced the explanatory power. Compared to the reduced model (epicenter–connectivity distance plus *MAPT* expression), the addition of amyloid-PET *z* scores as a predictor variable increased the proportion of explained variance by an additional 2 to 20% (ADNI: $R^2_{adj} = 0.460$ vs 0.479, $p = 0.005$; A05: $R^2_{adj} = 0.302$ vs 0.499, $p < 0.001$; BioFINDER-1: $R^2_{adj} = 0.343$ vs 0.450, $p < 0.001$). These results suggest that both regional *MAPT* expression levels and participant-level amyloid-PET *z* scores in a given ROI enhance the epicenter–connectivity distance model to explain regional ^{18}F-flortaucipir *z* scores.

We conducted sensitivity analyzes in clinically defined subgroups of Aβ$^+$ participants in ADNI and A05 (note that we did not attempt subgroup analysis in the BioFINDER-1 sample and the Aβ$^+$ CN subgroup of A05 due to smaller sample size). The above intermodel differences remained in the Aβ$^+$ MCI and AD dementia participants, but not the Aβ$^+$ CN group (Supplementary Fig S3). Specifically, regional *MAPT* expression did not explain the group-averaged ROI values of ^{18}F-flortaucipir *z* scores in the Aβ$^+$ CN group ($R^2_{adj} = 0.037$, $p_{spin} = 0.092$), potentially due to the low-level, spatially restricted ^{18}F-flortaucipir deposition in that group.

Participant-Level Analysis of ^{18}F-Flortaucipir PET Prediction

Based on previous findings explaining the group-average spatial pattern of ^{18}F-flortaucipir *z* scores in the Aβ$^+$ participants, we next asked whether the model also explains the spatial variability in the individual tau-PET deposition. Therefore, we repeated the analysis, this time testing the models to explain ^{18}F-flortaucipir *z* scores at the participant level. Consistent with the previous analysis reported above based on group-average ^{18}F-flortaucipir *z* scores, adding *MAPT* expression to epicenter–connectivity distance led to an increase in the proportion of explained variability in participant-level tau *z* scores (connectivity-only model vs 2-predictor combined model, ADNI: mean $R^2_{adj} = 0.118$ vs 0.156, $p < 0.001$; A05: mean $R^2_{adj} = 0.148$ vs 0.196, $p < 0.001$; BioFINDER-1: mean $R^2_{adj} = 0.119$ vs 0.162, $p < 0.001$; see Table 2, Fig 4). Adding amyloid-PET *z* scores increased the proportion of explained variance in ^{18}F-flortaucipir *z* scores by an additional 8 to 15% (ADNI: mean $R^2_{adj} = 0.156$ vs 0.333, $p < 0.001$; A05: mean $R^2_{adj} = 0.196$ vs 0.282, $p < 0.001$; BioFINDER-1: mean $R^2_{adj} = 0.162$ vs 0.251, $p < 0.001$). Sensitivity analysis in clinically defined subgroups showed enhanced explanatory value of the full models (including *MAPT* expression and amyloid-PET) in each of the clinical subgroups within Aβ$^+$ participants (Supplementary Fig S4).

Discussion

Our main finding was that the spatial patterns of *MAPT* expression and regional amyloid-PET *z* scores enhanced the epicenter–connectivity distance-based model for explaining spatial ^{18}F-flortaucipir patterns in AD. We reproduced these findings across samples from 3 studies,

ANNALS *of Neurology*

TABLE 2. Regression Models to Predict Group-Averaged and Participant-Level ^{18}F-Flortaucipir SUVRs

	ADNI		A05		BioFINDER-1	
Statistical model	**β (95% CI)**	**R^2_{adj} (95% CI)**	**β (95% CI)**	**R^2_{adj} (95% CI)**	**β (95% CI)**	**R^2_{adj} (95% CI)**
Group-averaged ^{18}F-flortaucipir PET						
Model A		0.392 (0.282 to 0.495)		0.218 (0.122 to 0.324)		0.221 (0.124 to 0.327)
Epicenter–connectivity distance	−0.629 (−0.739 to −0.518)		−0.471 (−0.597 to −0.346)		−0.474 (−0.599 to −0.349)	
Model B		0.115 (0.043 to 0.208)		0.136 (0.057 to 0.233)		0.157 (0.073 to 0.258)
Regional *MAPT* expression	0.345 (0.212 to 0.479)		0.374 (0.243 to 0.506)		0.402 (0.272 to 0.532)	
Model C		0.460 (0.349 to 0.555)		0.302 (0.192 to 0.406)		0.343 (0.231 to 0.446)
Epicenter–connectivity distance	−0.593 (−0.698 to −0.488)		−0.418 (−0.538 to −0.297)		−0.437 (−0.552 to −0.321)	
Regional *MAPT* expression	0.268 (0.163 to 0.373)		0.300 (0.179 to 0.420)		0.356 (0.241 to 0.472)	
Model D		0.479 (0.365 to 0.570)		0.499 (0.387 to 0.588)		0.450 (0.335 to 0.543)
Epicenter–connectivity distance	−0.562 (−0.667 to −0.456)		−0.472 (−0.574 to −0.369)		−0.484 (−0.591 to −0.377)	
Regional *MAPT* expression	0.252 (0.148 to 0.355)		0.302 (0.200 to 0.404)		0.297 (0.190 to 0.405)	
Regional amyloid	0.150 (0.045 to 0.256)		0.448 (0.347 to 0.549)		0.337 (0.230 to 0.445)	
Participant-level ^{18}F-flortaucipir PET[a]						
Model A		0.118 (0.101 to 0.134)		0.148 (0.127 to 0.169)		0.119 (0.085 to 0.152)
Epicenter–connectivity distance	−0.304 (−0.328 to −0.280)		−0.345 (−0.374 to −0.316)		−0.313 (−0.365 to −0.262)	
Model B		0.043 (0.036 to 0.050)		0.058 (0.049 to 0.068)		0.051 (0.034 to 0.068)
Regional *MAPT* expression	0.106 (0.079 to 0.132)		0.203 (0.181 to 0.227)		0.189 (0.143 to 0.236)	
Model C		0.156 (0.137 to 0.174)		0.196 (0.173 to 0.220)		0.162 (0.122 to 0.202)
Epicenter–connectivity distance	−0.296 (−0.320 to −0.272)		−0.332 (−0.360 to −0.303)		−0.301 (−0.353 to −0.250)	
Regional *MAPT* expression	0.092 (0.066 to 0.117)		0.180 (0.157 to 0.202)		0.167 (0.121 to 0.213)	
Model D		0.333 (0.313 to 0.354)		0.282 (0.260 to 0.304)		0.251 (0.204 to 0.298)
Epicenter–connectivity distance	−0.216 (−0.244 to −0.189)		−0.308 (−0.338 to −0.279)		−0.275 (−0.329 to −0.221)	
Regional *MAPT* expression	0.092 (0.069 to 0.116)		0.183 (0.161 to 0.205)		0.137 (0.085 to 0.190)	
Regional amyloid	0.417 (0.390 to 0.444)		0.260 (0.234 to 0.286)		0.225 (0.150 to 0.299)	

[a]For the participant-level regression models, the β and R^2_{adj} averaged across participants and their 95% CI are presented.
Abbreviations: A05 = ^{18}F-AV-1451-A05; ADNI = Alzheimer's Disease Neuroimaging Initiative; CI = confidence interval; PET = positron emission tomography; R^2_{adj} = adjusted proportion variance explained; β = standardized regression coefficient.

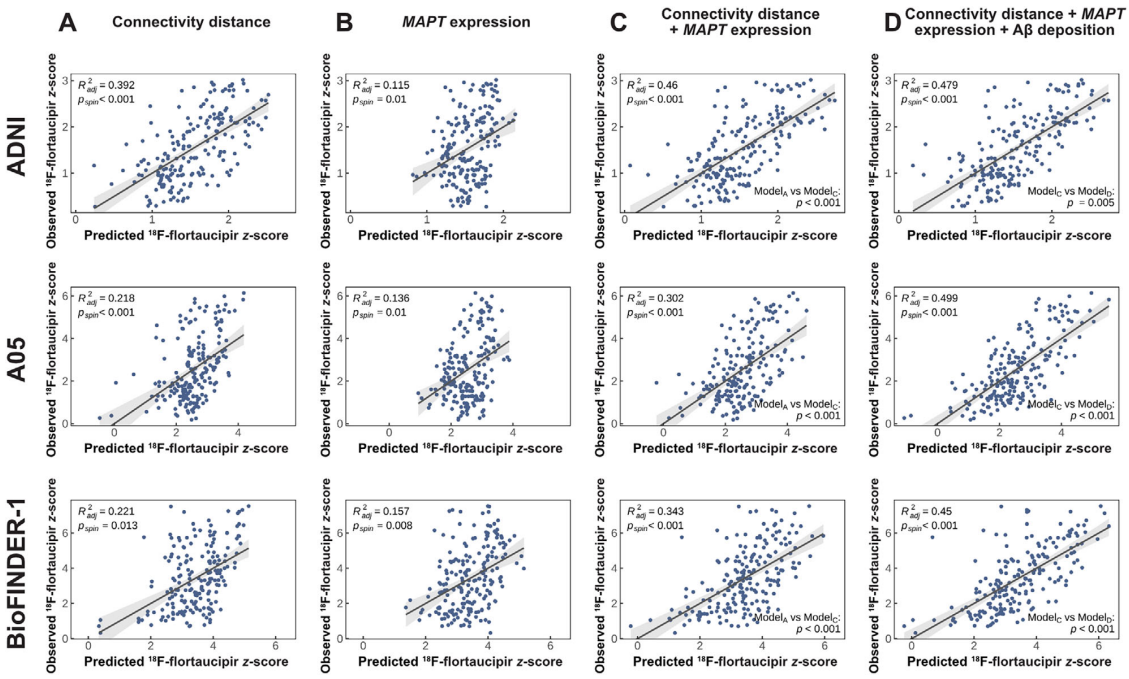

FIGURE 3: Prediction of group-average ^{18}F-flortaucipir *z* scores. Regression plots show the association between the predicted versus observed ^{18}F-flortaucipir *z* scores for each regression model including connectivity only (A), *MAPT* expression only (B), connectivity plus *MAPT* expression (C), and all 3 modalities combined (D). A05 = ^{18}F-AV-1451-A05; ADNI = Alzheimer's Disease Neuroimaging Initiative; Aβ = amyloid-beta; p_{spin} = spatial autocorrelation-corrected *p* value for spin-based permutation testing; R^2_{adj} = adjusted proportion variance explained.

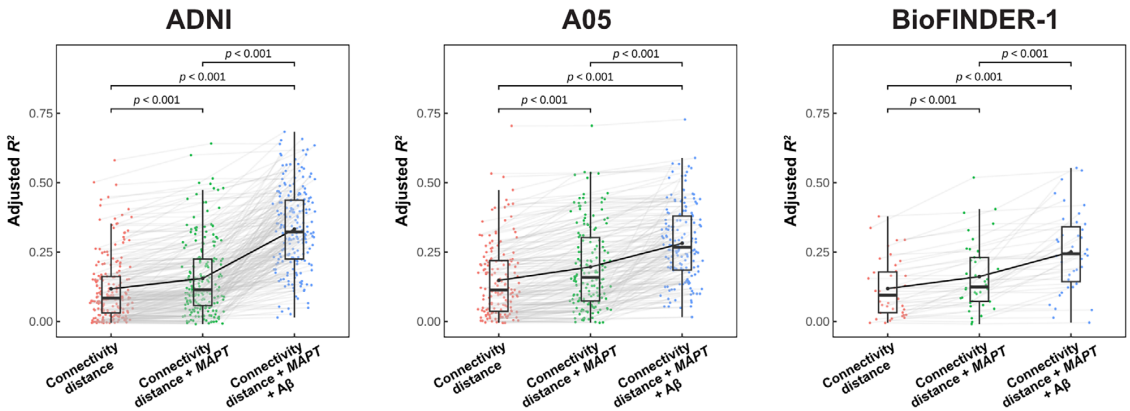

FIGURE 4: Prediction of participant-level ^{18}F-flortaucipir *z* scores. Box plots show the distribution of adjusted R^2 values for each regression model including connectivity-only models (*red dots*), connectivity plus *MAPT* expression (*green dots*), and all 3 modalities combined (*blue dots*) for each study. The R^2 values were compared between models using paired *t* tests. A05 = ^{18}F-AV-1451-A05; ADNI = Alzheimer's Disease Neuroimaging Initiative; Aβ = amyloid-beta.

suggesting a robust benefit of our multimodal model over connectivity for the prediction of ^{18}F-flortaucipir *z* scores in patients with biomarker evidence of AD. Our findings advance the results of previous studies to explain regional patterns of tau pathology.[3,10] Compared to connectivity-only models, the introduction of local gene expression and individual-level amyloid-PET increased the explained proportion of variance by 9 to 28% to a total of 45 to 50% across 3 samples, demonstrating a substantial benefit of the integrated multimodal model compared to

previous results. Toward precision medicine, we also performed a patient-level modeling of regional tau-PET deposition in addition to the group-level analysis. This is a more difficult task, as individual patterns in ^{18}F-flortaucipir *z* scores vary more than the group average. Our results showed a slightly reduced explanatory value for patient-level compared to group-level ^{18}F-flortaucipir *z* scores, but still demonstrated a significant increase in the effect size of the fully integrated prediction model compared to reduced models. Our approach, therefore, provides an important step forward to identify the factors that may underlie regional susceptibility to tau accumulation and yields a framework to build an integrated multidimensional model of regional tau-PET deposition applicable at the individual level in AD.

For the gene expression mapping, we focused, in a hypothesis-driven manner, on *MAPT* among more than 18,000 protein-encoding genes mapped in the AHBA. Our focus on the *MAPT* gene was driven by previous findings of a spatial match of regional *MAPT* gene expression and trajectories of tau spreading in the brain.[11] Supporting those previous findings, we found that *MAPT* gene expression showed a spatial association with tau-PET deposition surpassing the top 5th percentile among all genes mapped in the AHBA and when considering only those protein-encoding genes exhibiting enhanced expression in the brain. A potential mechanisms that may link *MAPT* expression with regional tau pathology is that higher *MAPT* transcript levels are associated with higher regional levels of soluble tau,[52] which may undergo fibrillization and transsynaptic spreading in disease.[7,8] In line with this, we recently found that increased levels of soluble tau are strongly associated with greater tau spread and accumulation over time in early AD.[53] We caution, however, that the proposed pathomechanistic model of tau spreading remains to be demonstrated in future studies.

In addition to *MAPT* expression levels, we found that regional amyloid-PET assessed in each participant was associated with higher regional tau-PET in spatially corresponding ROIs, suggesting that higher regional amyloid-PET adds to the explanation of regional tau PET levels. This finding may at first be surprising, given the spatial divergence of predilected brain areas of amyloid plaques (ie, the default mode network)[54] and tau (ie, medial temporal lobe, locus coeruleus).[2] However, the progression of tau pathology from medial temporal to higher cortical areas (Braak stage III–IV) is typically not seen in the absence of amyloid plaques,[55,56] suggesting that accumulation of fibrillar tau in higher cortical brain areas is facilitated by the presence of amyloid pathology.[13] Converging evidence comes from studies in transgenic animal models of Aβ and pathologic tau, where the spreading of tau from the entorhinal cortex to other cortical brain areas is dramatically enhanced in the presence of cortical Aβ.[57] Our findings are consistent with these previous findings, suggesting an association between regional amyloid-PET levels and tau-PET deposition in AD.

Some caveats should be considered for the interpretation of the current results. First, we focused in the current study on explaining regional variance in tau-PET accumulation averaged across subjects in one of our major analyses. However, previous studies suggest the predominance of spatial subtypes of fibrillar tau spreading in AD, such as the limbic-only or hippocampal sparing subtypes,[4] which we did not take into account. Such subtypes may provide a heuristic for stratified analysis of tau-PET patterns. Rather than stratifying our analysis by tau subtype, we chose to focus on the epicenter-based prediction models. The advantage is that epicenter locations can be individually determined and thus allow for patient-tailored prediction of tau-PET patterns rather than relying on categorical subtyping, where the assignment of individuals to subtypes can be ambiguous. Second, for mapping gene expression, we focused in a hypothesis-driven manner on the *MAPT* gene, but we caution that the expression patterns of *APOE*,[58,59] or other yet-to-be-identified genes, may show similar or even stronger spatial similarity to tau-PET. However, given the large number of potential genes, an exploratory analysis bears the risk of overfitting and would require extensive cross-validation, which was beyond the scope of the current study. Lastly, we employed an out-of-sample functional connectivity template to test our hypothesis that regions typically more strongly connected to tau epicenters exhibit higher tau-PET deposition. However, previous studies have shown that the functional connectome shows interindividual variability[60] that cannot be captured using group-averaged connectivity templates. Furthermore, functional connectivity may change during the disease course,[61] which in turn may influence the progression of tau pathology between connected brain areas. Precision fMRI with extended acquisition times may be particularly suitable to capture idiosyncratic maps of the functional connectome.[62] The current findings encourage future studies using precision fMRI to test whether individual functional connectomes can improve the prediction of AD pathologies beyond the use of connectivity templates.

Overall, our current results demonstrate the additive value of patient-level amyloid-PET scans and atlas-based *MAPT* gene expression mapping to enhance the connectivity-based explanation of tau accumulation. Therefore, the current findings provide important insight into potential sources underlying region-specific

deposition of tau pathology, and encourage future studies to test in patients with AD whether spatial subtypes of amyloid accumulation[63,64] or polymorphisms in tau-related genes are predictive of regional differences in tau deposition and associated domain-specific cognitive impairment.

Acknowledgments

The study was funded by grants from Deutsches Zentrum für Luft- und Raumfahrt (01KU2203 to M.E.), ERA PerMed (to O.H.), and Legerlotz (to M.E.). L.Z. received a scholarship from the China Scholarship Council (202006240090). ADNI data collection and sharing for this project was funded by ADNI (NIH National Institute of Aging (NIA) grant U01 AG024904) and DOD ADNI (Department of Defense award W81XWH-12-2-0012). ADNI is funded by the National Institute on Aging and the National Institute of Biomedical Imaging and Bioengineering, and through generous contributions from the following: AbbVie, Alzheimer's Association, Alzheimer's Drug Discovery Foundation, Araclon Biotech, BioClinica, Biogen, Bristol-Myers Squibb Company, CereSpir, Eisai, Elan Pharmaceuticals, Eli Lilly and Company, EuroImmun, F. Hoffmann-La Roche and its affiliated company Genentech, Fujirebio, GE Healthcare, IXICO, Janssen Alzheimer Immunotherapy Research & Development, Johnson & Johnson Pharmaceutical Research & Development, Lumosity, Lundbeck, Merck & Co, Meso Scale Diagnostics, NeuroRx Research, Neurotrack Technologies, Novartis Pharmaceuticals Corporation, Pfizer, Piramal Imaging, Servier, Takeda Pharmaceutical Company, and Transition Therapeutics. The Canadian Institutes of Health Research provides funds to support ADNI clinical sites in Canada. Private sector contributions are facilitated by the Foundation for the National Institutes of Health (www.fnih.org). The grantee organization is the Northern California Institute for Research and Education, and the study is coordinated by the Alzheimer's Disease Cooperative Study at the University of California, San Diego. ADNI data are disseminated by the Laboratory for Neuro Imaging at the University of Southern California. The 18F-AV-1451-A05 study was sponsored by Avid Radiopharmaceuticals, a wholly owned subsidiary of Eli Lilly and Company. The BioFINDER-1 study was supported by the Swedish Research Council (2022-00775), ERA PerMed (ERAPERMED2021-184), the Knut and Alice Wallenberg Foundation (2017-0383), the Strategic Research Area MultiPark (Multidisciplinary Research in Parkinson's Disease) at Lund University, the Swedish Alzheimer Foundation (AF-980907), the Swedish Brain Foundation (FO2021-0293), the Parkinson Foundation of Sweden (1412/22), the Cure Alzheimer's fund, the Konung Gustaf V:s och Drottning Victorias Frimurarestiftelse, the Skåne University Hospital Foundation (2020-O000028), Regionalt Forskningsstöd (2022-1259), and the Swedish federal government under the ALF agreement (2022-Projekt0080). Doses of flutemetamol injection were sponsored by GE Healthcare. The precursor of flortaucipir was provided by Avid Radiopharmaceuticals. Open Access funding enabled and organized by Projekt DEAL.

Author Contributions

M.E. and N.F. contributed to the conception and design of the study. All authors contributed to the acquisition and analysis of data. L.Z., M.E., and N.F. contributed to drafting the manuscript and preparing the figures.

Potential Conflicts of Interest

The ^{18}F-flortaucipir tracer was licensed by Avid Radiopharmaceuticals, a wholly owned subsidiary of Eli Lilly and Company. I.A.H., D.O.S., S.S., and M.J.P. are employees of Eli Lilly and Company. M.E., N.F., and O.H. have received research funding from Eli Lilly and Company. The other authors report no conflicts of interests.

Data Availability

The data can be made available upon reasonable request to the study-specific principal investigator of A05 (Avid Radiopharmaceuticals, a wholly owned subsidiary of Eli Lilly and Company) and BioFINDER-1 (O.H.) or according to the data access stipulations of the open-access data banks of ADNI, AHBA, and HCP.

References

1. Xia C, Makaretz SJ, Caso C, et al. Association of in vivo [18F] AV-1451 tau PET imaging results with cortical atrophy and symptoms in typical and atypical Alzheimer disease. JAMA Neurol 2017;74: 427–436.

2. Braak H, Alafuzoff I, Arzberger T, et al. Staging of Alzheimer disease-associated neurofibrillary pathology using paraffin sections and immunocytochemistry. Acta Neuropathol 2006;112: 389–404.

3. Franzmeier N, Dewenter A, Frontzkowski L, et al. Patient-centered connectivity-based prediction of tau pathology spread in Alzheimer's disease. Sci Adv 2020;6:eabd1327.

4. Vogel JW, Young AL, Oxtoby NP, et al. Four distinct trajectories of tau deposition identified in Alzheimer's disease. Nat Med 2021;27: 871–881.

5. Bejanin A, Schonhaut DR, la Joie R, et al. Tau pathology and neurodegeneration contribute to cognitive impairment in Alzheimer's disease. Brain 2017;140:3286–3300.

6. Brier MR, Gordon B, Friedrichsen K, et al. Tau and Aβ imaging, CSF measures, and cognition in Alzheimer's disease. Sci Transl Med 2016;8:338ra66.
7. Calafate S, Buist A, Miskiewicz K, et al. Synaptic contacts enhance cell-to-cell tau pathology propagation. Cell Rep 2015;11:1176–1183.
8. Clavaguera F, Bolmont T, Crowther RA, et al. Transmission and spreading of tauopathy in transgenic mouse brain. Nat Cell Biol 2009;11:909–913.
9. Mudher A, Colin M, Dujardin S, et al. What is the evidence that tau pathology spreads through prion-like propagation? Acta Neuropathol Commun 2017;5:99.
10. Vogel JW, Iturria-Medina Y, Strandberg OT, et al. Spread of pathological tau proteins through communicating neurons in human Alzheimer's disease. Nat Commun 2020;11:2612.
11. Sepulcre J, Grothe MJ, d'Oleire Uquillas F, et al. Neurogenetic contributions to amyloid beta and tau spreading in the human cortex. Nat Med 2018;24:1910–1918.
12. Montal V, Diez I, Kim C-M, et al. Network tau spreading is vulnerable to the expression gradients of APOE and glutamatergic-related genes. Sci Transl Med 2022;14:eabn7273.
13. Lee WJ, Brown JA, Kim HR, et al. Regional Aβ-tau interactions promote onset and acceleration of Alzheimer's disease tau spreading. Neuron 2022;110:1932–1943.e5.
14. Grothe MJ, Sepulcre J, Gonzalez-Escamilla G, et al. Molecular properties underlying regional vulnerability to Alzheimer's disease pathology. Brain 2018;141:2755–2771.
15. He Z, Guo JL, McBride JD, et al. Amyloid-β plaques enhance Alzheimer's brain tau-seeded pathologies by facilitating neuritic plaque tau aggregation. Nat Med 2018;24:29–38.
16. DeVos SL, Corjuc BT, Commins C, et al. Tau reduction in the presence of amyloid-β prevents tau pathology and neuronal death in vivo. Brain 2018;141:2194–2212.
17. Wang L, Benzinger TL, Su Y, et al. Evaluation of tau imaging in staging Alzheimer disease and revealing interactions between β-amyloid and Tauopathy. JAMA Neurol 2016;73:1070–1077.
18. Ossenkoppele R, Rabinovici GD, Smith R, et al. Discriminative accuracy of [18F]flortaucipir positron emission tomography for Alzheimer disease vs other neurodegenerative disorders. JAMA 2018;320:1151–1162.
19. Weiner MW, Veitch DP, Aisen PS, et al. The Alzheimer's disease neuroimaging initiative 3: continued innovation for clinical trial improvement. Alzheimers Dement 2017;13:561–571.
20. Alzheimer's Disease Neuroimaging Initiative. ADNI General Procedures Manual, Available from: https://adni.loni.usc.edu/wp-content/uploads/2010/09/ADNI_GeneralProceduresManual.pdf.
21. Petersen RC, Aisen PS, Beckett LA, et al. Alzheimer's disease neuroimaging initiative (ADNI): clinical characterization. Neurology 2010;74:201–209.
22. Tierney MC, Fisher RH, Lewis AJ, et al. The NINCDS-ADRDA work group criteria for the clinical diagnosis of probable Alzheimer's disease: a clinicopathologic study of 57 cases. Neurology 1988;38:359.
23. Pontecorvo MJ, Devous MD Sr, Navitsky M, et al. Relationships between flortaucipir PET tau binding and amyloid burden, clinical diagnosis, age and cognition. Brain 2017;140:748–763.
24. Albert MS, DeKosky ST, Dickson D, et al. The diagnosis of mild cognitive impairment due to Alzheimer's disease: recommendations from the National Institute on Aging-Alzheimer's Association workgroups on diagnostic guidelines for Alzheimer's disease. Alzheimers Dement 2011;7:270–279.
25. McKhann GM, Knopman DS, Chertkow H, et al. The diagnosis of dementia due to Alzheimer's disease: recommendations from the National Institute on Aging-Alzheimer's Association workgroups on diagnostic guidelines for Alzheimer's disease. Alzheimers Dement 2011;7:263–269.
26. Pontecorvo MJ, Devous MD, Kennedy I, et al. A multicentre longitudinal study of flortaucipir (18F) in normal ageing, mild cognitive impairment and Alzheimer's disease dementia. Brain 2019;142:1723–1735.
27. Mattsson N, Smith R, Strandberg O, et al. Comparing 18F-AV-1451 with CSF t-tau and p-tau for diagnosis of Alzheimer disease. Neurology 2018;90:e388–e395.
28. Gertje EC, Dv W, Panizo C, et al. Association of Enlarged Perivascular Spaces and Measures of small vessel and Alzheimer disease. Neurology 2021;96:e193–e202.
29. American Psychiatric Association. *Diagnostic and statistical manual of mental disorders (third edition—revised): DSM-III-R*. Washington, DC, USA: Am Psychiatric Assoc, 1987.
30. Alzheimer's Disease Neuroimaging Initiative. ADNI Study Documents, Available from: http://adni.loni.usc.edu/methods/documents.
31. Grabner G, Janke AL, Budge MM, et al. Symmetric atlasing and model based segmentation: an application to the hippocampus in older adults. Med Image Comput Comput Assist Interv 2006;9:58–66.
32. Tustison NJ, Holbrook AJ, Avants BB, et al. The ANTs Longitudinal Cortical Thickness Pipeline2018.
33. Maass A, Landau S, Baker SL, et al. Comparison of multiple tau-PET measures as biomarkers in aging and Alzheimer's disease. Neuroimage 2017;157:448–463.
34. Schaefer A, Kong R, Gordon EM, et al. Local-global Parcellation of the human cerebral cortex from intrinsic functional connectivity MRI. Cereb Cortex 2018;28:3095–3114.
35. Vemuri P, Lowe VJ, Knopman DS, et al. Tau-PET uptake: regional variation in average SUVR and impact of amyloid deposition. Alzheimers Dement (Amst) 2017;6:21–30.
36. Jagust WJ, Landau SM, Koeppe RA, et al. The Alzheimer's disease neuroimaging initiative 2 PET Core: 2015. Alzheimers Dement 2015;11:757–771.
37. Yoon B, Guo T, Provost K, et al. Abnormal tau in amyloid PET negative individuals. Neurobiol Aging 2022;109:125–134.
38. Jenkinson M, Beckmann CF, Behrens TEJ, et al. Fsl. NeuroImage 2012;62:782–790.
39. Smith R, Puschmann A, Schöll M, et al. 18F-AV-1451 tau PET imaging correlates strongly with tau neuropathology in MAPT mutation carriers. Brain 2016;139:2372–2379.
40. Hansson O, Grothe MJ, Strandberg TO, et al. Tau pathology distribution in Alzheimer's disease corresponds differentially to cognition-relevant functional brain networks. Front Neurosci 2017;11:11.
41. Fischl B. FreeSurfer. NeuroImage 2012;62:774–781.
42. Lundqvist R, Lilja J, Thomas BA, et al. Implementation and validation of an adaptive template registration method for 18F-Flutemetamol imaging data. J Nucl Med 2013;54:1472–1478.
43. Thurfjell L, Lilja J, Lundqvist R, et al. Automated quantification of 18F-Flutemetamol PET activity for categorizing scans as negative or positive for brain amyloid: concordance with visual image reads. J Nucl Med 2014;55:1623–1628.
44. Smith SM, Beckmann CF, Andersson J, et al. Resting-state fMRI in the human connectome project. Neuroimage 2013;80:144–168.
45. Rubinov M, Sporns O. Complex network measures of brain connectivity: uses and interpretations. Neuroimage 2010;52:1059–1069.
46. Floyd RW. Algorithm 97: shortest path. Commun ACM 1962;5:345.
47. Shen EH, Overly CC, Jones AR. The Allen human brain atlas: comprehensive gene expression mapping of the human brain. Trends Neurosci 2012;35:711–714.
48. Gryglewski G, Seiger R, James GM, et al. Spatial analysis and high resolution mapping of the human whole-brain transcriptome for integrative analysis in neuroimaging. Neuroimage 2018;176:259–267.

49. Sjöstedt E, Zhong W, Fagerberg L, et al. An atlas of the protein-coding genes in the human, pig, and mouse brain. Science 2020; 367:eaay5947.

50. Váša F, Seidlitz J, Romero-Garcia R, et al. Adolescent tuning of association cortex in human structural brain networks. Cereb Cortex 2018;28:281–294.

51. Franzmeier N, Rubinski A, Neitzel J, et al. Functional connectivity associated with tau levels in ageing, Alzheimer's, and small vessel disease. Brain 2019;142:1093–1107.

52. Trabzuni D, Wray S, Vandrovcova J, et al. MAPT expression and splicing is differentially regulated by brain region: relation to genotype and implication for tauopathies. Hum Mol Genet 2012;21: 4094–4103.

53. Pichet Binette A, Franzmeier N, Spotorno N, et al. Ayloid-associated increases in soluble tau relate to tau aggregation rates and cognitive decline in early Alzheimer's disease. Nat Commun 2022;13:6635.

54. Palmqvist S, Scholl M, Strandberg O, et al. Earliest accumulation of beta-amyloid occurs within the default-mode network and concurrently affects brain connectivity. Nat Commun 2017;8:1214.

55. Braak H, Braak E. Neuropathological stageing of Alzheimer-related changes. Acta Neuropathol 1991;82:239–259.

56. Sanchez JS, Becker JA, Jacobs HIL, et al. The cortical origin and initial spread of medial temporal tauopathy in Alzheimer's disease assessed with positron emission tomography. Sci Transl Med 2021; 13:eabc0655.

57. Pooler AM, Polydoro M, Maury EA, et al. Amyloid accelerates tau propagation and toxicity in a model of early Alzheimer's disease. Acta Neuropathol Commun 2015;3:14.

58. Dincer A, Chen CD, McKay NS, et al. APOE epsilon4 genotype, amyloid-beta, and sex interact to predict tau in regions of high APOE mRNA expression. Sci Transl Med 2022;14:eabl7646.

59. Ferrari-Souza JP, Lussier FZ, Leffa DT, et al. APOEepsilon4 associates with microglial activation independently of Abeta plaques and tau tangles. Sci Adv 2023;9:eade1474.

60. Gordon EM, Laumann TO, Gilmore AW, et al. Precision functional mapping of individual human brains. Neuron 2017;95:791–807 e7.

61. Badhwar A, Tam A, Dansereau C, et al. Resting-state network dysfunction in Alzheimer's disease: a systematic review and meta-analysis. Alzheimers Dement (Amst) 2017;8:73–85.

62. Gratton C, Laumann TO, Nielsen AN, et al. Functional brain networks are dominated by stable group and individual factors, not cognitive or daily variation. Neuron 2018;98:439–452 e5.

63. Sun Y, Zhao Y, Hu K, et al. Distinct spatiotemporal subtypes of amyloid deposition are associated with diverging disease profiles in cognitively normal and mild cognitive impairment individuals. Transl Psychiatry 2023;13:35.

64. Collij LE, Salvadó G, Wottschel V, et al. Spatial-temporal patterns of beta-amyloid accumulation: a subtype and stage inference model analysis. Neurology 2022;98:e1692–e1703.

Supplemental material

Combined Connectomics, *MAPT* Gene Expression, and Amyloid Deposition to Explain Regional Tau Deposition in Alzheimer's Disease

Lukai Zheng, MD, MMed; Anna Rubinski, PhD; Jannis Denecke, MSc; Ying Luan, MD, PhD; Ruben Smith, MD, PhD; Olof Strandberg, PhD; Erik Stomrud, MD, PhD; Rik Ossenkoppele, PhD; Diana Otero Svaldi, PhD; Ixavier Alonzo Higgins, PhD; Sergey Shcherbinin, PhD; Michael J. Pontecorvo, PhD; Oskar Hansson, MD, PhD; Nicolai Franzmeier, PhD; Michael Ewers, PhD for the Alzheimer's Disease Neuroimaging Initiative (ADNI)

Supplementary Figure 1. Group-average ^{18}F-flortaucipir *z*-score maps in clinically defined subgroups of amyloid-positive participants.

Supplementary Figure 2. Association between ^{18}F-flortaucipir and gene expression across 2,098 genes that are highly expressed in the brain.

Supplementary Figure 3. Model performance in explaining group-average ^{18}F-flortaucipir maps in clinically defined subgroups.

Supplementary Figure 4. Prediction of participant-level ^{18}F-flortaucipir *z*-score in clinical subgroups.

Supplementary Figure 1. Group-average ^{18}F-flortaucipir *z*-score maps in clinically defined subgroups of amyloid-positive participants.

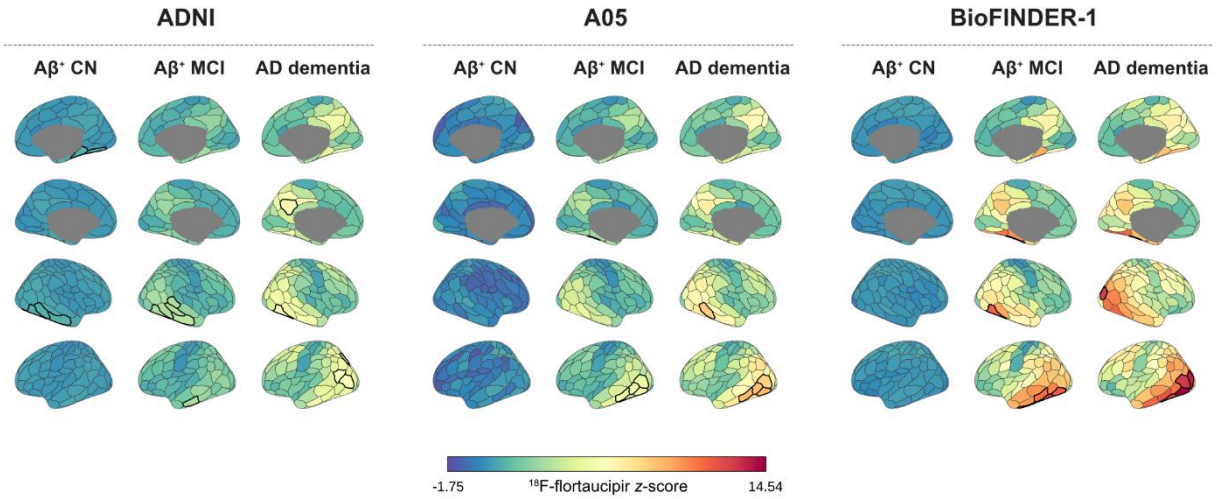

Tau epicenters (six ROIs with the highest ^{18}F-flortaucipir *z*-score) are shown in bold black contours. *$A\beta^-$ = amyloid negative; $A\beta^+$ = amyloid positive; CN = cognitively normal; MCI = mild cognitive impairment.*

Supplementary Figure 2. Association between ^{18}F-flortaucipir and gene expression across 2,098 genes that are highly expressed in the brain.

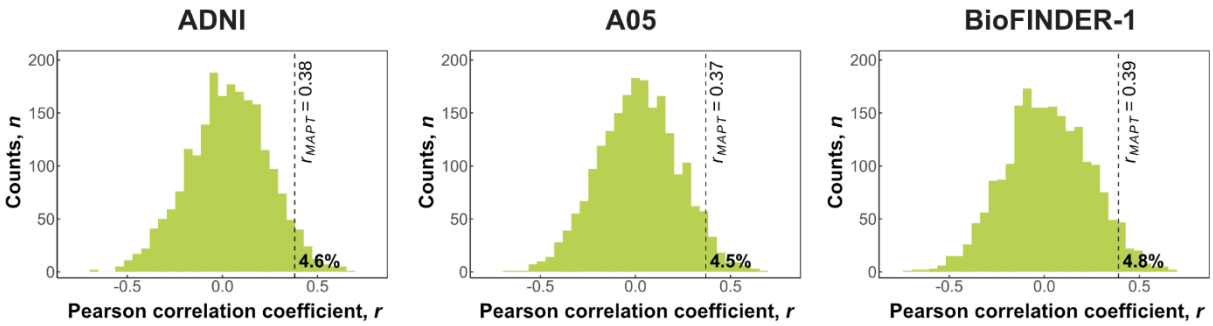

The vertical dotted lines indicate the percentiles of the correlation coefficients for the associations between *MAPT* gene expression vs ^{18}F-flortaucipir *z*-scores for each of the three studies.

Supplementary Figure 3. Model performance in explaining group-average ^{18}F-flortaucipir maps in clinically defined subgroups.

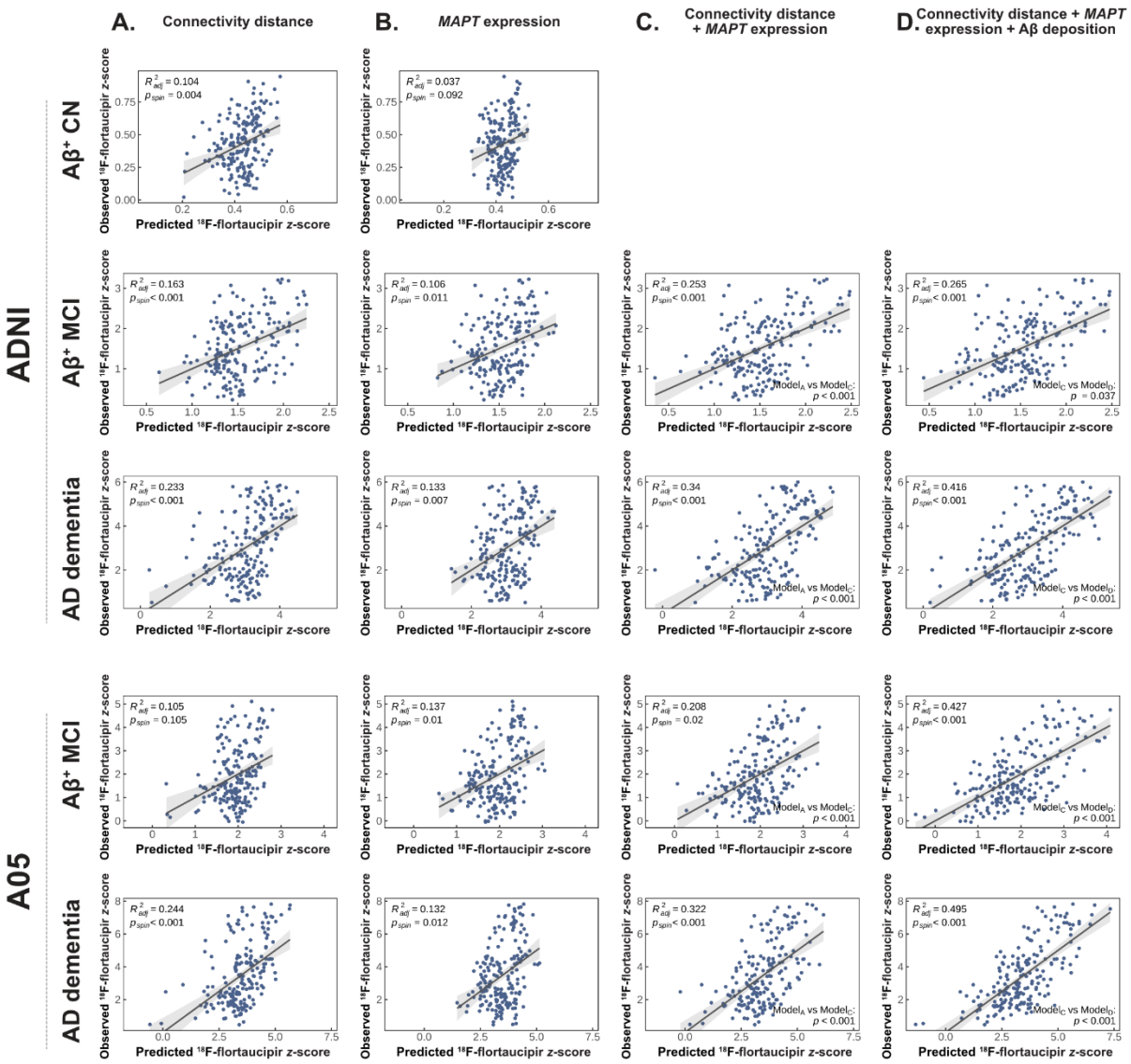

Regression plots showing the associations between the predicted and observed ^{18}F-flortaucipir *z*-scores stratified by clinical subgroup (rows) and statistical model (columns). The models included epicenter-connectivity distance (A), regional *MAPT* expression (B), or the combination of connectivity plus *MAPT* expression (C) plus amyloid-PET (D), assessed in amyloid-positive participants from ADNI and A05. R^2_{adj} *= adjusted proportion variance explained;* p_{spin} *= spatial autocorrelation-corrected p value for spin-based permutation testing.*

Supplementary Figure 4. Prediction of participant-level ^{18}F-flortaucipir *z*-scores in clinical subgroups.

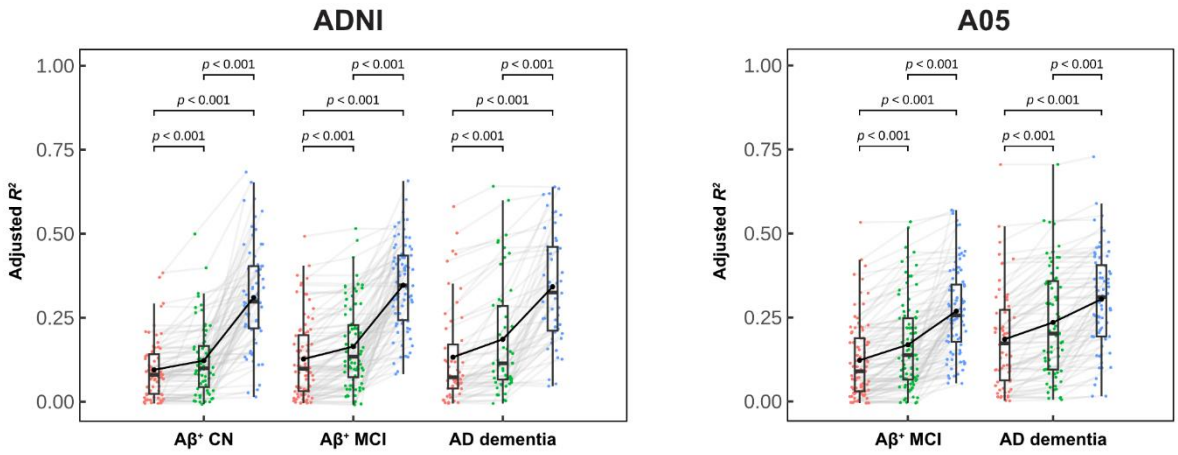

Box plots showing the adjusted R^2 for each statistical prediction model stratified by clinical subgroup and statistical model for explaining patient-level ^{18}F-flortaucipir *z*-scores. The statistical models included connectivity-only models (red dots), connectivity and *MAPT* expression (green dots), and all three modalities combined (blue dots). Participant-level adjusted R^2 values were compared between models using paired *t* tests. *Aβ⁺ = amyloid positive; CN = cognitively normal; MCI = mild cognitive impairment.*

Manuscript II

Florbetapir PET-assessed demyelination is associated with faster tau accumulation in an *APOE ε4*-dependent manner

European Journal of Nuclear Medicine and Molecular Imaging (2024) 51:1035–1049
https://doi.org/10.1007/s00259-023-06530-8

ORIGINAL ARTICLE

Florbetapir PET-assessed demyelination is associated with faster tau accumulation in an APOE ε4-dependent manner

Anna Rubinski[1] · Anna Dewenter[1] · Lukai Zheng[1] · Nicolai Franzmeier[1] · Henry Stephenson[2] · Yuetiva Deming[2] · Marco Duering[1,3] · Benno Gesierich[3] · Jannis Denecke[1] · An-Vi Pham[1,4] · Barbara Bendlin[2] · Michael Ewers[1,5] · for the Alzheimer's Disease Neuroimaging Initiative

Received: 18 May 2023 / Accepted: 14 November 2023 / Published online: 5 December 2023

Abstract

Purpose The main objectives were to test whether (1) a decrease in myelin is associated with enhanced rate of fibrillar tau accumulation and cognitive decline in Alzheimer's disease, and (2) whether apolipoprotein E (APOE) ε4 genotype is associated with worse myelin decrease and thus tau accumulation.

Methods To address our objectives, we repurposed florbetapir-PET as a marker of myelin in the white matter (WM) based on previous validation studies showing that beta-amyloid (Aβ) PET tracers bind to WM myelin. We assessed 43 Aβ-biomarker negative (Aβ−) cognitively normal participants and 108 Aβ+ participants within the AD spectrum with florbetapir-PET at baseline and longitudinal flortaucipir-PET as a measure of fibrillar tau (tau-PET) over ~ 2 years. In linear regression analyses, we tested florbetapir-PET in the whole WM and major fiber tracts as predictors of tau-PET accumulation in a priori defined regions of interest (ROIs) and fiber-tract projection areas. In mediation analyses we tested whether tau-PET accumulation mediates the effect of florbetapir-PET in the whole WM on cognition. Finally, we assessed the role of myelin alteration on the association between APOE and tau-PET accumulation.

Results Lower florbetapir-PET in the whole WM or at a given fiber tract was predictive of faster tau-PET accumulation in Braak stages or the connected grey matter areas in Aβ+ participants. Faster tau-PET accumulation in higher cortical brain areas mediated the association between a decrease in florbetapir-PET in the WM and a faster rate of decline in global cognition and episodic memory. APOE ε4 genotype was associated with a worse decrease in the whole WM florbetapir-PET and thus enhanced tau-PET accumulation.

Conclusion Myelin alterations are associated in an APOE ε4 dependent manner with faster tau progression and cognitive decline, and may therefore play a role in the etiology of AD.

Keywords Myelin · Florbetapir-PET · Tau · APOE

✉ Michael Ewers
Michael.ewers@med.uni-muenchen.de

1 Institute for Stroke and Dementia Research, University Hospital, Ludwig-Maximilian-University Munich, Munich, Germany

2 Department of Medicine, School of Medicine and Public Health, University of Wisconsin- Madison, Madison, WI, USA

3 Medical Image Analysis Center (MIAC) and Department of Biomedical Engineering, University of Basel, Basel, Switzerland

4 Department of Neuroradiology, School of Medicine, Technical University of Munich, Munich, Germany

5 German Center for Neurodegenerative Diseases (DZNE), Munich, Germany

Introduction

Alzheimer's disease (AD) is the major cause of age-related dementia. The disease defining pathologies are beta-amyloid (Aβ) plaques and neurofibrillary tau tangles. In particular, fibrillar tau is associated with neurodegeneration and cognitive decline [1], and is thus a key pathology driving clinical progression. During the course of AD, fibrillar tau preferentially progresses between connected brain regions [2, 3], suggesting that tau spreads along axonal connections [4, 5]. The spatial pattern of regional tau progression resembles the level of myelination of the connecting fibers, where regions connected by ontogenetically lower myelinated fiber tracts show higher susceptibility to tau deposition [6, 7]. These

findings suggest that lower myelination may provide a vulnerability factor to the development of tau pathology in AD.

In patients with AD, myelin in the white matter (WM) is reduced as detected by single-cell transcriptomics of myelinating oligodendrocytes [8, 9], histochemical staining [8–10], and neuroimaging [11–13] of myelin alterations. In transgenic mouse models of Aβ and tau pathology, myelin alterations can be observed before the overt occurrence of amyloid plaques and fibrillar tau [14, 15]. Taken together, these observations raise the possibility that myelin alterations are associated with the formation of fibrillar tau in AD [16, 17]. However, it remains to be addressed whether in patients with AD, a decrease in myelin is associated with the progression of tau deposition. Therefore, our first major aim was to test the association between lower degree of myelin in fiber tracts and higher rates of tau-accumulation in the connected grey matter (GM) areas. Motivated by previous observations that those regions connected by ontogenetically lower myelinated fiber tracts are more susceptible to tau accumulation in AD [6, 7], our auxiliary aim was to test whether any association between myelin impairment and tau accumulation in patients with AD is particularly pronounced for typically lower myelinated fiber tracts.

In order to address these aims, we combined florbetapir-PET for the measurement of myelin with longitudinal assessment of fibrillar tau accumulation in a sample of clinically well-characterized patients with biomarker evidence of AD [18]. Florbetapir-PET was originally developed for the assessment of amyloid plaques [19], but — among other amyloid-sensitive PET tracers — has been recently repurposed for the assessment of myelin in the brain [20]. Amyloid-PET tracers may bind not only to the beta-sheet structure of fibrillar Aβ, but also to that of myelin-binding protein [21], enabling the quantification of myelin in the brain [22].

Our second major aim was to test whether the association between WM myelin and tau pathology is modulated by the presence of the APOE ε4 allele, i.e., the most important genetic risk factor of AD [23, 24]. The rationale for this aim is that APOE is the main transporter protein of cholesterol [25], i.e., a major component of myelin [26]. The APOE ε4 polymorphism was associated with reduced cholesterol biosynthesis in myelinating oligodendrocytes [27] and accelerated myelin reduction in normal aging [28, 29]. APOE ε4 expression in a transgenic mouse model of AD was associated with a substantial loss of myelin and increased tau pathology [30], suggesting that APOE ε4 is linked to tau pathology potentially via myelin alterations. In humans, APOE ε4 was strongly associated with increased levels of amyloid deposition in the brain [31]; however, APOE ε4 was also associated with higher tau accumulation independently from its effect on amyloid deposition in AD [32]. Therefore, our aim was to test whether myelin alterations assessed by florbetapir PET interact with APOE ε4 status to influence the rate of tau-PET increase.

Methods

ADNI participants

We included a sample of 151 participants from the Alzheimer's Disease Neuroimaging Initiative (ADNI; http://adni.loni.usc.edu/), including a control group with 43 CN Aβ− participants and 108 participants within the AD spectrum consisting of 56 CN Aβ+, 32 MCI Aβ+, and 20 Aβ+ AD dementia. ADNI is a prospective multicenter study on biomarker and neuroimaging changes in AD [18]. The inclusion criteria for the current study beyond those of ADNI were the availability of T1-weighted MRI, FLAIR, [^{18}F]-florbetapir amyloid-PET, at least 2 measures of [^{18}F]-flortaucipir tau-PET (for follow-up duration see Table 1) and cognitive measures. In addition, participants were selected based on the inclusion in either a control group of CN Aβ− or AD spectrum group with abnormally elevated amyloid deposition (Aβ+). The Aβ+ was defined as a global standardized uptake value ratio (SUVR) cutoff > 1.11 for [^{18}F]-florbetapir-PET as established previously [33]. Participants were clinically diagnosed as cognitively normal (CN, Mini-Mental State Exam (MMSE) > 24, Clinical Dementia Rating (CDR) = 0, nondepressed), mildly cognitively impaired (MCI, MMSE > 24, CDR = 0.5, objective memory loss on the education adjusted Wechsler Memory Scale II, preserved activities of daily living), or demented (AD, MMSE of 20 to 26, CDR > 0.5, NINCDS/ADRDA criteria for probable AD).

Ethical approval was obtained by the ADNI investigators at each participating ADNI site. All participants provided written informed consent.

MRI acquisition and processing

MRI scans were performed on different 3T MRI scanners using standardized scanning protocols (detailed scan protocols can be found on https://adni.loni.usc.edu/wp-content/uploads/2017/07/ADNI3-MRI-protocols.pdf). T1w images were acquired using a 3D MPRAGE sequence with 1 mm isotropic voxel-size and a TR = 2300 ms. Fluid-attenuated inversion recovery (FLAIR) images were acquired using a 3D FLAIR sequence with 1.2×1×1 mm voxel-size and TR = 4800 ms.

Using the Advanced Normalization Tools (ANTs) longitudinal cortical thickness pipeline [34, 35], T1-weighted images underwent bias field correction, followed by brain extraction and non-linear normalization to MNI space through a high-dimensional warping algorithm [34, 35]. Using the estimated normalization parameters, we further

European Journal of Nuclear Medicine and Molecular Imaging (2024) 51:1035–1049

Table 1 Sample characteristics

	Control	AD spectrum		
	CN Aβ− (*n*=43)	CN Aβ+ (*n*=56)	MCI Aβ+ (*n*=32)	AD Aβ+ (*n*=20)
Age, year	72.6 (7.1)	76.2 (7.0)	76.1 (6.7)	77.5 (9.9)
Sex (M/F)	18M/25F	23M/33F	17M/15F	11M/9F
Education, year	16.5 (2.4)	16.7 (2.2)	16.7 (2.5)	14.6 (2.3)
ADAS13 score	7.2 (2.9)	8.8 (5.2)	17.2 (6.6)	30.7 (9.8)
ADNI-MEM score	1.2 (0.5)	1.0 (0.7)	0.0 (0.6)	-0.9 (0.6)
APOE ε4 carriers −/+[a]	30-/13+	26-/30+	7-/24+	11-/8+
Global AV45-PET SUVR	1.0 (0.0)	1.3 (0.2)	1.4 (0.1)	1.5 (0.2)
Global tau-PET SUVR[b]	0.9 (0.0)	0.9 (0.1)	1.0 (0.1)	1.0 (0.2)
Tau-PET follow-up time, year	2.7 (1.3)	2.3 (1.2)	1.9 (1.0)	1.7 (0.7)
WMH volume (ml)[c]	2.4 (3.4)	6.2 (9.8)	11.0 (24.8)	14.0 (28.3)
Global WM SUVR[c]	2.1 (0.2)	2.3 (0.2)	2.1 (0.3)	2.1 (0.2)

Aβ amyloid-beta, *AD* Alzheimer's disease, *APOE* apolipoprotein E, *CN* cognitive normal, *F* female, *M* male, *MCI* mild cognitive impairment, *MMSE* Mini-Mental State Exam

[a]APOE status is missing for one MCI and one AD dementia participants. The mean and standard deviation (in brackets) are shown for each continuous variable

[b]Global Tau-PET at baseline, using eroded WM as reference region

[c]Raw, non-transformed data

transformed the Desikan-Killiany atlas (Desikan et al., 2006) and the reference regions for intensity normalization of PET images from MNI space to native space.

PET acquisition and processing

Tau-PET was recorded in 6×5 min frames, 75-105 min post-injection of [^{18}F]flortaucipir. Amyloid-PET was recorded in 4 × 5 min frames, 50–70 min post injection of [^{18}F]florbetapir. PET images were realigned, averaged, and further standardized with respect to the orientation, voxel size and intensity by the ADNI PET core [36].

Tau-PET images were rigidly co-registered to the participant's T1-weighted image and Tau-PET SUVRs were computed by normalizing the tau-PET images to the mean tau-PET tracer uptake of the eroded white matter reference region, based on recent recommendations for longitudinal tau-PET assessments [37, 38]. Because tau-PET uptake in the white matter reference region can be altered in AD [39], we also computed tau-PET SUVRs using the inferior cerebellar grey as an alternate reference region [37]. ROI-level tau-PET SUVRs were computed for three a priori established composite regions including Braak 1 (entorhinal), Braak 3+4 (limbic) and Braak 5+6 (neocortical), as defined by the Braak post-mortem staging of tau pathology [40]. The Braak-stage 2 region (hippocampus) was not included due to potential spill-in from known off-target binding of the flortaucipir tracer in the choroid plexus [41]. In addition, global tau-PET SUVRs were determined as the average of neocortical tau-PET SUVRs across multiple cortical regions within temporal, parietal, and frontal lobes as specified previously by us [42]. Tau-PET SUVR measures were log-transformed prior to analysis to approximate a normal distribution.

Myelin in white matter

Assessment of global myelin

The florbetapir-PET images were acquired up to 1 year spaced apart from the first tau-PET scan and cognitive assessment. In order to derive masks to compute global white matter (WM) measures of florbetapir-PET, we first segmented the T1-weighted images using SynthSeg [43]. For each participant, we generated WM and GM masks in native space by thresholding and binarizing the estimated tissue segmentation at a threshold of 0.5 for WM to be consistent with a previous publication using florbetapir-PET signal as a proxy of myelin [13]and a threshold of 0.3 for GM which is commonly used and is consistent with our previous publications [7, 44]. We eroded the WM mask so that voxels within 1-mm distance from any non-WM voxel were excluded. In addition, for each participant, we derived a normal appearing white matter (NAWM) mask and white matter hyperintensities (WMH) mask.

WMH were segmented using a fully automated, deep learning algorithm based on multi-dimensional gated recurrent units [45] (https://github.com/miac-research/mdgru) with 3D FLAIR and 3D T1w images as inputs. Small WMH clusters with fewer than 5 voxels were excluded. For each

participant, we generated NAWM masks by subtracting the WMH binary masks from the WM masks.

Florbetapir-PET images were rigidly co-registered to the participant's T1-weighted images in native space and intensity normalized with the cerebellar grey as the reference regions, resulting in SUVR values [13]. Finally, using the individual WM, NAWM, WMH, or GM masks we computed the median florbetapir-PET SUVR values within each mask for each individual. For all further SUVRs calculations, we have used the median and not the mean as the median is more robust to outliers.

Assessment of regional fiber-tract myelin and tau-PET in projection zones

Next, we extracted florbetapir-PET SUVRs from fiber-tract ROIs. To this end, we employed an unbiased fiber orientation distribution (FOD) template using a similar approach as previously described [46]. Specifically, we analyzed multi-shell diffusion data from 45 individuals included in ADNI across the AD continuum and performed multi-tissue constrained spherical deconvolution to build the FOD template. We applied TractSeg, a deep learning-based method for automated white matter bundle segmentation, based on the FOD template to construct 72 anatomically well-established white matter fiber tracts [47]. We excluded fiber tracts located in the cerebellum and the pons as we were interested in tracts with cortical projections. In addition, we excluded the fornix due to CSF partial-volume effects that rendered the tracking unreliable. This procedure resulted in a final sample of 58 white matter fiber tracts (see supplementary Table 1 for a list of fiber tracts included in the current study).

We estimated the normalization parameters from T1-weighted images to FOD template space, using non-linear spatial normalization with ANTs [34]. Florbetapir-PET SUVR images were then spatially normalized to FOD template space using the ANTs-derived normalization parameters. We then derived median florbetapir-PET SUVRs from each of the 58 white-matter fiber tracts for each participant, by superimposing the florbetapir-PET SUVR images onto the fiber tracts and sampling the voxels along the streamlines using MRtrix3 [48].

To assess regional associations between tract-specific florbetapir-PET SUVRs and regional tau pathology, we determined regional tau-PET SUVRs in cortical GM projection areas of each of the fiber tracts. To this end, we used masks from the beginning and ending of the fiber tracts as obtained by TractSeg [47]. Using the ANT-derived normalization parameters, we spatially normalized the cortical GM projection area masks to MNI space. The spatially normalized masks were further masked with a cortical GM mask and applied to the tau-PET SUVR images in MNI space to extract the median regional tau-PET SUVRs in each cortical GM projection area.

Finally, in order to assess the normal myelin levels in cognitively normal individuals for the 58 white-matter fiber tracts, we employed a myelin water fraction (MWF) template derived from young to middle-age healthy adults (mean age = 25 years) [49]. We spatially normalized the MWF template from MNI space to FOD template space using the ANTs-derived normalization parameters. We then derived median MWF levels along each of the fiber tracts, by superimposing the MWF template onto the fiber tracts and sampling the voxels along the streamlines using MRtrix3 [48]. The tract-specific effect size of the associations between florbetapir-PET SUVR in the fiber tracts and tau-PET SUVR changes in the tract's projection zones in the AD spectrum group were projected onto the fiber-tract map of MWF to test the hypothesis that late-developing normally lower-myelinated fiber tracts (as assessed in the healthy individuals) are prone to exhibit a stronger effect of myelin alterations on tau deposition in AD.

APOE genotyping

APOE allele counts were provided by ADNI, and participants were classified as APOE ε4 carriers when at least one ε4 allele was detected, otherwise participants were classified as APOE ε4 non-carriers. In addition, we calculated a neuropathology-based weighted risk score for APOE (APOE-npscore) as previously described [50]. Briefly, to generate the APOE-npscore we weighted the different allele combinations (including ε2, ε3, ε4 alleles) by the natural log (ln) transformed odds ratios of the association of each allele combination with the risk of brain-autopsy confirmed cases with AD [51]. This yields a neuropathology-validated pseudo-continuous APOE risk score that was previously shown to be more sensitive to predict AD progression compared to alternative forms of APOE scores, such as the binary classification into APOE ε4 carriers vs non-carriers [50].

Neuropsychological measures

To assess global cognition we used the extended Alzheimer's Disease Assessment Scale (ADAS13), which is an extension of the 11-item cognitive subscale of the ADAS [52], including an additional test of delayed word recall and number cancellation [53]. To assess memory performance we used the pre-established composite memory score ADNI-MEM [54], which includes the Rey Auditory Verbal Learning Test, the ADAS, the Wechsler Logical Memory I and II, and the word recall of the MMSE [54].

Statistical analysis

Adjustment of florbetapir-PET SUVRs

Our main predictor variable was florbetapir-PET SUVR in the WM as a measure of myelin. In order to reduce any influence of florbetapir binding to amyloid-plaques in the GM on the florbetapir binding in the WM, we adjusted the WM florbetapir SUVR as previously described [13]. Briefly, we fitted a linear regression model with the global GM florbetapir-PET SUVR as the predictor and the global florbetapir-PET SUVR in the WM as the dependent variable in the CN group including both Aβ+ and Aβ- participants. We then adjusted the florbetapir-PET SUVRs in the WM for the GM florbetapir-PET signal by subtracting the predicted SUVRs (using the estimated linear models) from each observed global SUVR in the WM. Furthermore, in order to quantify to what extent, the florbetapir-PET SUVR in the WM of the symptomatic Aβ+ participants deviate from those in the CN group, we computed z scores of WM florbetapir-PET SUVRs, using the CN group as a reference. For sensitivity analyses we computed florbetapir z scores also for NAWM and WMH (for distribution see Supplementary Figure 1). For fiber-tract level analyses, we performed the same procedure using fiber tract-specific florbetapir-PET SUVRs as the dependent variables. All subsequent analyses were conducted based on the florbetapir z scores in the WM.

Association between florbetapir z scores in the WM and tau accumulation rates

In our main analysis, we tested whether a decrease in myelin levels in the WM is associated with higher rates of change in tau-PET. To this end, we first determined the subject-level annual rate of change in tau-PET, using a previously established approach [55]. We fitted linear mixed effects models with tau-PET SUVR as the dependent variable, time from baseline as the independent variable, with random slope and intercept. Using the thus estimated rates of change of tau-PET as the dependent variables, we tested in a linear regression analyses the global florbetapir z scores in the WM as the predictor. In sensitivity analyses, we tested whether global florbetapir z score alterations in areas of WMH are driving the results. We thus repeated the regression analyses, this time using florbetapir z scores within either the NAWM or WMH as predictors of the rates of change of tau-PET.

Association between florbetapir z scores in the WM and cognitive decline & mediation analysis

In order to assess whether a decrease in myelin levels in the WM is associated with faster cognitive decline, we calculated the rate of change in cognitive measures (including composite scores ADNI-MEM and ADAS13) using linear-mixed effect models as mentioned above. Using linear regression, we tested global florbetapir z scores in the WM as a predictor of change rate in cognitive measures. To test whether the association between myelin and changes in cognition were mediated via changes in tau-PET, we conducted mediation analyses. To that end we treated the global florbetapir z scores in the WM as the predictor, change rate in global tau-PET as a mediator, and ADNI-MEM or ADAS13 scores as outcomes. The significance of the mediation was assessed using 1000 bootstrapped iterations, as implemented in the "mediation" R package [56]. The effect size of the mediated effect was computed as the proportion of the average causal mediation effect to the total effects expressed as percentage [56].

Association between fiber tract-level florbetapir z scores and tau-PET accumulation in connected brain areas

In the next step, we assessed the regional associations between fiber tract-specific myelin and tau-PET changes in projection areas. To that end, for each fiber tract, we first computed the association between fiber tract-specific florbetapir z scores and tau-PET changes in the connected areas for each fiber tract, and the resulting distribution of β-values was tested against zero, using a one-sample t-test. Next, in order to test the hypothesis that the association between myelin alterations and tau change is particularly pronounced in ontogenetically less myelinated fiber tracts, we computed a spatial correlation between the fiber-tract β-values from the fiber tract-specific regressions and the fiber tract-specific MWF values from the MWF template of healthy individuals [49].

The effect of APOE ε4 on the association between florbetapir z scores in the WM and tau-PET accumulation

Finally, we assessed the role of APOE using an ANCOVA analysis where APOE ε4 status was tested as a predictor of global florbetapir z scores in the WM or tau-PET changes. To test whether the association between APOE ε4 status and tau-PET changes is mediated via global

florbetapir z scores in WM, we conducted a mediation analysis. To that end we treated the APOE ε4 status as the predictor, global florbetapir z scores in WM as a mediator, and tau-PET changes as the outcome. We next tested whether APOE ε4 status modulates the association between myelin and tau change by testing the interaction APOE ε4 status by global florbetapir z scores in the WM on tau-PET changes.

All above-mentioned models were controlled for age, sex, education, diagnosis, cortical florbetapir-PET SUVR, maximum follow-up duration, and time difference between florbetapir scan and tau-PET/cognitive measures. In addition, as sensitivity analyses to control for baseline severity of tau pathology, we controlled all above-mentioned models for the global tau-PET levels at baseline. All statistical analyses were performed using R statistical software (http://www.R-project.org). P-values were considered significant when meeting the α-threshold of 0.05. In the current study we chose not to implement correction for multiple comparisons in accordance with statistical guidelines that advise against utilizing correction for multiple comparisons in studies with a limited number of planned comparisons and are hypothesis driven [57].

Results

We included a total of 108 participants on the AD continuum (Aβ+ CN/MC/AD) and 43 control participants (Aβ- CN) with longitudinal tau-PET and a baseline florbetapir-PET measure. Sample characteristics are shown in Table 1.

Lower florbetapir PET in the WM is associated with higher tau accumulation rates

First, we addressed our aim to test whether a decrease in myelin levels in the WM is associated with higher tau-PET accumulation in participants within the AD spectrum (Aβ+ participants, Table 1). We found that lower florbetapir z scores in the global WM were significantly associated with higher rates of subsequent tau-PET accumulation in higher cortical areas among Aβ+ participants (Braak 3+4: β=−0.291, p=0.002; Braak 5+6: β=−0.181, p=0.048; Fig. 1) but not in the entorhinal cortex (Braak 1, β=−0.191, p=0.079; Fig. 1). Note that these and all subsequent analyses were controlled for florbetapir binding in the GM — among other covariates — to partial out any influence of amyloid plaque deposition in the GM. As expected, no associations were observed in the control group consisting of cognitively normal (CN) participants without biomarker evidence of elevated Aβ deposition (CN Aβ−, Braak 1: β=−0.103, p=0.6; Braak 3+4: β=−0.157, p=0.4; Braak 5+6: β=−0.162, p=0.4). These results suggest that reduced myelin levels in the WM are associated with faster rates of tau accumulation in subjects with biomarker evidence of AD.

When controlling the analyses for baseline global tau-PET levels, we confirmed a significant association between the florbetapir z scores in the WM and the rate of change of tau-PET in Braak stage 1 (β=−0.219, p = 0.049) and Braak stage 3+4 (β=−0.124, p = 0.036).

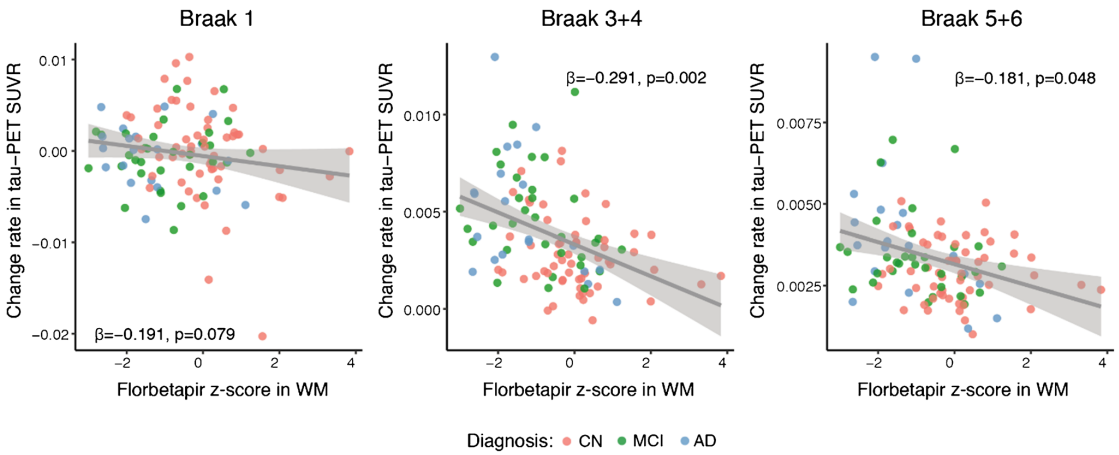

Fig. 1 Association between florbetapir z scores in WM and change rate in tau-PET SUVRs. The scatterplots show the associations between florbetapir z scores in WM and change rate in tau-PET SUVRs for Aβ+ participants. Observations are color-coded by diagnosis and standardized β-values with p-values are displayed. AD = Alzheimer's disease; CN = Cognitive normal; MCI = Mild cognitive impairment; WM = White matter

As sensitivity analyses, we repeated these analyses using a cerebellar reference region instead of the white matter reference region for the calculation of tau-PET SUVRs. We found consistent results where lower florbetapir *z* scores in the global WM were significantly associated with higher rates of subsequent tau-PET accumulation in all Braak stages among Aβ+ participants (Braak 1: β=−0.258, p=0.018, Braak 3+4: β=−0.309, p=0.0008; Braak 5+6: β=−0.227, p=0.011; Supplementary Figure 1).

Florbetapir uptake was significantly reduced in WMH areas compared to those within the NAWM (t(295)=7.024, $p < 0.001$), replicating previous findings [13]. Next, we tested whether the observed association between florbetapir *z* scores in the WM and tau-PET accumulation depends on the presence of WMH. To this end, we extracted the global florbetapir *z* scores in areas of WMH, or alternatively exclusively in the NAWM excluding WMH. Consistent with the results for the whole WM, lower global florbetapir *z* scores both in the WMH and NAWM were associated with higher tau-PET accumulation in higher cortical regions among the Aβ+ participants (Supplementary Figure 2), suggesting that the association between florbetapir *z* scores in the WM and tau-PET accumulation was not exclusively driven by WMH.

Lower florbetapir PET in the WM was associated with cognitive decline via tau accumulation

Next, we tested the association between the decrease in myelin and the rate of cognitive decline. We found that lower global florbetapir *z* scores in the WM were significantly associated with a faster decline in memory performance (ADNI-MEM: β=0.182, p=0.021; Fig. 2A) and global cognition (ADAS13: β=−0.151, p=0.047; Fig. 2B). Using bootstrapped mediation analyses, we found that higher rates of global tau-PET accumulation mediated the effect of lower global florbetapir *z* scores in the WM on the rate of change in memory (ADNI-MEM: β=0.063 [95% CI: 0.01, 0.133], p=0.014, proportion mediated = 33.8%; Fig. 2C) and global cognition (ADAS13: β=−0.095 [95% CI: −0.180, −0.015], p=0.026, proportion mediated = 63.8%; Fig. 2D), suggesting that the effect of myelin on tau explains the association between demyelination and faster cognitive decline.

Fiber tract-level florbetapir PET was associated with tau-PET accumulation in connected brain areas

In the next step, we tested whether there is a spatial correspondence between fiber tract-level alterations in florbetapir *z* scores and tau-PET accumulation in the connected GM regions. To this end, we extracted the florbetapir *z* scores in each of the 58 major well-established fiber tracts and tau-PET change rates in each of the tracts' cortical projection areas in each participant. For each fiber tract, we regressed the rate of tau accumulation in the tract's projection area on the tract-level florbetapir *z* scores. In a second-level analysis, we found that the associations between the fiber tract-specific florbetapir *z* scores and change rate in tau-PET in projection areas were significant across fiber tracts (t(57)= −14.099, p<0.001; Fig. 3A).

Due to heterochronicity of the myelination of the brain during development, fiber tracts in the normal brain show substantial differences in the degree of myelin [58]. Given that we and others previously observed that brain regions connected by typically lower myelinated fiber tracts are more susceptible to accumulate tau pathology in AD [59], we tested here our auxiliary hypothesis that the association between myelin impairment and tau accumulation is particularly pronounced for typically lower myelinated fiber tracts, using a MRI-derived template of myelin in the normal brain [49]. We observed for those fiber tracts that are lower myelinated in the normal brain a stronger association between the florbetapir *z* scores and tau-PET increases in the connected GM areas (β=0.406, p=0.002; Fig. 3B), suggesting that the association between demyelination and tau accumulation is stronger for those fiber tracts that are typically lower myelinated in the brain.

When controlling for global tau-PET levels at baseline, we found that the associations between the fiber tract-specific florbetapir *z* scores and change rate in tau-PET in projection areas were significant across fiber tracts (t(57)= −3.671, p<0.001).

APOE ε4 influences the association between florbetapir z score in the WM and tau-PET accumulation

For our second major aim, we tested the effect of APOE ε4 on both florbetapir *z* score and tau-PET accumulation. We found that florbetapir *z* scores in the WM were reduced in the APOE ε4 carriers compared to those in the APOE ε4 non-carriers within the Aβ+ group (F(1,99) = 8.622, 0.004; Fig. 4A). Furthermore, APOE ε4 carriers showed higher rates of tau-PET accumulation in Braak-stage 3+4 ROIs (F(1,97) = 5.942, 0.017; Fig. 4B).

Next, we tested whether the effect of APOE ε4 status on tau-PET accumulation is mediated by global florbetapir *z* scores in the WM. Using bootstrapped mediation analysis, we found that global florbetapir *z* scores in the WM mediated the effect of APOE ε4 status on the rate of tau-PET accumulation in Braak 3+4 ROIs (β=0.064 [95% CI: 0.009, 0.140], p=0.008, proportion mediated = 39.3%; Fig. 4C). These results suggest that APOE ε4 is associated with tau accumulation through its effect on myelin impairment. In addition, we tested whether APOE ε4 status also worsens the association between myelin alterations and tau accumulation. In an interaction analysis, we found a significant interaction between APOE ε4 status and florbetapir *z* scores

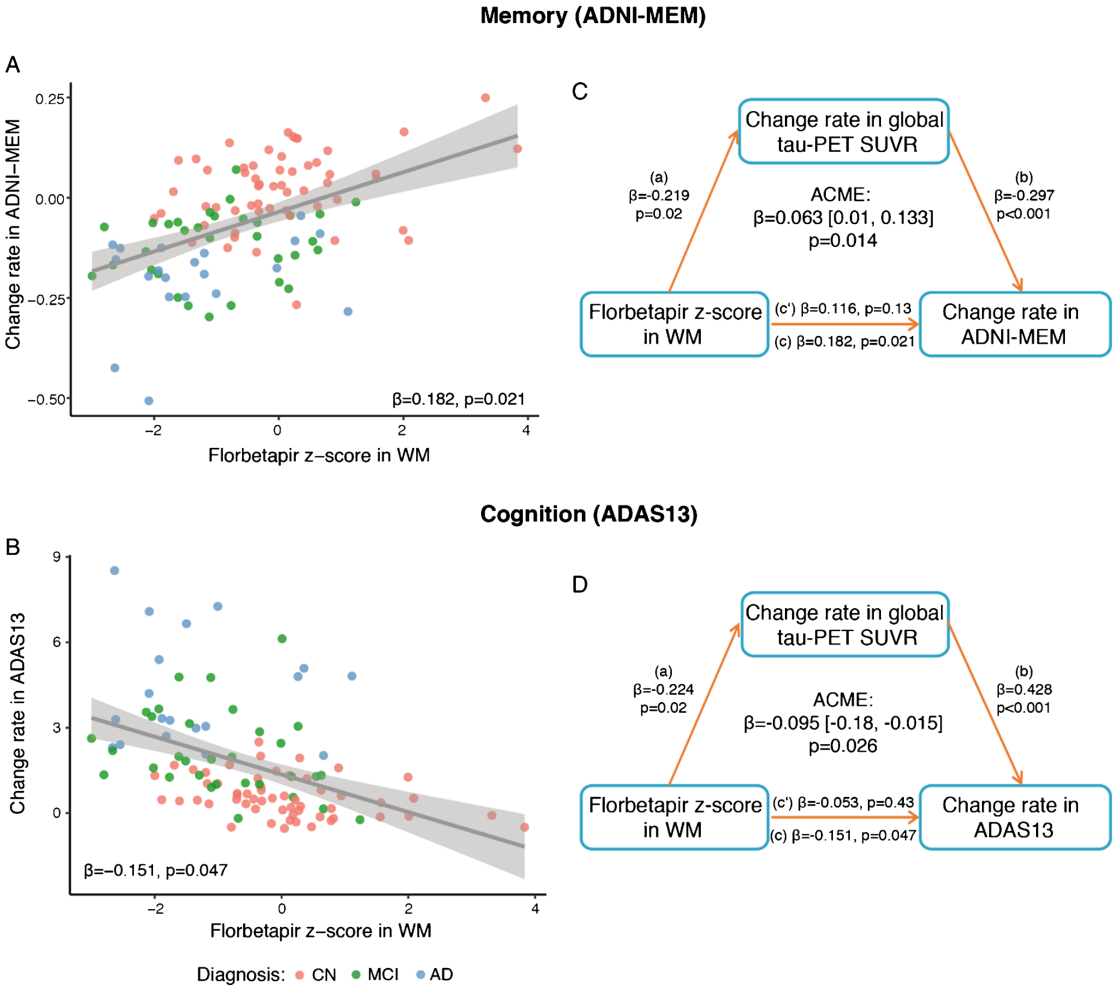

Fig. 2 Tau-PET accumulation mediates the association between florbetapir *z* scores in WM and cognitive decline. **A**, **B** Scatterplots showing the association between florbetapir *z* scores in WM and change rate in memory (ADNI-MEM; **A**) or cognition (ADAS13; **B**). Observations are color coded by diagnosis and standardized *β*-values with *p*-values are displayed. **C, D** Mediation analyses showing that the association between florbetapir *z* scores in WM and changes in memory performance (**C**) or cognition (**D**) is mediated by the change rate in global tau-PET SUVR. Path values are displayed as *β*-values with *p*-values. The path weight c indicates the effect of florbetapir *z* scores in WM on changes in memory or cognition without taking change rate in global tau-PET SUVR into account, the path coefficient c' indicates the corresponding effect of florbetapir *z* scores in WM after accounting for the mediator change rate in global tau-PET SUVR. Mediation effects were determined based on bootstrapping with 1000 iterations. All paths are controlled for age, sex, education, diagnosis, cortical florbetapir-PET SUVR, maximum follow-up duration, and time difference between florbetapir scan and cognitive measures. AD = Alzheimer's disease; ADAS13 = Alzheimer's Disease Assessment Scale cognitive subscale; ACME = Average causal mediation effect; ADNI-MEM = Alzheimer's Disease Neuroimaging Initiative memory composite; CN = cognitive normal; MCI = mild cognitive impairment; WM = white matter

in the WM, where APOE ε4 carriers showed stronger association between lower global florbetapir *z* scores in the WM and higher tau-PET accumulation in Braak stage 3+4 ROIs (β=−0.323, p=0.009; Fig. 5A) and 5+6 ROIs (β=−0.248, p=0.045; Fig. 5A). When controlling for global-tau PET values, the interaction did not reach significance, probably due to limited power for testing interaction terms.

In order to ensure that analysis of the effects of the APOE e4 allele does not depend on the binary classification of the APOE ε4 status, we repeated the analysis based

European Journal of Nuclear Medicine and Molecular Imaging (2024) 51:1035–1049 1043

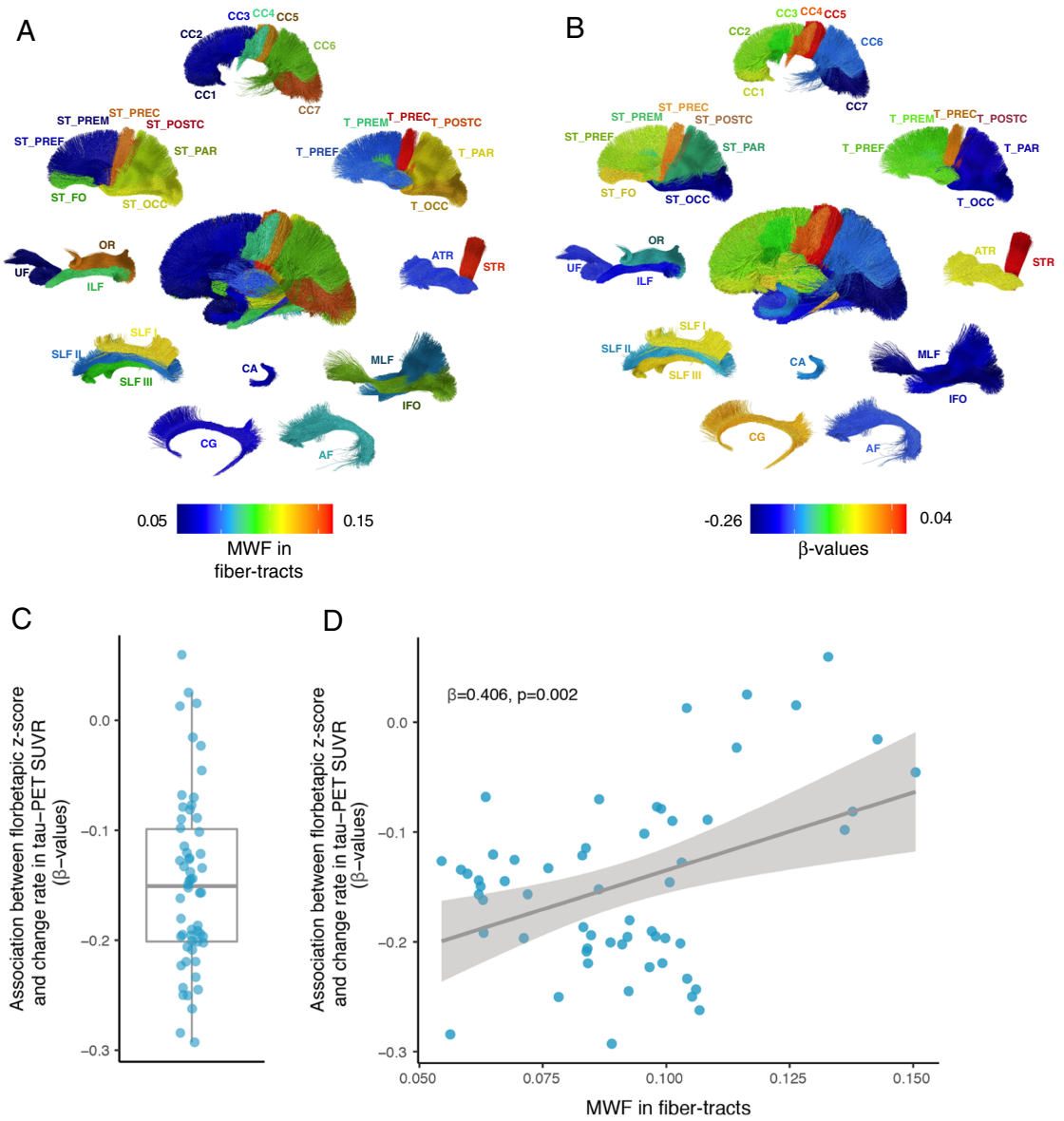

Fig. 3 Association between florbetapir z scores in fiber tracts and change rate in tau-PET SUVRs in connected regions. **A** The myelin water fraction (MWF) quantifying the myelin levels for each major fiber tract in cognitively normal subjects. The color coding refers to the MWF level, with warmer colors corresponding to higher MWF levels. **B** The effect sizes (standardized β-value) from the linear regression analyses including fiber tract-level florbetapir z scores as a predictor of tau-PET in the connected cortical areas are plotted for each fiber tract. Warmer colors correspond to a stronger β-coefficient of the association between lower florbetapir z scores in a given fiber tract and higher rate of tau-PET increase in the connected cortical areas. **C** Boxplot showing the β-values derived from the correlation between florbetapir z scores in fiber tracts and change rate in tau-PET in connected regions. Each dot represents a specific fiber tract. **D** Scatterplot showing the association between normative MWF in fiber tracts derived from healthy participants (x-axis) and β-values derived from the correlation between florbetapir z scores in fiber tracts and change rate in tau-PET in connected regions. MWF = myelin water fraction

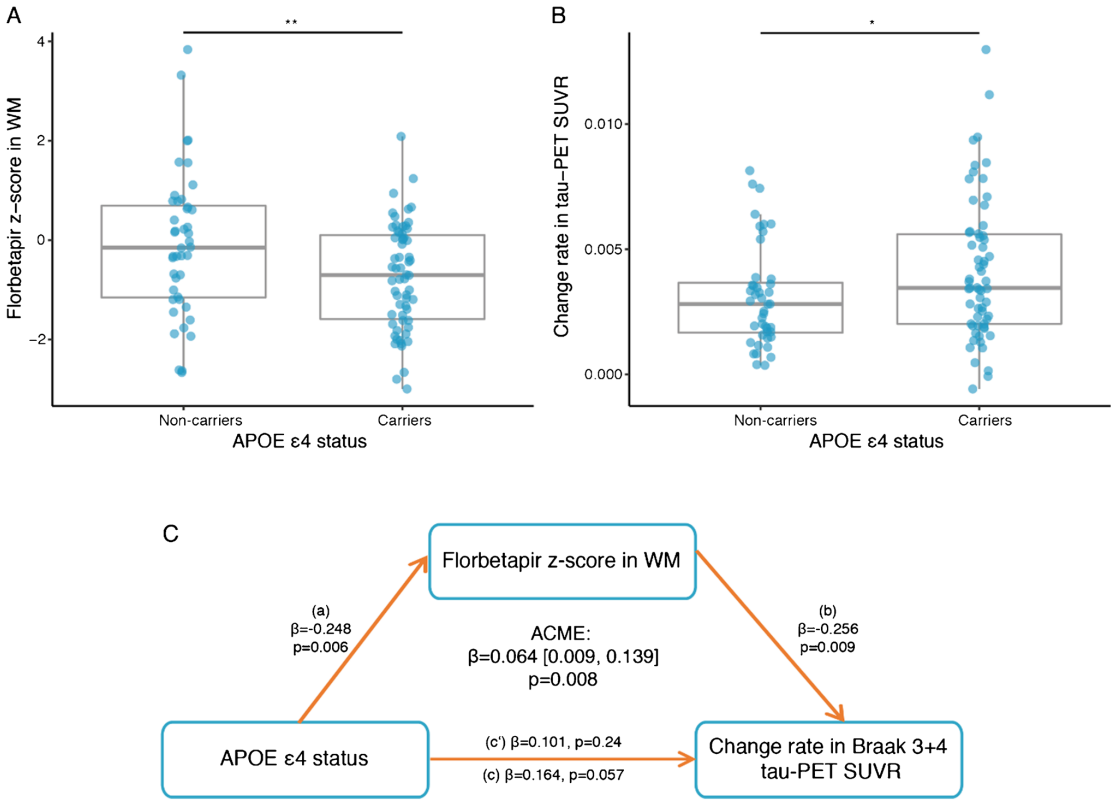

Fig. 4 Florbetapir *z* scores mediate the effect of APOE ε4 status on change rate in tau-PET SUVRs. **A** Boxplot showing the effect of APOE ε4 status on florbetapir *z* scores in WM. **B** Boxplot showing the effect of APOE ε4 status on change rate in Braak 3+4 tau-PET SUVR. **C** Mediation analysis showing that the association between APOE ε4 status and change rate in Braak 3+4 tau-PET SUVR is mediated by florbetapir *z* scores in WM. Path values are displayed as *β*-values with *p*-values. The path weight c indicates the effect of APOE ε4 status on changes in tau-PET without taking florbetapir *z* score into account, the path coefficient c' indicates the corresponding effect of APOE-npscore after accounting for the mediator including florbetapir *z* scores in WM. Mediation effect was determined based on bootstrapping with 1000 iterations. All paths are controlled for age, sex, education, diagnosis, cortical florbetapir-PET SUVR, maximum follow-up duration, and time difference between florbetapir scan and tau-PET scan. ACME = average causal mediation effect; APOE = apolipoprotein E; WM = white matter

on a recently developed neuropathology-weighted measure of APOE gene dosage [60]. The result pattern remained the same (Supplementary results and Supplementary Figure 3), supporting the robustness of our analysis.

Discussion

Myelin alterations frequently occur in AD [16] and are exacerbated in APOE ε4 carriers [29, 61], but the association between APOE ε4, myelin alterations, and primary AD pathology remains unclear [62]. By repurposing the florbetpir-PET tracer to measure myelin in the WM, we found that decreased florbetapir *z* scores in the WM were associated with faster rates of cortical tau-PET accumulation, which mediated the effect on cognitive decline. APOE ε4 was associated with worse florbetapir *z* score reduction and interacted with florbetapir *z* scores in enhancing the rate of tau-PET accumulation, suggesting that APOE ε4 and myelin alterations show a synergistic effect on tau accumulation. Together, these results when controlled for amyloid levels in the GM suggest that a decrease in WM myelin is associated with accelerated fibrillar tau accumulation and thus cognitive decline, where the presence of APOE ε4 exacerbate the association between myelin loss and tau accumulation.

For our first major finding, we demonstrated that lower florbetapir *z* scores were associated with faster subsequent tau-PET accumulation in isocortical brain areas, suggesting that a decrease in myelin is predictive of faster tau accumulation in AD. Our results are in general agreement with

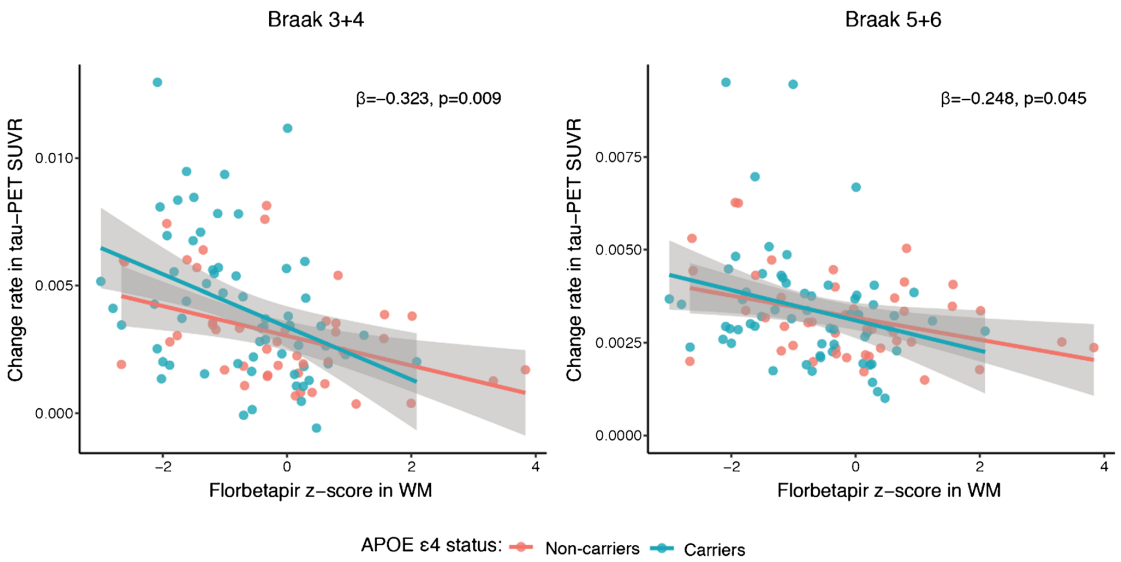

Fig. 5 APOE ε4 status modulates the effect of florbetapir *z* scores on change rate in tau-PET SUVRs. Scatterplots showing the interaction between APOE ε4 status and global florbetapir *z* scores in the WM on change rate in tau-PET in Braak stages 3+4 and 5+6. Red line is the regression line for APOE ε4 non-carriers and the blue regression line is for APOE ε4 carriers

previous neuroimaging and brain autopsy studies reporting reduced WM myelin in AD [12, 63–65]. Consistent with the current results, available evidence from previous studies suggest that myelin alterations occur early in the development of tau pathology: Lower MRI-assessed myelin water fraction in the WM was associated with higher CSF biomarker levels of phospho-tau in preclinical AD [12], and post-mortem assessed myelin-specific ceramide levels were reduced in early Braak-stage region of tau pathology including the medial temporal lobe [10]. Likewise, myelin changes emerged before overt deposition of fibrillar tau in a transgenic mouse model of tau pathology [14], providing experimental support for an early involvement of myelin alterations in the development of tau pathology. Our longitudinal tau-PET imaging study in patients with AD significantly advances these previous cross-sectional studies, demonstrating for the first time that myelin alterations are predictive of faster tau accumulation. While we caution that the current findings should not be interpreted in a causative manner, our findings suggest that myelin alterations may play a role in the etiology of tau pathology.

Furthermore, we demonstrated in our fiber tract-level analysis that the associations between fiber-tract myelin alterations on tau PET accumulation were strongest for those fiber tracts that are typically lower myelinated in the human brain. These findings are in agreement with previous observations of enhanced regional susceptibility to tau accumulation of those brain regions connected by lower myelinated fiber tracts [6, 7]. Furthermore, in humans, we and others previously showed that tau pathology preferentially progresses along closely connected brain regions in patients with AD [3, 4, 66], suggesting that interregional connections provide pathways for the progression of tau pathology in the brain [67, 68]. Therefore, one possibility is that myelin alterations, particularly in late-developing lower myelinated fiber tracts, may enhance the spreading of tau pathology. However, the exact molecular mechanisms need to be still deciphered.

Our second major finding suggests that myelin alteration play an important role in the association between APOE and tau pathology. Our mediation analysis suggested that myelin alterations contribute to the association between APOE ε4 and tau progression, suggesting that APOE and myelin alterations are part of a common pathomechanistic pathway linked to tau pathology. APOE ε4 was previously found to be associated with reduced cholesterol localization and homeostasis in myelinating oligodendrocytes [27]. In transgenic mouse models of tau pathology, myelin was impaired [69, 70], and expression of human APOE ε4 was associated with both higher levels of myelin damage and tau pathology [30, 70]. These studies substantiate a link between APOE ε4, myelin alterations, and tau pathology. Furthermore, we found that in APOE ε4 carriers, the association between myelin alterations and tau accumulation was pronounced. A potential pathomechanism underlying this interaction between APOE ε4 and myelin is that microglial

phagocytosis of cholesterol-rich lipid droplets from impaired myelin may lead to microglial senescence [71, 72] which is exacerbated by microglial APOE ε4 expression [66], rendering microglia less efficient in phagocyting core AD pathologies [67]. Therefore, APOE ε4 may interact with myelin loss such that impaired microglial activation and increased release of inflammasome [70] enhance the accumulation of tau pathology in AD [68]. Our results encourage future experimental studies to uncover the molecular mechanisms that explain the association between APOE, myelin alterations and tau pathology. It should be also noted that consistent with previous findings [13], we observed worse florbetapir-PET signal loss in areas of WMH compared to NAWM. WMH may stem from small vessel disease related processes or, alternatively, relate to primary AD pathology [73, 74]. The disentanglement of the sources of WMH and associated myelin loss warrants further investigation.

In order to interpret the current findings, some caveats need to be taken into account. First, the florbetapir-PET tracer which was originally developed for the detection of amyloid plaques in the GM was repurposed as a measure of myelin in the WM in the current study. In AD the potential influence of amyloid plaque deposition on the florbetapir-PET binding in the WM is particularly pertinent. In order to mitigate any potential influence of binding to amyloid plaques in the GM, we adopted several steps including (1) the erosion of the WM in order to reduce any spill-over effects from GM regions, and (2) adjusting the florbetapir-PET WM signal for the florbetapir-PET GM signal, which rendered the WM and GM florbetapir signal uncorrelated and thus removed the influence of GM signal on the WM. Furthermore, histochemical brain autopsy results suggest that amyloid deposition occurs predominantly close to the WM border and vanishes rapidly within less than 1 mm [75], and may not account for amyloid-PET binding in the WM [76]. Eroding the WM border as implemented in our study may have effectively reduced any PET binding to amyloid in the WM. We note further that there is now solid evidence that amyloid-PET tracers bind to the beta-sheet structure of amyloid and the myelin binding protein in the WM [77, 78], supporting the validity of our approach. In conclusion, while the substrate of amyloid-PET tracer binding in the WM remains to be fully clarified and an influence of amyloid on WM binding cannot be excluded in AD, the current findings provide convincing evidence for myelin alterations assessed by florbetapir-PET binding in AD.

Another caveat is that we could not assess whether the observed effects differ by clinical disease stage due to limited sample size. In particular, in the early asymptomatic phase of AD, any myelin reductions and tau-PET increases are more limited and thus will require larger future studies. Lastly, we caution that most participants were highly educated individuals of Caucasian background with limited cerebrovascular disease. Therefore, the current results remain to be replicated in a group of individuals with a more heterogeneous socio-economic and cultural background. We further note that future studies may investigate the association between myelin alterations and the development of the deposition of amyloid plaques, which we could not test in the current study due to the necessity to correct the florbetapir-PET signal in the WM for the GM signal. Our results therefore suggest that the association between myelin alterations and tau pathology hold when controlling for amyloid GM levels. Yet, our results do not preclude that there is also an association between myelin alterations and amyloid plaque deposition[67, 79], which may synergistically influence the deposition of fibrillar tau. Lastly, we note the difficulty of disentangling effects on the cumulative level of tau-PET and the rates of tau-PET accumulation, given that both are intrinsically linked. In the current study we focused on the rates of tau-accumulation to model differences in the intra-individual increase in tau accumulation.

In summary, the current study provides to our best knowledge the first evidence for the association between APOE genotype, myelin alterations, and tau progression in AD. Myelin is a druggable target, and several already FDA-approved drugs such as clemastine, fingolimod, and rolipram could be potentially repurposed for enhancing myelination and thus slowing AD progression and cognitive decline [80]. Therefore, it is pivotal to better understand the association between myelin alterations and the formation of primary AD pathologies in AD to pave the way for drug interventions that may complement anti-amyloid drugs.

Supplementary Information The online version contains supplementary material available at https://doi.org/10.1007/s00259-023-06530-8.

Funding Open Access funding enabled and organized by Projekt DEAL. The study was funded by grants from Deutsches Zentrum für Luft- und Raumfahrt (DLR, 01KU2203 to M. Ewers), Legerlotz (to M. Ewers). ADNI data collection and sharing for this project was funded by the Alzheimer's Disease Neuroimaging Initiative (ADNI) (National Institutes of Health Grant U01 AG024904) and DOD ADNI (Department of Defense award number W81XWH-12-2-0012). L. Zheng received a scholarship from the China Scholarship Council (no. 202006240090). ADNI is funded by the National Institute on Aging, the National Institute of Biomedical Imaging and Bioengineering, and through generous contributions from the following: AbbVie, Alzheimer's Association; Alzheimer's Drug Discovery Foundation; Araclon Biotech; BioClinica, Inc.; Biogen; Bristol-Myers Squibb Company; CereSpir, Inc.; Eisai Inc.; Elan Pharmaceuticals, Inc.; Eli Lilly and Company; EuroImmun; F. Hoffmann-La Roche Ltd and its affiliated company Genentech, Inc.; Fujirebio; GE Healthcare; IXICO Ltd.; Janssen Alzheimer Immunotherapy Research & Development, LLC.; Johnson & Johnson Pharmaceutical Research & Development LLC.; Lumosity; Lundbeck; Merck & Co., Inc.; Meso Scale Diagnostics, LLC.; NeuroRx Research; Neurotrack Technologies; Novartis Pharmaceuticals Corporation; Pfizer Inc.; Piramal Imaging; Servier; Takeda Pharmaceutical Company; and Transition Therapeutics. The Canadian

Institutes of Health Research is providing funds to support ADNI clinical sites in Canada. Private sector contributions are facilitated by the Foundation for the National Institutes of Health (www.fnih.org). The grantee organization is the Northern California Institute for Research and Education, and the study is coordinated by the Alzheimer's Disease Cooperative Study at the University of California, San Diego. ADNI data are disseminated by the Laboratory for Neuro Imaging at the University of Southern California.

Data availability Data used in this study are available from the ADNI database (adni.loni.usc.edu) upon registration and compliance with the data usage agreement.

Code availability The custom R scripting used for the analysis of the data will be made available upon reasonable request.

Declarations

Ethics approval All participants provided written informed consent approved by the institutional ethics committee of each ADNI participating institution.

Competing interests ME and NF receive research funding from Eli Lilly, ME received consulting feeds from Eli Lilly.

References

1. Franzmeier N, Dewenter A, Frontzkowski L, Dichgans M, Rubinski A, Neitzel J, et al. Patient-centered connectivity-based prediction of tau pathology spread in Alzheimer's disease. Sci Adv. 2020;6. https://doi.org/10.1126/sciadv.abd1327.
2. Vogel JW, Young AL, Oxtoby NP, Smith R, Ossenkoppele R, Strandberg OT, et al. Four distinct trajectories of tau deposition identified in Alzheimer's disease. Nature Med. 2021;27:871–81. https://doi.org/10.1038/s41591-021-01309-6.
3. Franzmeier N, Brendel M, Beyer L, Slemann L, Kovacs GG, Arzberger T, et al. Tau deposition patterns are associated with functional connectivity in primary tauopathies. Nat Commun. 2022;13:1362. https://doi.org/10.1038/s41467-022-28896-3.
4. Clavaguera F, Bolmont T, Crowther RA, Abramowski D, Frank S, Probst A, et al. Transmission and spreading of tauopathy in transgenic mouse brain. Nature Cell Bio. 2009;11:909–13. https://doi.org/10.1038/ncb1901.
5. Mudher A, Colin M, Dujardin S, Medina M, Dewachter I, Alavi Naini SM, et al. What is the evidence that tau pathology spreads through prion-like propagation? Acta Neuropathol Commun. 2017;5:99. https://doi.org/10.1186/s40478-017-0488-7.
6. Braak H, Del Tredici K. Spreading of Tau Pathology in Sporadic Alzheimer's Disease Along Cortico-cortical Top-Down Connections. Cereb Cortex. 2018;28:3372–84. https://doi.org/10.1093/cercor/bhy152.
7. Rubinski A, Franzmeier N, Dewenter A, Luan Y, Smith R, Strandberg O, et al. Higher levels of myelin are associated with higher resistance against tau pathology in Alzheimer's disease. Alzheimers Res Ther. 2022;14:139. https://doi.org/10.1186/s13195-022-01074-9.
8. Sjobeck M, Haglund M, Englund E. White matter mapping in Alzheimer's disease: a neuropathological study. Neurobiol Aging. 2006;27:673–80. https://doi.org/10.1016/j.neurobiolaging.2005.03.007.
9. Zhan X, Jickling GC, Ander BP, Liu D, Stamova B, Cox C, et al. Myelin injury and degraded myelin vesicles in Alzheimer's disease. Curr Alzheimer Res. 2014;11:232–8. https://doi.org/10.2174/1567205011666140131120922.
10. Couttas TA, Kain N, Suchowerska AK, Quek LE, Turner N, Fath T, et al. Loss of ceramide synthase 2 activity, necessary for myelin biosynthesis, precedes tau pathology in the cortical pathogenesis of Alzheimer's disease. Neurobiol Aging. 2016;43:89–100. https://doi.org/10.1016/j.neurobiolaging.2016.03.027.
11. Bouhrara M, Reiter DA, Bergeron CM, Zukley LM, Ferrucci L, Resnick SM, et al. Evidence of demyelination in mild cognitive impairment and dementia using a direct and specific magnetic resonance imaging measure of myelin content. Alzheimers Dement. 2018;14:998–1004. https://doi.org/10.1016/j.jalz.2018.03.007.
12. Dean DC 3rd, Hurley SA, Kecskemeti SR, O'Grady JP, Canda C, Davenport-Sis NJ, et al. Association of amyloid pathology with myelin alteration in preclinical Alzheimer disease. JAMA Neurology. 2017;74:41–9. https://doi.org/10.1001/jamaneurol.2016.3232.
13. Moscoso A, Silva-Rodríguez J, Aldrey JM, Cortés J, Pías-Peleteiro JM, Ruibal Á, et al. (18)F-florbetapir PET as a marker of myelin integrity across the Alzheimer's disease spectrum. Eur J Nucl Med Mol Imaging. 2022;49:1242–53. https://doi.org/10.1007/s00259-021-05493-y.
14. Desai MK, Mastrangelo MA, Ryan DA, Sudol KL, Narrow WC, Bowers WJ. Early oligodendrocyte/myelin pathology in Alzheimer's disease mice constitutes a novel therapeutic target. Am J Pathol. 2010;177:1422–35. https://doi.org/10.2353/ajpath.2010.100087.
15. Desai MK, Sudol KL, Janelsins MC, Mastrangelo MA, Frazer ME, Bowers WJ. Triple-transgenic Alzheimer's disease mice exhibit region-specific abnormalities in brain myelination patterns prior to appearance of amyloid and tau pathology. Glia. 2009;57:54–65. https://doi.org/10.1002/glia.20734.
16. Nasrabady SE, Rizvi B, Goldman JE, Brickman AM. White matter changes in Alzheimer's disease: a focus on myelin and oligodendrocytes. Acta Neuropathol Commun. 2018;6:22. https://doi.org/10.1186/s40478-018-0515-3.
17. De Strooper B, Karran E. The Cellular Phase of Alzheimer's Disease. Cell. 2016;164:603–15. https://doi.org/10.1016/j.cell.2015.12.056.
18. Weiner MW, Veitch DP, Aisen PS, Beckett LA, Cairns NJ, Green RC, et al. The Alzheimer's disease neuroimaging initiative 3: continued innovation for clinical trial improvement. Alzheimers Dement. 2017;13:561–71. https://doi.org/10.1016/j.jalz.2016.10.006.
19. Clark CM, Schneider JA, Bedell BJ, Beach TG, Bilker WB, Mintun MA, et al. Use of florbetapir-PET for imaging beta-amyloid pathology. JAMA. 2011;305:275–83. https://doi.org/10.1001/jama.2010.2008.
20. Auvity S, Tonietto M, Caille F, Bodini B, Bottlaender M, Tournier N, et al. Repurposing radiotracers for myelin imaging: a study comparing 18F-florbetaben, 18F-florbetapir, 18F-flutemetamol,11C-MeDAS, and 11C-PiB. Eur J Nucl Med Mol Imaging. 2020;47:490–501. https://doi.org/10.1007/s00259-019-04516-z.

21. Bajaj A, LaPlante NE, Cotero VE, Fish KM, Bjerke RM, Siclovan T, et al. Identification of the protein target of myelin-binding ligands by immunohistochemistry and biochemical analyses. J Histochem Cytochem. 2013;61:19–30. https://doi.org/10.1369/0022155412467353.
22. Veronese M, Rizzo G, Belzunce M, Schubert J, Searle G, Whittington A, et al. Reproducibility of findings in modern PET neuroimaging: insight from the NRM2018 grand challenge. J Cereb Blood Flow Metab. 2021;41:2778–96. https://doi.org/10.1177/0271678X211015101.
23. Corder EH, Saunders AM, Strittmatter WJ, Schmechel DE, Gaskell PC, Small GW, et al. Gene dose of apolipoprotein E type 4 allele and the risk of Alzheimer's disease in late onset families. Science. 1993;261:921–3.
24. Bertram L, McQueen MB, Mullin K, Blacker D, Tanzi RE. Systematic meta-analyses of Alzheimer disease genetic association studies: the AlzGene database. Nat Genet. 2007;39:17–23. https://doi.org/10.1038/ng1934.
25. Mahley RW. Apolipoprotein E: cholesterol transport protein with expanding role in cell biology. Science. 1988;240:622–30. https://doi.org/10.1126/science.3283935.
26. Saher G, Stumpf SK. Cholesterol in myelin biogenesis and hypomyelinating disorders. Biochim Biophys Acta. 2015;1851:1083–94. https://doi.org/10.1016/j.bbalip.2015.02.010.
27. Blanchard JW, Akay LA, Davila-Velderrain J, von Maydell D, Mathys H, Davidson SM, et al. APOE4 impairs myelination via cholesterol dysregulation in oligodendrocytes. Nature. 2022;611:769–79. https://doi.org/10.1038/s41586-022-05439-w.
28. Bartzokis G, Lu PH, Geschwind DH, Tingus K, Huang D, Mendez MF, et al. Apolipoprotein E affects both myelin breakdown and cognition: implications for age-related trajectories of decline into dementia. Biol Psychiatry. 2007;62:1380–7. https://doi.org/10.1016/j.biopsych.2007.03.024.
29. Operto G, Molinuevo JL, Cacciaglia R, Falcon C, Brugulat-Serrat A, Suarez-Calvet M, et al. Interactive effect of age and APOE-epsilon4 allele load on white matter myelin content in cognitively normal middle-aged subjects. NeuroImage Clin. 2019;24:101983. https://doi.org/10.1016/j.nicl.2019.101983.
30. Koutsodendris N, Blumenfeld J, Agrawal A, Traglia M, Grone B, Zilberter M, et al. Neuronal APOE4 removal protects against tau-mediated gliosis, neurodegeneration and myelin deficits. Nature Aging. 2023. https://doi.org/10.1038/s43587-023-00368-3.
31. Ossenkoppele R, Jansen WJ, Rabinovici GD, Knol DL, van der Flier WM, van Berckel BN, et al. Prevalence of amyloid PET positivity in dementia syndromes: a meta-analysis. JAMA. 2015;313:1939–49. https://doi.org/10.1001/jama.2015.4669.
32. Salvado G, Grothe MJ, Groot C, Moscoso A, Scholl M, Gispert JD, et al. Differential associations of APOE-epsilon2 and APOE-epsilon4 alleles with PET-measured amyloid-beta and tau deposition in older individuals without dementia. Eur J Nucl Med Mol Imaging. 2021;48:2212–24. https://doi.org/10.1007/s00259-021-05192-8.
33. Landau SM, Mintun MA, Joshi AD, Koeppe RA, Petersen RC, Aisen PS, et al. Amyloid deposition, hypometabolism, and longitudinal cognitive decline. Annals of neurology. 2012;72:578–86. https://doi.org/10.1002/ana.23650.
34. Avants BB, Tustison NJ, Song G, Cook PA, Klein A, Gee JC. A reproducible evaluation of ANTs similarity metric performance in brain image registration. NeuroImage. 2011;54:2033–44. https://doi.org/10.1016/j.neuroimage.2010.09.025.
35. Tustison NJ, Cook PA, Klein A, Song G, Das SR, Duda JT, et al. Large-scale evaluation of ANTs and FreeSurfer cortical thickness measurements. NeuroImage. 2014;99:166–79. https://doi.org/10.1016/j.neuroimage.2014.05.044.
36. Jagust WJ, Landau SM, Koeppe RA, Reiman EM, Chen K, Mathis CA, et al. The ADNI PET Core: 2015. Alzheimer's & dementia : the journal of the Alzheimer's Association. 2015;11:757–71. https://doi.org/10.1016/j.jalz.2015.05.001.
37. Young CB, Landau SM, Harrison TM, Poston KL, Mormino EC. Influence of common reference regions on regional tau patterns in cross-sectional and longitudinal [18F]-AV-1451 PET data. NeuroImage. 2021;243:118553. https://doi.org/10.1016/j.neuroimage.2021.118553.
38. Schwarz CG, Therneau TM, Weigand SD, Gunter JL, Lowe VJ, Przybelski SA, et al. Selecting software pipelines for change in flortaucipir SUVR: Balancing repeatability and group separation. NeuroImage. 2021;238:118259. https://doi.org/10.1016/j.neuroimage.2021.118259.
39. Moscoso A, Grothe MJ, Scholl M. Alzheimer's Disease Neuroimaging I. Reduced [(18)F]flortaucipir retention in white matter hyperintensities compared to normal-appearing white matter. Eur J Nucl Med Mol Imaging. 2021;48:2283–94. https://doi.org/10.1007/s00259-021-05195-5.
40. Braak H, Braak E. Neuropathological stageing of Alzheimer-related changes. Acta Neuropathologica. 1991;82:239–59.
41. Marquie M, Normandin MD, Vanderburg CR, Costantino IM, Bien EA, Rycyna LG, et al. Validating novel tau positron emission tomography tracer [F-18]-AV-1451 (T807) on postmortem brain tissue. Annals of neurology. 2015;78:787–800. https://doi.org/10.1002/ana.24517.
42. Franzmeier N, Ossenkoppele R, Brendel M, Rubinski A, Smith R, Kumar A, et al. The BIN1 rs744373 Alzheimer's disease risk SNP is associated with faster Abeta-associated tau accumulation and cognitive decline. Alzheimers Dement. 2022;18:103–15. https://doi.org/10.1002/alz.12371.
43. Billot B, Greve DN, Puonti O, Thielscher A, Van Leemput K, Fischl B, et al. Synthseg: Domain randomisation for segmentation of brain mri scans of any contrast and resolution. arXiv preprint arXiv:210709559. 2021.
44. Rubinski A, Franzmeier N, Neitzel J, Ewers M, Alzheimer's Disease Neuroimaging I. FDG-PET hypermetabolism is associated with higher tau-PET in mild cognitive impairment at low amyloid-PET levels. Alzheimers Res Ther. 2020;12:133. https://doi.org/10.1186/s13195-020-00702-6.
45. Kuijf HJ, Biesbroek JM, Bresser JD, Heinen R, Andermatt S, Bento M, et al. Standardized assessment of automatic segmentation of white matter hyperintensities and results of the WMH segmentation challenge. IEEE Trans Med Imaging. 2019;38:2556–68. https://doi.org/10.1109/TMI.2019.2905770.
46. Dewenter A, Jacob MA, Cai M, Gesierich B, Hager P, Kopczak A, et al. Disentangling the effects of Alzheimer's and small vessel disease on white matter fibre tracts. Brain. 2022:awac265 https://doi.org/10.1093/brain/awac265.
47. Wasserthal J, Neher P, Maier-Hein KH. TractSeg - fast and accurate white matter tract segmentation. NeuroImage. 2018;183:239–53. https://doi.org/10.1016/j.neuroimage.2018.07.070.
48. Tournier JD, Smith R, Raffelt D, Tabbara R, Dhollander T, Pietsch M, et al. MRtrix3: A fast, flexible and open software framework for medical image processing and visualisation. NeuroImage. 2019;202:116137. https://doi.org/10.1016/j.neuroimage.2019.116137.
49. Liu H, Rubino C, Dvorak AV, Jarrett M, Ljungberg E, Vavasour IM, et al. Myelin Water Atlas: A Template for Myelin Distribution in the Brain. J Neuroimaging. 2019;29:699–706. https://doi.org/10.1111/jon.12657.
50. Deming Y, Vasiljevic E, Morrow A, Miao J, Van Hulle C, Jonaitis E, et al. Neuropathology-based APOE genetic risk score better quantifies Alzheimer's risk. medRxiv. 2022:2022.10.12.22280874. https://doi.org/10.1101/2022.10.12.22280874.

51. Reiman EM, Arboleda-Velasquez JF, Quiroz YT, Huentelman MJ, Beach TG, Caselli RJ, et al. Exceptionally low likelihood of Alzheimer's dementia in APOE2 homozygotes from a 5,000-person neuropathological study. Nat Commun. 2020;11:667. https://doi.org/10.1038/s41467-019-14279-8.
52. Rosen WG, Mohs RC, Davis KL. A new rating scale for Alzheimer's disease. Am J Psychiatry. 1984;141:1356–64.
53. Mohs RC, Knopman D, Petersen RC, Ferris SH, Ernesto C, Grundman M, et al. Development of cognitive instruments for use in clinical trials of antidementia drugs: additions to the Alzheimer's Disease Assessment Scale that broaden its scope. The Alzheimer's Disease Cooperative Study. Alzheimer Dis Assoc Disord. 1997;11(Suppl 2):S13-21.
54. Crane PK, Carle A, Gibbons LE, Insel P, Mackin RS, Gross A, et al. Development and assessment of a composite score for memory in the Alzheimer's Disease Neuroimaging Initiative (ADNI). Brain Imaging Behav. 2012;6:502–16. https://doi.org/10.1007/s11682-012-9186-z.
55. Preische O, Schultz SA, Apel A, Kuhle J, Kaeser SA, Barro C, et al. Serum neurofilament dynamics predicts neurodegeneration and clinical progression in presymptomatic Alzheimer's disease. Nature Med. 2019;25:277–83. https://doi.org/10.1038/s41591-018-0304-3.
56. Tingley D, Yamamoto T, Hirose K, Keele L, Imai K. mediation: R Package for Causal Mediation Analysis. J Statistical Software. 2014;1(5):2014. https://doi.org/10.18637/jss.v059.i05.
57. Rothman KJ. No adjustments are needed for multiple comparisons. Epidemiology. 1990;1:43–6.
58. Yeatman JD, Wandell BA, Mezer AA. Lifespan maturation and degeneration of human brain white matter. Nat Commun. 2014;5:4932. https://doi.org/10.1038/ncomms5932.
59. Braak H, Braak E. Development of Alzheimer-related neurofibrillary changes in the neocortex inversely recapitulates cortical myelogenesis. Acta Neuropathologica. 1996;92:197–201. https://doi.org/10.1007/s004010050508.
60. Deming Y, Vasiljevic E, Morrow A, Miao J, Van Hulle C, Jonaitis E, et al. Neuropathology-based APOE genetic risk score better quantifies Alzheimer's risk. Alzheimers Dement. 2023. https://doi.org/10.1002/alz.12990.
61. Bartzokis G, Lu PH, Geschwind DH, Edwards N, Mintz J, Cummings JL. Apolipoprotein E genotype and age-related myelin breakdown in healthy individuals: implications for cognitive decline and dementia. Arch Gen Psychiatry. 2006;63:63–72. https://doi.org/10.1001/archpsyc.63.1.63.
62. Hirschfeld LR, Risacher SL, Nho K, Saykin AJ. Myelin repair in Alzheimer's disease: a review of biological pathways and potential therapeutics. Transl Neurodegener. 2022;11:47. https://doi.org/10.1186/s40035-022-00321-1.
63. Bulk M, Abdelmoula WM, Nabuurs RJA, van der Graaf LM, Mulders CWH, Mulder AA, et al. Postmortem MRI and histology demonstrate differential iron accumulation and cortical myelin organization in early- and late-onset Alzheimer's disease. Neurobiol Aging. 2018;62:231–42. https://doi.org/10.1016/j.neurobiolaging.2017.10.017.
64. Mitew S, Kirkcaldie MT, Halliday GM, Shepherd CE, Vickers JC, Dickson TC. Focal demyelination in Alzheimer's disease and transgenic mouse models. Acta neuropathologica. 2010;119:567–77. https://doi.org/10.1007/s00401-010-0657-2.
65. Nasrabady SE, Rizvi B, Goldman JE, Brickman AM. White matter changes in Alzheimer's disease: a focus on myelin and oligodendrocytes. Acta Neuropathologica Commun. 2018;6:22. https://doi.org/10.1186/s40478-018-0515-3.
66. Wang N, Wang M, Jeevaratnam S, Rosenberg C, Ikezu TC, Shue F, et al. Opposing effects of apoE2 and apoE4 on microglial activation and lipid metabolism in response to demyelination. Mol Neurodegener. 2022;17:75. https://doi.org/10.1186/s13024-022-00577-1.
67. Depp C, Sun T, Sasmita AO, Spieth L, Berghoff SA, Steixner-Kumar AA, et al. Ageing-associated myelin dysfunction drives amyloid deposition in mouse models of Alzheimer's disease. bioRxiv. 2021:2021.07.31.454562 https://doi.org/10.1101/2021.07.31.454562.
68. Ising C, Venegas C, Zhang S, Scheiblich H, Schmidt SV, Vieira-Saecker A, et al. NLRP3 inflammasome activation drives tau pathology. Nature. 2019;575:669–73. https://doi.org/10.1038/s41586-019-1769-z.
69. Shi Y, Andhey PS, Ising C, Wang K, Snipes LL, Boyer K, et al. Overexpressing low-density lipoprotein receptor reduces tau-associated neurodegeneration in relation to apoE-linked mechanisms. Neuron. 2021;109:2413-26 e7 https://doi.org/10.1016/j.neuron.2021.05.034
70. Shi Y, Yamada K, Liddelow SA, Smith ST, Zhao L, Luo W, et al. ApoE4 markedly exacerbates tau-mediated neurodegeneration in a mouse model of tauopathy. Nature. 2017;549:523–7. https://doi.org/10.1038/nature24016.
71. Safaiyan S, Kannaiyan N, Snaidero N, Brioschi S, Biber K, Yona S, et al. Age-related myelin degradation burdens the clearance function of microglia during aging. Nature Neurosci. 2016;19:995–8. https://doi.org/10.1038/nn.4325.
72. Cantuti-Castelvetri L, Fitzner D, Bosch-Queralt M, Weil MT, Su M, Sen P, et al. Defective cholesterol clearance limits remyelination in the aged central nervous system. Science. 2018;359:684–8. https://doi.org/10.1126/science.aan4183.
73. Garnier-Crussard A, Bougacha S, Wirth M, Dautricourt S, Sherif S, Landeau B, et al. White matter hyperintensity topography in Alzheimer's disease and links to cognition. Alzheimers Dement. 2022;18:422–33. https://doi.org/10.1002/alz.12410.
74. Wardlaw JM, Valdes Hernandez MC, Munoz-Maniega S. What are white matter hyperintensities made of? Relevance to vascular cognitive impairment. J Am Heart Assoc. 2015;4:001140. https://doi.org/10.1161/JAHA.114.001140.
75. Iwamoto N, Nishiyama E, Ohwada J, Arai H. Distribution of amyloid deposits in the cerebral white matter of the Alzheimer's disease brain: relationship to blood vessels. Acta Neuropathol. 1997;93:334–40. https://doi.org/10.1007/s004010050624.
76. Fodero-Tavoletti MT, Rowe CC, McLean CA, Leone L, Li QX, Masters CL, et al. Characterization of PiB binding to white matter in Alzheimer disease and other dementias. J Nucl Med. 2009;50:198–204. https://doi.org/10.2967/jnumed.108.057984.
77. Stankoff B, Wang Y, Bottlaender M, Aigrot MS, Dolle F, Wu C, et al. Imaging of CNS myelin by positron-emission tomography. Proc Natl Acad Sci U S A. 2006;103:9304–9. https://doi.org/10.1073/pnas.0600769103.
78. Stankoff B, Freeman L, Aigrot MS, Chardain A, Dolle F, Williams A, et al. Imaging central nervous system myelin by positron emission tomography in multiple sclerosis using [methyl-(11)C]-2-(4'-methylaminophenyl)- 6-hydroxybenzothiazole. Annals of neurology. 2011;69:673–80. https://doi.org/10.1002/ana.22320.
79. Bartzokis G, Lu PH, Mintz J. Human brain myelination and amyloid beta deposition in Alzheimer's disease. Alzheimers Dement. 2007;3:122–5. https://doi.org/10.1016/j.jalz.2007.01.019.
80. Fessel J. Reversing Alzheimer's disease dementia with clemastine, fingolimod, or rolipram, plus anti-amyloid therapy. Alzheimers Dement (N Y). 2022;8:e12242. https://doi.org/10.1002/trc2.12242.

Supplementary figures

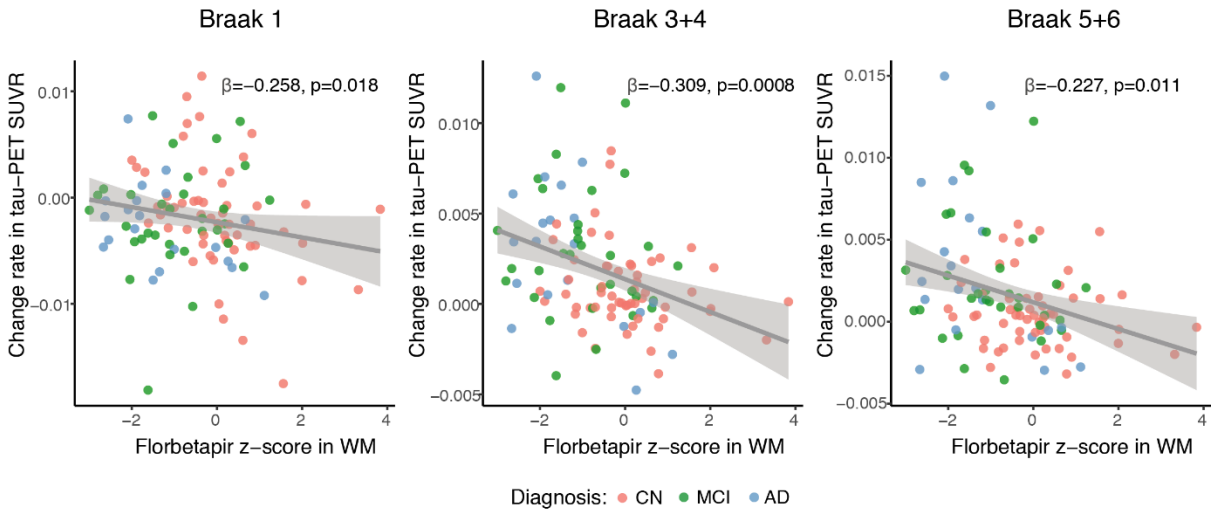

Supplementary Figure 1: Association between florbetapir z-score in WM and change rate in tau-PET SUVRs calculated using a standard cerebellar reference region

Scatterplots showing the association between florbetapir z-score in WM and change rate in tau-PET SUVRs for Aβ+ participants. Tau-PET SUVRs are calculated using a standard cerebellar reference region. Observations are color-coded by diagnosis and standardized β-values with p-values are displayed. AD = Alzheimer's disease; CN = Cognitive normal; MCI = Mild cognitive impairment; WM = White matter.

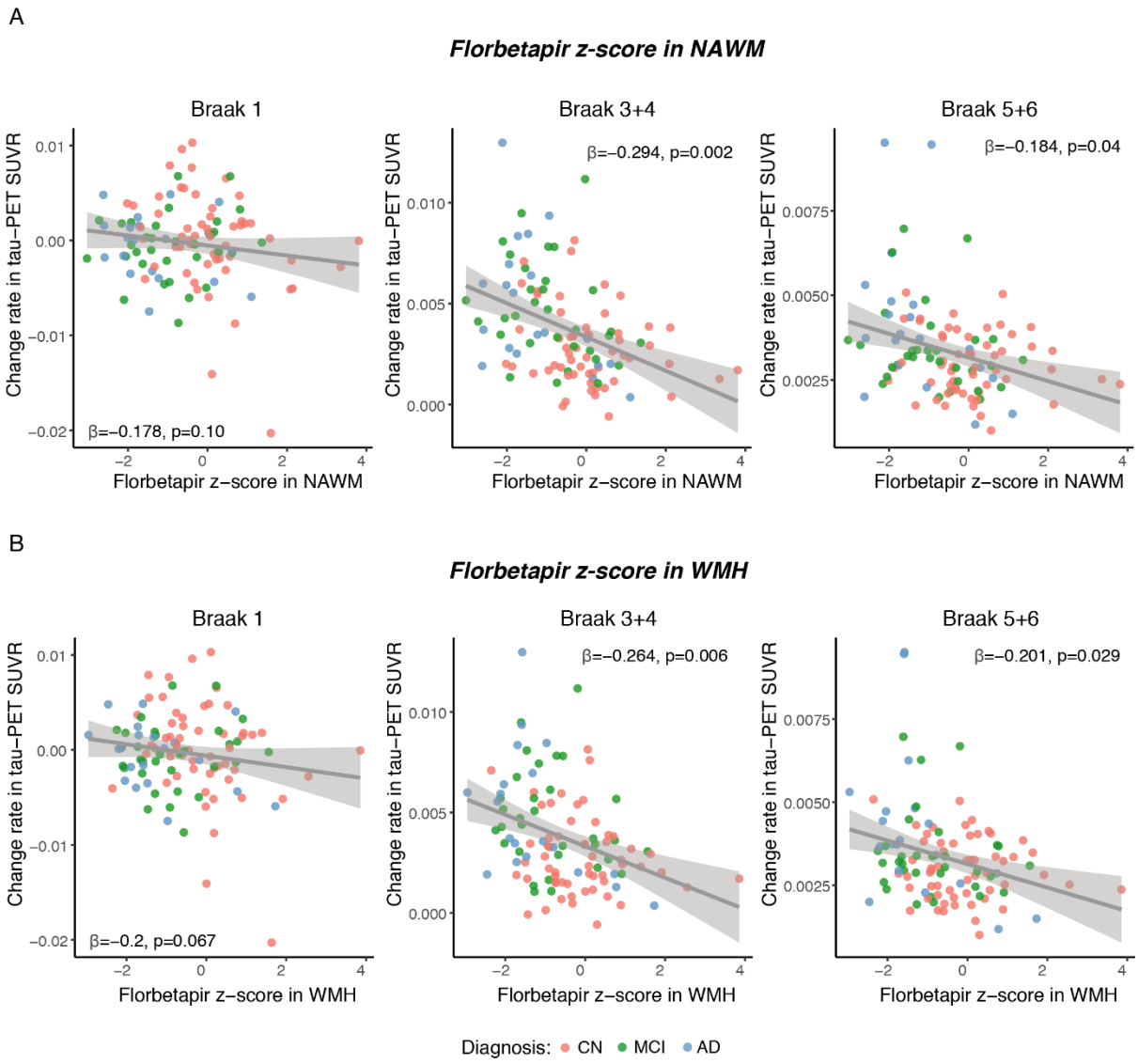

Supplementary Figure 2: Association between florbetapir z-score in NAWM or WMH and change rate in tau-PET SUVRs

Scatterplots showing the association between florbetapir z-score in NAWM (A) or WMH (B) and change rate in tau-PET SUVRs for Aβ+ participants. Observations are color coded by diagnosis and standardized β-values with p-values are displayed. AD = Alzheimer's disease; CN = Cognitive normal; MCI = Mild cognitive impairment; NAWM = Normal appearing white matter; WM = White matter; WMH = White matter hyperintensities.

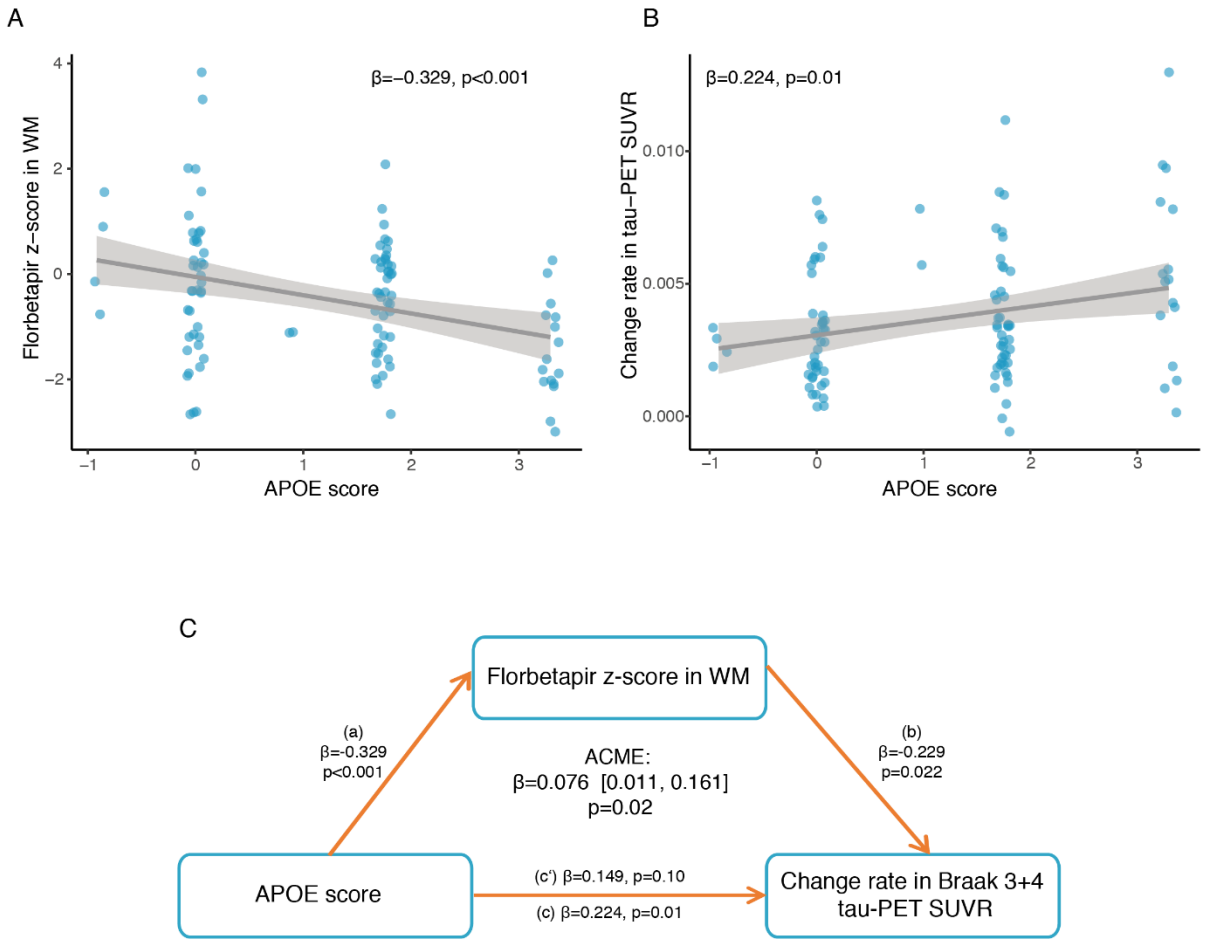

Supplementary Figure 3: Florbetapir z-score mediates the effect of APOE-npscore on change rate in tau-PET SUVRs

(A) Scatterplot showing the association between APOE-npscore and florbetapir z-score in WM. (B) Scatterplot showing the association between APOE-npscore and change rate in Braak 3+4 tau-PET SUVR. (C) Mediation analysis showing that the association between APOE-npscore and change rate in Braak 3+4 tau-PET SUVR is mediated by florbetapir z-score in WM. Path values are displayed as β-values with p-values. The path weight c indicates the effect of APOE-npscore on changes in tau-PET without taking florbetapir z-score into account, the path coefficient c' indicates the corresponding effect of APOE-npscore after accounting for the mediator flobrbetapir z-score in WM. Mediation effect was determined based on bootstrapping with 1,000 iterations. All paths are controlled for age, sex, education, diagnosis, cortical florbetapir-PET SUVR, maximum follow-up duration, and time difference between florbetapir scan and tau-PET scan. ACME = Average causal mediation effect; APOE = Apolipoprotein E; WM = White matter.

Acknowledgements

I express my gratitude to Prof. Dr. Michael Ewers, my supervisor, for his guidance and support throughout my PhD journey. I also express appreciation to the other members of my thesis advisory committee, Prof. Dr. med. Peter zu Eulenburg and Prof. Dr. med. Matthias Brendel, whose valuable feedback enhanced the quality of my work.

Special acknowledge goes to Dr. Anna Rubinski, Dr. Nicolai Franzmeier, and all co-authors and colleagues whose contributions played a pivotal role in the development of this dissertation.

Heartfelt thanks to my family, partner, and friends for their steadfast support.

In the words of Confucius, observing men of worth encourages emulation, while encountering those of a contrary nature prompts introspection (*Analects*, Chapter Benevolence).[1] Lastly, I extend my thanks to all those I encountered on this journey.

[1] The original Chinese text said “見賢思齊焉見不賢而內自省也”.

List of publications

Zheng, L., Rubinski, A., Denecke, J., Luan, Y., Smith, R., Strandberg, O., Stomrud, E., Ossenkoppele, R., Svaldi, D. O., Higgins, I. A., Shcherbinin, S., Pontecorvo, M. J., Hansson, O., Franzmeier, N., Ewers, M., for the Alzheimer's Disease Neuroimaging Initiative. (2024). Combined Connectomics, *MAPT* Gene Expression, and Amyloid Deposition to Explain Regional Tau Deposition in Alzheimer Disease. *Annals of Neurology*, 95(2), 274–287. https://doi.org/10.1002/ana.26818

Wang, H., Zhu, Y., **Zheng, L.**, Chen, M., Hao, Z., Guo, R., Feng, L., & Wang, D. (2024). Association of the *COL4A2* Gene Polymorphisms with Primary Intracerebral Hemorrhage Risk and Outcome in Chinese Han Population. *Molecular Neurobiology*. https://doi.org/10.1007/s12035-024-04146-z

Rubinski, A., Dewenter, A., **Zheng, L.**, Franzmeier, N., Stephenson, H., Deming, Y., Duering, M., Gesierich, B., Denecke, J., Pham, A.-V., Bendlin, B., Ewers, M., for the Alzheimer's Disease Neuroimaging Initiative. (2024). Florbetapir PET-assessed demyelination is associated with faster tau accumulation in an *APOE ε4*-dependent manner. *European Journal of Nuclear Medicine and Molecular Imaging*, 51(4), 1035–1049. https://doi.org/10.1007/s00259-023-06530-8

Song, X., Liu, J., Wang, Y., **Zheng, L.**, & Liu, M. (2022). Serum microRNA miR-491-5p/miR-206 Is Correlated with Poor Outcomes/Spontaneous Hemorrhagic Transformation after Ischemic Stroke: A Case Control Study. *Brain Sciences*, *12*(8), Article 8. https://doi.org/10.3390/brainsci12080999

Biel, D., Luan, Y., Brendel, M., Hager, P., Dewenter, A., Moscoso, A., Otero Svaldi, D., Higgins, I. A., Pontecorvo, M., Römer, S., Steward, A., Rubinski, A., **Zheng, L.**, Schöll, M., Shcherbinin, S., Ewers, M., Franzmeier, N., & Alzheimer's Disease Neuroimaging Initiative. (2022). Combining tau-PET and fMRI meta-analyses for patient-

centered prediction of cognitive decline in Alzheimer's disease. *Alzheimer's Research & Therapy*, *14*(1), 166. https://doi.org/10.1186/s13195-022-01105-5

Zheng, L., Wang, Z., Liu, J., Yang, X., Zhang, S., Hao, Z., Liu, M., & Wang, D. (2021). Association between admission blood fibrinogen-to-albumin ratio and clinical outcomes after acute lacunar stroke. *Biomarkers in Medicine*. https://doi.org/10.2217/bmm-2019-0537

Xu, M., Cheng, Y., Zhang, S., Zhang, S., Song, Q., **Zheng, L.**, Liu, M., & Liu, M. (2021). Higher cerebral small vessel disease burden is associated with smaller hematoma volume in mixed-location intracerebral hemorrhage. *Microcirculation*, *28*(6), e12705. https://doi.org/10.1111/micc.12705

Yang, X., Wang, L., **Zheng, L.**, Wu, J., Liu, J., Hao, Z., Zhang, S., Wu, B., Liu, M., & Wang, D. (2020). Serum albumin as a potential predictor of pneumonia after acute ischemic stroke. *Current Neurovascular Research*, *17*(4), 385–393. https://doi.org/10.2174/1567202617666200514120641

Zheng, L., Yang, C., Xiang, L., & Hao, Z. (2019). Genotype-guided antiplatelet therapy compared with conventional therapy for patients with acute coronary syndromes: A systematic review and meta-analysis. *Biomarkers*, *24*(6), 517–523. https://doi.org/10.1080/1354750X.2019.1634764

Zheng, L., Xiong, Y., Liu, J., Yang, X., Wang, L., Zhang, S., Liu, M., & Wang, D. (2019). MMP-9-Related microRNAs as Prognostic Markers for Hemorrhagic Transformation in Cardioembolic Stroke Patients. *Frontiers in Neurology*, *10*, 945. https://doi.org/10.3389/fneur.2019.00945

Wang, L., Song, Q., Wang, C., Wu, S., Deng, L., Li, Y., **Zheng, L.**, & Liu, M. (2019). Neutrophil to lymphocyte ratio predicts poor outcomes after acute ischemic stroke: A cohort study and systematic review. *Journal of the Neurological Sciences*, *406*, 116445. https://doi.org/10.1016/j.jns.2019.116445

Liu, J., **Zheng, L.**, Cheng, Y., Zhang, S., Wu, B., Wang, D., Zhang, S., Tao, W., Wu, S., & Liu, M. (2019). Trends in Outcomes of Patients With Ischemic Stroke Treated Between 2002 and 2016. *Circulation: Cardiovascular Quality and Outcomes*, *12*(12), e005610. https://doi.org/10.1161/CIRCOUTCOMES.119.005610

LMU LUDWIG-MAXIMILIANS-UNIVERSITÄT MÜNCHEN

Dekanat Medizinische Fakultät
Promotionsbüro

Affidavit

Zheng, Lukai

Surname, first name

Address

I hereby declare, that the submitted thesis entitled

Combining connectivity, related pathologies, and genetic factors to explain tau accumulation in Alzheimer's disease

is my own work. I have only used the sources indicated and have not made unauthorised use of services of a third party. Where the work of others has been quoted or reproduced, the source is always given.

I further declare that the dissertation presented here has not been submitted in the same or similar form to any other institution for the purpose of obtaining an academic degree.

Munich, 8.7.2024 Zheng, Lukai

Place, Date Signature doctoral candidate

LMU LUDWIG-MAXIMILIANS-UNIVERSITÄT MÜNCHEN

Dekanat Medizinische Fakultät
Promotionsbüro

Confirmation of congruency between printed and electronic version of the doctoral thesis

Doctoral candidate: Lukai Zheng

Address:

I hereby declare that the electronic version of the submitted thesis, entitled

Combining connectivity, related pathologies, and genetic factors to explain tau accumulation in Alzheimer's disease

is congruent with the printed version both in content and format.

Munich, 8.7.2024 Zheng, Lukai

Place, Date Signature doctoral candidate